Blue Globe Foresight

Studie #9/2015

Decentral Green H_2

Wasserstoff aus Biomasse zur CO_2-neutralen, effizienten und dezentralen Strom- und Wärmeerzeugung

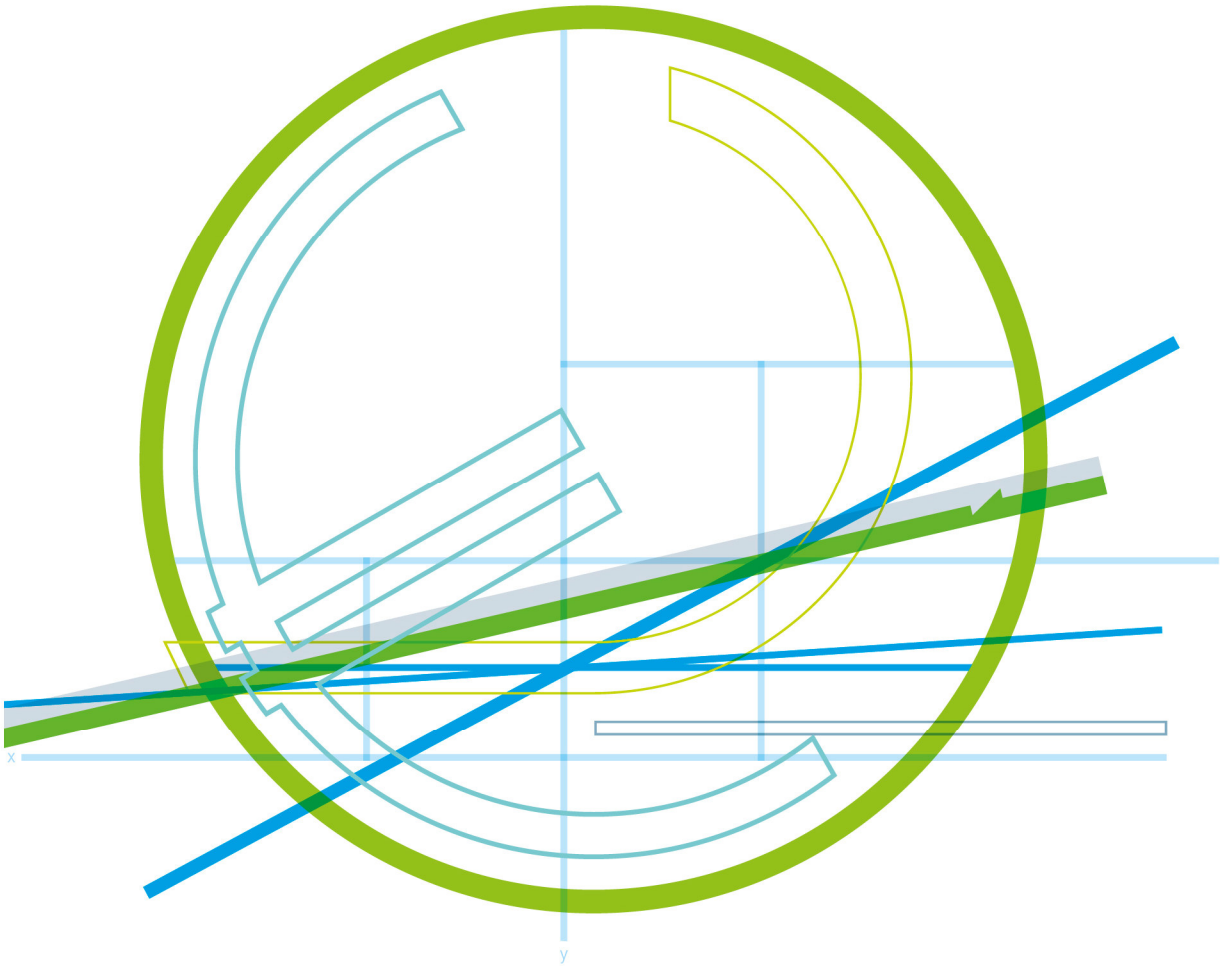

Hermann Hofbauer et al.

VORWORT

Die Publikationsreihe BLUE GLOBE REPORT macht die Kompetenz und Vielfalt, mit der die österreichische Industrie und Forschung für die Lösung der zentralen Zukunftsaufgaben arbeiten, sichtbar. Strategie des Klima- und Energiefonds ist, mit langfristig ausgerichteten Förderprogrammen gezielt Impulse zu setzen. Impulse, die heimischen Unternehmen und Institutionen im internationalen Wettbewerb eine ausgezeichnete Ausgangsposition verschaffen.

Jährlich stehen dem Klima- und Energiefonds bis zu 150 Mio. Euro für die Förderung von nachhaltigen Energie- und Verkehrsprojekten im Sinne des Klimaschutzes zur Verfügung. Mit diesem Geld unterstützt der Klima- und Energiefonds Ideen, Konzepte und Projekte in den Bereichen Forschung, Mobilität und Marktdurchdringung.

Mit dem BLUE GLOBE REPORT informiert der Klima- und Energiefonds über Projektergebnisse und unterstützt so die Anwendungen von Innovation in der Praxis. Neben technologischen Innovationen im Energie- und Verkehrsbereich werden gesellschaftliche Fragestellung und wissenschaftliche Grundlagen für politische Planungsprozesse präsentiert. Der BLUE GLOBE REPORT wird der interessierten Öffentlichkeit über die Homepage www.klimafonds.gv.at zugänglich gemacht und lädt zur kritischen Diskussion ein.

Der vorliegende Bericht dokumentiert die Ergebnisse eines Projekts aus dem Forschungs- und Technologieprogramm „Neue Energien 2020“. Mit diesem Programm verfolgt der Klima- und Energiefonds das Ziel, durch Innovationen und technischen Fortschritt den Übergang zu einem nachhaltigen Energiesystem voranzutreiben.

Wer die nachhaltige Zukunft mitgestalten will, ist bei uns richtig: Der Klima- und Energiefonds fördert innovative Lösungen für die Zukunft!

Ingmar Höbarth
Geschäftsführer, Klima- und Energiefonds

Theresia Vogel
Geschäftsführerin, Klima- und Energiefonds

Wasserstoff aus Biomasse zur CO_2-neutralen, effizienten und dezentralen Strom- und Wärmeerzeugung

Decentral Green H_2

AutorInnen:
Univ.Prof. Dipl.-Ing. Dr.techn. Hermann Hofbauer
Dipl.-Ing. Dr.techn. Klaus Bosch
Ing. Horst Binder

Unter Mitarbeit von:
Dipl. Ing. Dr.techn. Michael Harasek
Dipl. Ing. Florian Benedikt
Dipl. Ing. David Konlechner
Dipl. Ing. Michael Kraussler

1 Inhaltsverzeichnis

2 Einleitung

Wasserstoff wird heutzutage primär durch Dampfreformierung von Erdgas hergestellt. Dabei entstehen hohe CO_2 Emissionen. Die aktuelle Klimasituation macht es notwendig, alternative und erneuerbare Quellen für die Wasserstoffproduktion zu finden. Abseits der Wasserstoffproduktion durch Elektrolyse, wenn diese über erneuerbare Stromquellen betrieben wird, bietet sich die Wasserstoffproduktion aus Biomasse an.

Das bei der Biomasse-Dampfvergasung entstehende Produkt- oder Holzgas weist einen Wasserstoffanteil von ca. 40 vol. % auf. Über weitere Gasreinigungs- und Konditionierungsschritte kann aus dem Holzgas Wasserstoff mit einer Reinheit > 99,95 vol. % gewonnen werden. Dadurch, dass Biomasse als Ausgangsstoff verwendet wird, würden bei einer Wasserstoffproduktion auf Grundlage dieser Technologie keine zusätzlichen CO_2 Emissionen entstehen.

In diesem Projekt sollen Prozessketten evaluiert und getestet werden, die eine erneuerbare Wasserstoffproduktion aus Biomasse ermöglichen sollen.

Im Zuge des Projekts wurden diverse verfahrenstechnische Unit Operations zur Wasserstoffproduktion am Standort des Biomasse-Dampfvergasungskraftwerks in Oberwart getestet. Darunter eine dreistufige Wassergas-Shift (WGS) Unit zur Umwandlung von Kohlenmonoxid in Wasserstoff, eine Membran Unit zum Anreichern von Wasserstoff und gleichzeitigem Verringern von Kohlenmonoxid und Methan, ein Gaswäscher, der mit Hilfe des Waschmittels Rapsmethylester (RME) Teere abscheiden soll und einer Druckwechseladsorptions-Anlage (DWA) zur Feinreinigung des Wasserstoffs, um Reinheiten > 99 vol. % zu erreichen. Zum Nachweis der erzeugten Wasserstoffqualität wurde mit dem aus Biomasse erzeugten Wasserstoff eine PEM Brennstoffzelle betrieben, deren Anforderungen an die eingesetzte Reinheit sehr hoch sind.

Es gab insgesamt zwei Langzeitversuche mit unterschiedlichen Prozesskettenkonfigurationen. Die Prozesskette 1 zur Wasserstofferzeugung aus Biomasse bestand aus dem RME Gaswäscher, der Membran Unit, der Druckwechseladsorption und der PEM Brennstoffzelle. Die Prozesskette 2 bestand aus einer dreistufigen WGS Unit, dem RME Gaswäscher, der Druckwechseladsorption und der PEM Brennstoffzelle. Beide Prozessketten ermöglichten die Erzeugung von Wasserstoff aus Biomasse. In beiden Fällen wurde eine Reinheit > 99,95 vol. % erreicht. Diese hohe Reinheit ermöglichte auch einen problemlosen Betrieb der PEM Brennstoffzelle. Vor und parallel zum Betrieb der Prozessketten wurden umfangreiche Untersuchungen und Optimierungen zu den einzelnen Prozessschritten (Membran, DWA, WGS, PEM) durchgeführt, um eine verlässliche und kontrollierbare Performance dieser Stufen zu haben. Im ersten Teil dieses Berichtes werden die bei den Versuchen verwendeten Anlagenteile beschrieben, sowie die verwendeten Messmethoden mit denen das erzeugte Gas analysiert wurde. Anschließend werden die beiden Prozessketten beschrieben und dargestellt. Die wichtigsten Highlights aus den Untersuchungen an den einzelnen Stufen der Prozessketten sind Inhalt eines weiteren Kapitels Basierend auf diesen Versuchsdaten wurde eine IPSEpro Simulation der beiden Prozessketten zur Wasserstofferzeugung durchgeführt. Anhand der Ergebnisse dieser Simulationen wurde in weiterer Folge ein Konzept für einen Scale-Up der Anlage zur Wasserstoffherstellung erstellt.

3 Inhaltliche Darstellung

In diesem Kapitel wird das experimentelle Umfeld der Versuche dargestellt. Zunächst wird das Dual Fluidized Bed (DFB) Biomass Steam Gasification (Biomasse-Dampfvergasung) Verfahren erläutert, welches Holzgas mit hohem Wasserstoffanteil bereitstellt. Als nächstes wird das Biomassekraftwerk Oberwart beschrieben, welches das Holzgas für die Versuche zur Verfügung gestellt hat. Schließlich werden sowohl die beiden Prozessketten zur Produktion von Wasserstoff aus Holzgas vorgestellt, als auch die verwendeten Analysemethoden, mit denen das Holzgas entlang der Prozessketten auf Haupt- und Nebenkomponenten untersucht wurde.

3.1 Biomasse-Dampfvergasung

Die Grundlage der Versuche zur Erzeugung von Wasserstoff aus Biomasse bildet das DFB-Biomasse-Dampfvergasungsverfahren. Dieses ist in Abbildung 1 dargestellt.

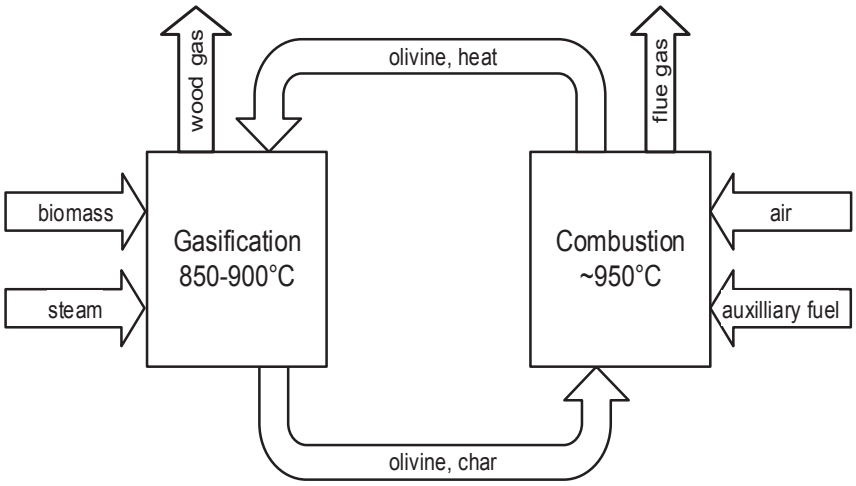

Abbildung 1: Grundprinzip der allothermen Biomasse-Dampfvergasung (Benedikt, 2014).

Das Verfahren basiert auf der allothermen Vergasung von Biomasse. Dabei wird Biomasse mit Dampf als Vergasungsmedium vergast. Die für die ablaufenden Vergasungsreaktionen notwendige Wärme (endothermer Prozess) wird über ein zirkulierendes Bettmaterial, in diesem Falle Olivin, bereitgestellt. Olivin wird in der Verbrennungskammer mit aus der Vergasung zurückbleibendem Koks, einem Teil des Holzgases und Luft aufgeheizt. Danach wird es in den Vergasungsreaktor transportiert und gibt dort seine Wärme an die Vergasungsreaktionen ab. Anschließend gelangt das Olivin wieder in den Verbrennungsteil, wird dort wieder aufgewärmt und der Kreislauf beginnt von vorne.
Das entstehende Holzgas besitzt einen vergleichsweise hohen Heizwert. Die durchschnittliche Gaszusammensetzung ist in Tabelle 1 dargestellt.

Tabelle 1: Durchschnittliche trockene Holzgaszusammensetzung der Biomasse-Dampfvergasung bei der Anlage Oberwart (Kraussler, 2014).

Komponente	Anteil (trocken)	Einheit
Wasserstoff H_2	40	Vol. %
Kohlenmonoxid CO	25	Vol. %
Kohlendioxid CO_2	20	Vol. %
Methan CH_4	10	Vol. %
Höhere Kohlenwasserstoffe C_xH_y	4	Vol. %
Stickstoff N_2	1	Vol. %

3.2 Beschreibung des KWK-Biomassekraftwerks Oberwart

Ausgangspunkt der beiden Langzeitversuche zur Wasserstoffproduktion aus Biomasse war das Biomassekraftwerk Oberwart, welches das notwendige Holzgas zur Verfügung gestellt hat. Das Kraftwerk basiert auf dem Prinzip der Biomasse Dampfvergasung (siehe Abschnitt 3.1). Das Fließbild des Kraftwerks ist in Abbildung 2 dargestellt.

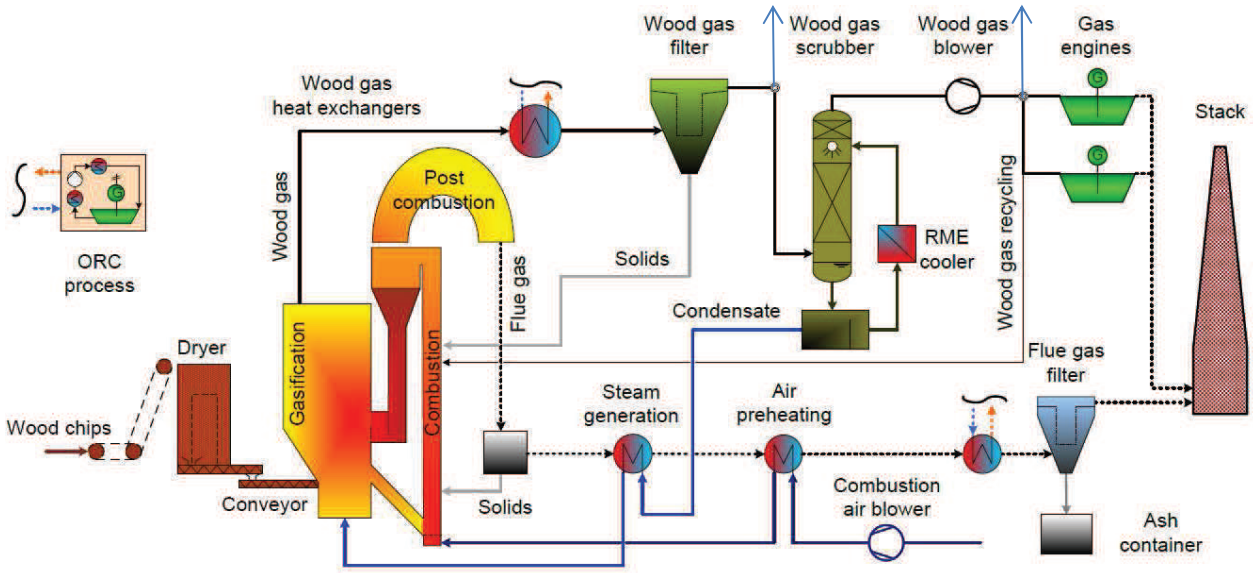

Abbildung 2: Vereinfachtes Fließschema des Biomassekraftwerks Oberwart nach dem Prinzip der Biomasse Dampfvergasung. Das Holzgas zur Erzeugung von Wasserstoff kann vor und nach dem Gaswäscher des Kraftwerks entnommen werden, siehe blaue Pfeile (Benedikt, 2014).

Die Biomasse in Form von Hackschnitzeln wird mit erwärmter Umgebungsluft getrocknet und gelangt in den Vergaser. Das entstehende Holzgas wird anschließend gekühlt und im Holzgasfilter vom Großteil der Partikel befreit. Im RME Gaswäscher wird Wasser und Teer (höhere Kohlenwasserstoffe) kondensiert. Zusätzlich wird Teer in RME gelöst und dadurch aus dem Holzgasstrom entfernt. Anschließend gelangt das Holzgas über ein Gebläse in zwei Gasmotoren, in denen Strom und Wärme produziert werden.

Das in der Verbrennungskammer entstehende Abgas wird in einer Nachbrennkammer fertig oxidiert und im Anschluss in einer Absetzkammer von Partikeln befreit. Danach wird aus dem noch heißen Abgas Wärme für den Prozess ausgekoppelt, bevor es durch den Abgasfilter geleitet wird. Schließlich gelangt es zusammen mit den Abgasen der Gasmotoren in den Kamin. Zusätzlich zur Stromerzeugung mittels Gasmotoren wird auch noch über einen ORC (Organic Rankine Cycle) Prozess Elektrizität erzeugt. Der ORC Prozess verwendet dazu einen Teil der Prozesswärme des Kraftwerks. Tabelle 2 zeigt typische Betriebsparameter des Biomassekraftwerks in Oberwart.

Tabelle 2: Auslegungs-Kennzahlen des Biomassekraftwerks Oberwart (Kraussler, 2014).

Parameter	Wert	Einheit
Brennstoffleistung	8,7	MW
Elektrische Leistung Gasmotoren	2,4	MW_{el}
Elektrische Leistung ORC	0,4	MW_{el}
Fernwärmeleistung	4,0	MW_{th}
Elektrischer Wirkungsgrad	32	%
Thermischer Wirkungsgrad	46	%
Gesamtnutzungsgrad	78	%

Für den Betrieb der beiden Prozessketten zur Wasserstoffproduktion aus Biomasse wurde Holzgas nach dem RME Gaswäscher des Kraftwerks entnommen (siehe Abbildung 2).

3.3 Beschreibung von Prozesskette 1 zur Wasserstoffproduktion aus Biomasse

In Abbildung 3 ist die Prozesskette 1 dargestellt, mit der Langzeitversuche zur Wasserstoffproduktion aus Holzgas durchgeführt wurde. Sie besteht aus dem RME Gaswäscher, der Membraneinheit, der DWA Anlage und der PEM Brennstoffzelle. Das Holzgas für diesen Langzeitversuch wurde vom Biomassekraftwerk Oberwart nach dem Kraftwerkswäscher entnommen (siehe Abbildung 2).

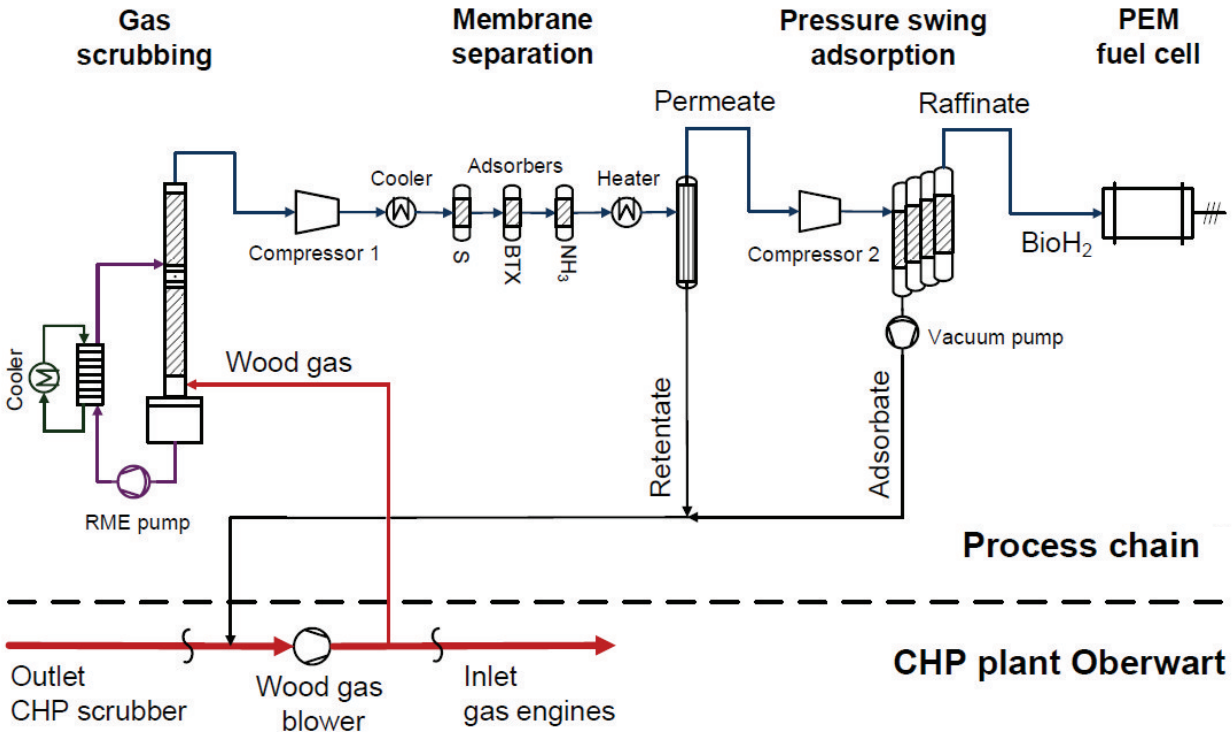

Abbildung 3: Fließbild der Prozesskette 1 zur Wasserstoffproduktion aus Biomasse. (Hinteregger, 2014).

In der ersten Stufe, dem RME Gaswäscher, wurde der Teergehalt im Holzgas weiter verringert und Kondensat abgeschieden, um das Gas anschließend verdichten zu können. Das Holzgas wurde so weit aufbereitet, dass es bedenkenlos in den nächsten Prozessschritt, die Membraneinheit (ca. 13 bar), geleitet werden konnte. Dort erhält man eine wasserstoff- und kohlendioxidreiche Fraktion, das Permeat und eine methan- und kohlenmonoxidreiche Fraktion, das Retentat. Dieses Retentat wurde zum Kraftwerk zurückgeleitet. Die wasserstoffreiche Fraktion wurde verdichtet (6,5 bar) und in der DWA Anlage aufbereitet. Dabei konnte reiner Wasserstoff aus dem Feedstrom der DWA Anlage abgetrennt werden und im Raffinat gewonnen werden. Das Adsorbat, welches die anderen Gaskomponenten enthielt, wurde wieder zum Kraftwerk geleitet. Im letzten Schritt der Prozesskette wurde mit dem erzeugten Wasserstoff die PEM Brennstoffzelle betrieben.

3.4 Beschreibung von Prozesskette 2 zur Wasserstoffproduktion aus Biomasse

In Abbildung 4 ist die Prozesskette 2 dargestellt, mit der ebenfalls ein Langzeitversuch zur Wasserstoffproduktion aus Holzgas durchgeführt wurde. Sie besteht aus der WGS Einheit, dem RME Gaswäscher, der DWA Anlage und der PEM Brennstoffzelle. Für den Langzeitversuch wurde Holzgas nach dem Kraftwerks RME Wäscher entnommen.

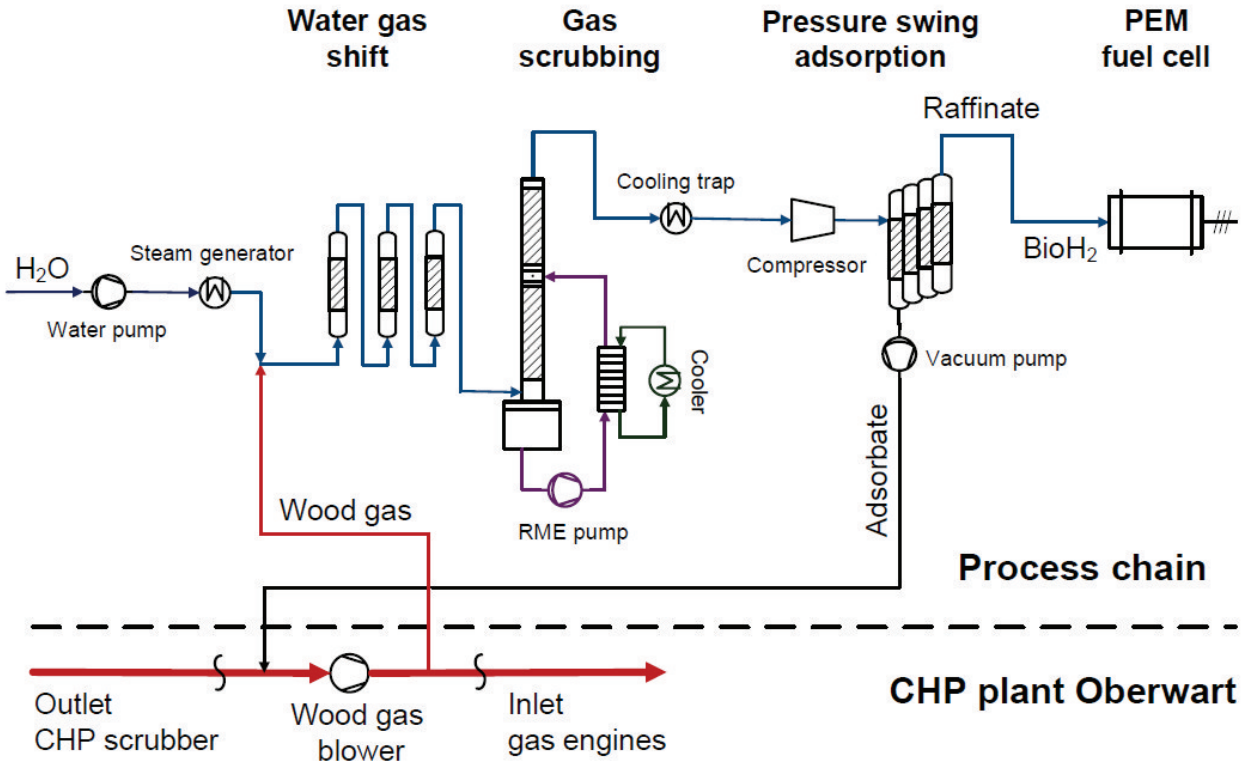

Abbildung 4: Fließbild der Prozesskette 2 zur Wasserstoffproduktion aus Biomasse. (Hinteregger, 2014).

In der WGS Einheit (atmosphärischer Druck) wurde der Wasserstoffanteil des Holzgases auf Kosten des Kohlenmonoxidanteils erhöht. Dafür ist zusätzlicher Wasserdampf notwendig. Im nächsten Schritt wurde das Gas über den RME Gaswäscher geleitet. Dort wurde Teer entfernt sowie Kondensat abgeschieden. Daraufhin wurde das Gas verdichtet (6,5 bar) und in der DWA in die Wasserstofffraktion (Raffinat) und die restlichen Gaskomponenten (Adsorbat) aufgetrennt. Das Adsorbat wurde zum Kraftwerk zurückgeschickt. Schlussendlich wurde die PEM Brennstoffzelle mit dem erzeugten hochreinen Wasserstoff betrieben.

3.5 Verwendete Analysemethoden

Ein Gaschromatograph mit Wärmeleitfähigkeitsdetektor (TCD) wurde zur Analyse der Hauptkomponenten (CO, CO_2, CH_4, N_2, O_2, C_2H_6, C_2H_4 und C_2H_2) eingesetzt. Zur Analyse der Schwefelkomponenten (H_2S, COS und C_4H_4S) wurde ein FPD (Flame Photometric Detector) verwendet.
Im Zuge der Versuchsreihen wurden auch Teerproben genommen. Der genaue Ablauf der Probennahme und der Analyse kann in (Fail S. , et al., 2014, Anhang) nachgelesen werden.
Neben Teeranalysen wurden auch NH_3 sowie Benzol, Toluol und Xylol (BTX) Analysen durchgeführt. Auch hier sei auf die weiterführende Literatur verwiesen (Diaz, 2013) und (Fail, Biohydrogen Production Based on the Catalyzed Water Gas Shift Reaction in Wood Gas, 2014)

3.6 Untersuchungen und Optimierungen bei den Einzelkomponenten

3.6.1 Membrantrennprozess

Der Membranversuchsaufbau wurde zu Beginn der Arbeit übernommen und im Zuge der durchgeführten Arbeit sukzessive den Erfordernissen der Experimente zur Wasserstoffseparation angepasst. Abbildung 5 zeigt den Membranversuchsstand inklusive des Kompressors in der zu Beginn der Arbeit übernommenen Form.

Abbildung 5: Membranversuchsstand am Standort Oberwart während des Aufbaus der Versuchskette Juli 2011 (Konlechner, Aufbereitung von Wasserstoff aus der Biomassevergasung mittels Membrantechnologie, 2015).

Im Membranversuchsstand erfolgt die Abtrennung von Wasserstoff aus dem vorbehandelten Produktgas und dessen Anreicherung im sogenannten Permeatgasstrom. Mittels Kompressor wird der Druck im zugeführten Gas erhöht um die Triebkraft für den Trennungsprozess bereitzustellen. Wasserstoff hat ein größeres Diffusionsvermögen durch das Membranmaterial als die übrigen im Produktgas enthaltenen Gaskomponenten, wodurch sich die Trenneigenschaften dieses Prozessschrittes ergeben. Im vorliegenden Fall hat der Membrantrennschritt die Aufgabe eines effektiven und wirtschaftlichen Vorreinigungsprozesses. Der Wasserstoffanteil im Gasstrom wird signifikant gesteigert und die in der Feinreinigung zu handhabenden Volumenströme können deutlich reduziert werden.

Durch die Einflussnahme auf Systemdruck, Systemtemperatur, Zuflussmenge oder die Anordnung weitere Membranmodule kann Einfluss auf die Trennleistung des Systems genommen werden.
Im Zuge der durchgeführten Arbeit wurden am Versuchsstand Hohlfaser-Polymer-Membrane der Firma Air Liquide in verschiedenen Prozessanordnungen und unter unterschiedlichen Betriebsbedingungen untersucht. Ausgehend von Wasserstoffkonzentration von 35 bis 40 vol. % im Eingangsgasstrom konnten Wasserstoffkonzentrationen von bis zu 90 vol. % im Zuge dieses Reinigungsschrittes erzielt werden.
In der nachfolgenden Abbildung 6 ist ein vereinfachtes Prozessflussdiagramm des Membranversuchsstandes dargestellt. Bei der abgebildeten zweistufigen Anordnung entsteht das finale Produktgas (Permeat) in der ersten Stufe. Das mit Wasserstoff angereicherte Gas der zweiten Stufe wird rückgeführt, wodurch eine Wasserstoffanreicherung in der ersten Stufe erzielt wird. Durch diesen Recyclingvorgang können höhere Wasserstoffreinheiten im finalen Produktgas sowie größere Ausbeuten erzielt werden.
Die Steuerung der Versuchsanlage erfolgt automatisch mittels einer eigenen, industriellen speicherprogrammierbaren Steuerung (SPS). Die aufgezeichneten Versuchsdaten werden in einem Datenbanksystem abgelegt. Die Anlage ist so ausgeführt, dass ein permanenter Betrieb auch ohne permanent anwesendes Bedienpersonal möglich ist. Dies ermöglicht einen kontinuierlichen Versuchsbetrieb auch über einen längeren Zeitraum. Eine kontinuierliche Messung und Aufzeichnung der Gaszusammensetzung mittels industrieller Gasanalytik ist ebenfalls direkt im Versuchsaufbau umgesetzt.

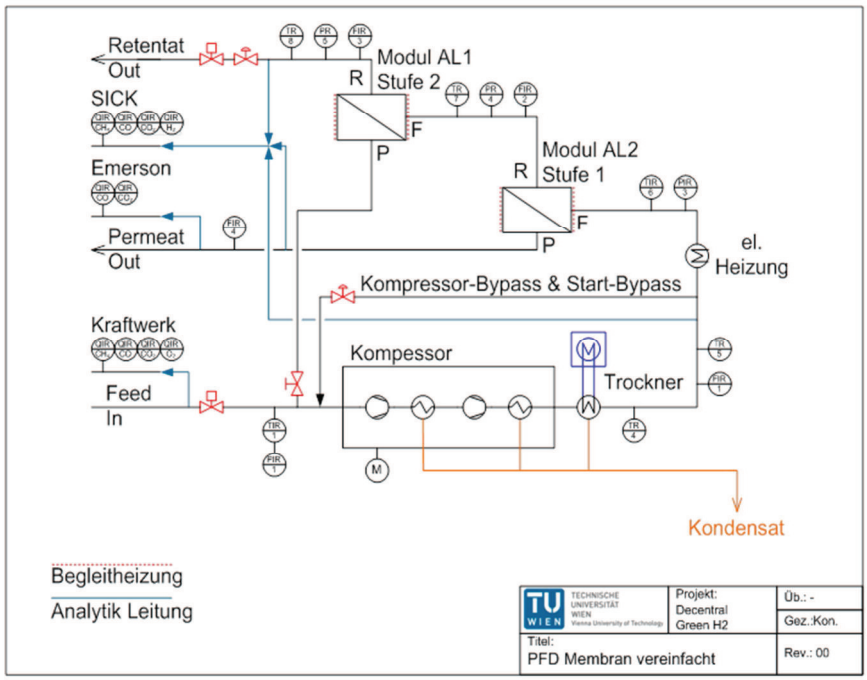

Abbildung 6: Vereinfachtes Prozessflussdiagramm zweistufiger Membranversuchsstand inklusive eingesetzter Analytik (Konlechner, Aufbereitung von Wasserstoff aus der Biomassevergasung mittels Membrantechnologie, 2015).

Als Eingangsstrom in den Membranversuchsstand dient mittels Wäscher vorbehandeltes Produktgas vom Kraftwerk oder der WGS Anlage. Das an Wasserstoff abgereicherte und unter Druck stehende Restgas wird entspannt und zurück zum Kraftwerk geführt und verwertet. Das mit Wasserstoff angereicherte Produktgas kann ebenfalls zum Kraftwerk rückgeführt werden, für den Fall, dass ausschließlich der Membranversuchsstand betrieben wird. Alternativ kann das Produktgas oder Teile davon zur Druckwechseladsorptionsanlage zur Herstellung von hochreinem Wasserstoff geschickt werden.

Im Zuge des Projekts wurden mit den beiden seitens Air Liquid bereitgestellten Membranmodulen intensive Parametervariationsversuche durchgeführt. Die beiden folgenden Diagramme (Abbildung 7 und Abbildung 8) zeigen exemplarisch die erreichten Gasqualitäten als auch die im Zuge der Variationsexperimente erzielten Wasserstoffausbeuten für einen Feedgasstrom im Bereich von 3 Nm³/h.

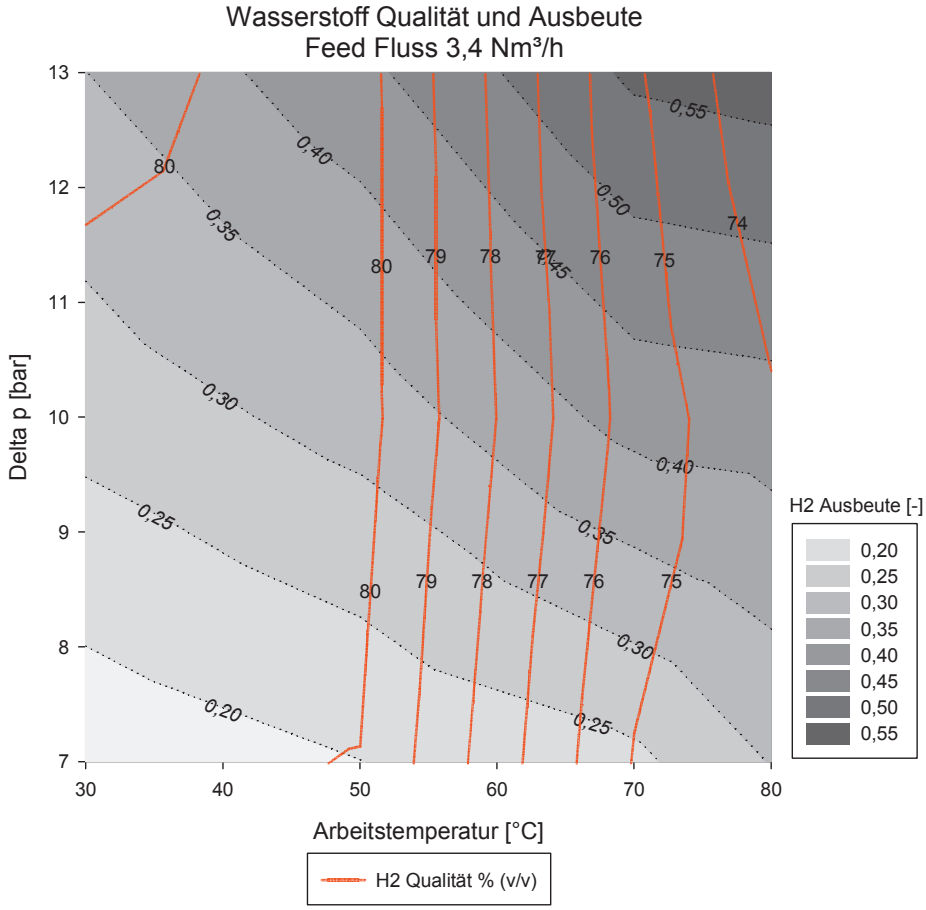

Abbildung 7: Wasserstoff Qualität und Ausbeute AL Modul A (Konlechner, Aufbereitung von Wasserstoff aus der Biomassevergasung mittels Membrantechnologie, 2015).

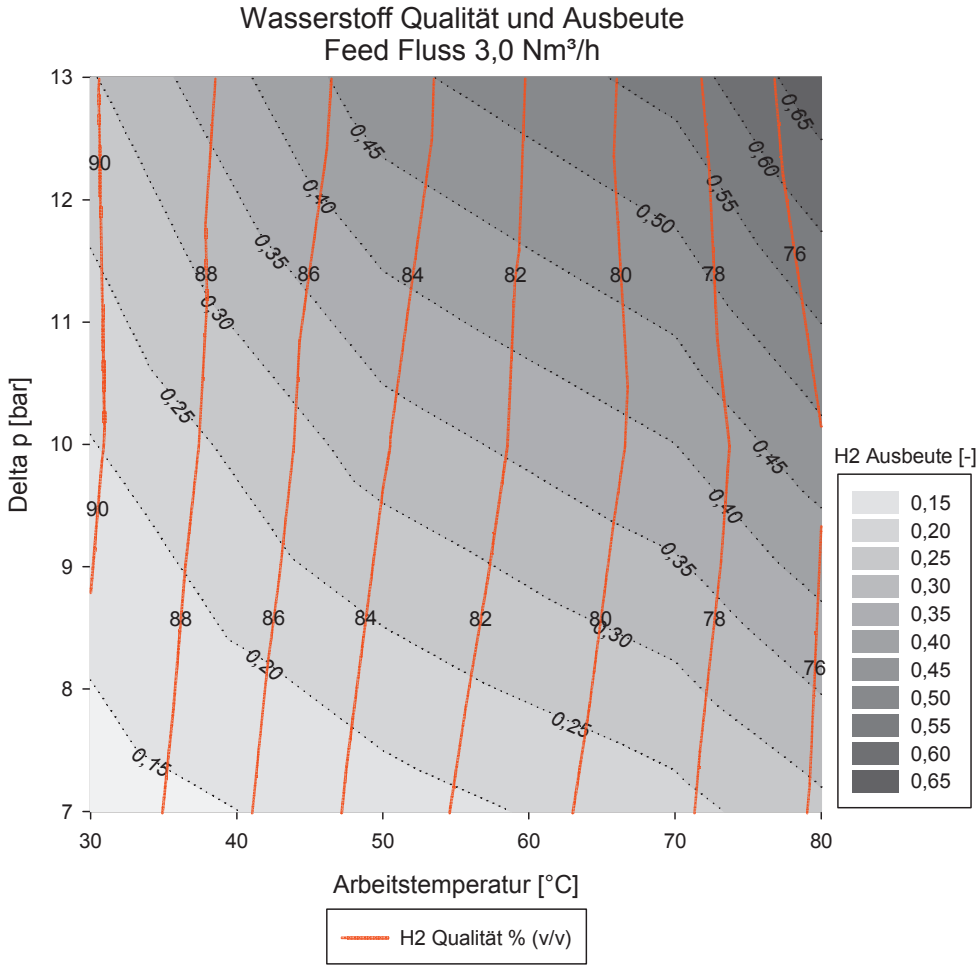

Abbildung 8: Wasserstoff Qualität und Ausbeute AL Modul B (Konlechner, Aufbereitung von Wasserstoff aus der Biomassevergasung mittels Membrantechnologie, 2015).

Es ist zu erkennen, dass mit Modul B deutlich bessere Reinheiten erzielt werden können. Mit steigender Temperatur nimmt diese Eigenschaft deutlich ab und nähert sich im Bereich von 80°C jener des Moduls A. Die gewonnenen Daten für die Aufbereitung von realem Gas können in die Auslegung zukünftiger Anlagen einfließen.

3.6.2 Druckwechseladsorption (DWA)

Es wurden umfangreiche Versuche in einer Laboranlage durchgeführt. Diese dienten in erster Linie dem Screening verschiedener Adsorbentien für die Abtrennung von Kohlenstoffmonoxid und Kohlenstoffdioxid, sowohl in Hinsicht auf deren Adsorptions- als auch Desorptionsverhalten für die genannten Komponenten. Als Adsorbens für Kohlenstoffdioxid und teilweise auch Kohlenstoffmonoxid wurden unterschiedliche Aktivkohlen getestet, für die selektive Adsorption von Kohlenstoffmonoxid erfolgte die Untersuchung verschiedener Zeolithe. Die als am geeignetsten ermittelten Adsorbentien sollen in der Prozesskette eingesetzt werden. Tabelle 3 zeigt eine Auflistung aller im Rahmen dieser Versuchsserien getesteten Adsorbentien.

Tabelle 3: Gestestete Adsorbentien

Firma	Adsorbens	Adsorbenstyp
CarboTech	CMS H2 55/2	Aktivkohle
Chemviron Carbon	AP1-60	Aktivkohle
Norit	RB2	Aktivkohle
CarboTech	Köstrolith 5AK	Zeolith
Roth	Molekularsieb 5A	Zeolith
UOP	5A HP 8x12	Zeolith

Abbildung 9 zeigt die Beladung der getesteten Aktivkohlen für die Komponenten Kohlenstoffdioxid und Kohlenstoffmonoxid in Abhängigkeit des Adsorptionsdruckes. Aus der Abbildung geht der signifikante Unterschied zwischen den Beladungskapazitäten der Aktivkohlen für Kohlenstoffdioxid und Kohlenstoffmonoxid klar hervor. Während sich die Beladungswerte für Kohlenstoffdioxid im Bereich von 6 gew. % bei einem Adsorptionsdruck von 3,1 bar g bis 9,7 gew. % bei einem Adsorptionsdruck von 5,6 bar g bewegen, sind die Beladungswerte für Kohlenstoffmonoxid um eine Größenordnung niedriger. Diese schwanken im Bereich von etwa 0,08 gew. % (Adsorptionsdruck von 3,1 bar g) bis 0,25 gew. % (Adsorptionsdruck von 5,6 bar g). Unter den getesteten Aktivkohlen weisen die Aktivkohlen Norit und CarboTech die höchsten Beladungskapazitäten für Kohlenstoffdioxid und Kohlenstoffmonoxid auf.

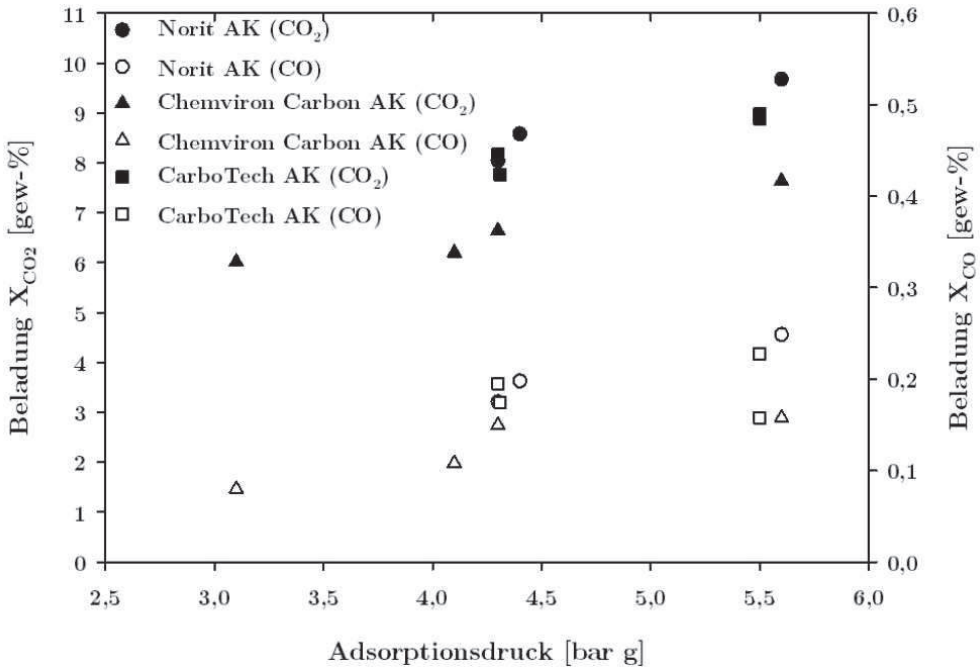

Abbildung 9: Ausgewählte Beispiele von Beladungskapazitäten der getesteten Aktivkohlen für Kohlenstoffdioxid und Kohlenstoffmonoxid in Abhängigkeit des Adsorptionsdruckes.

Weitere Ergebnisse für die Aktivkohlen und jene für die Zeolithe können (Mayer, 2012) entnommen werden.

Vollautomatische Funktion der DWA-Anlage

Des Weiteren wurde mithilfe von Versuchen die vollautomatische Funktion der DWA-Anlage getestet und die optimalen Betriebsparameter für eine möglichst gute Adsorption mit hoher Wasserstoffausbeute bestimmt. Zudem wurde mittels Gasanalyse überprüft, ob die Gaszusammensetzung nach der Druckwechseladsorptionsanlage (DWA) den Anforderungen einer Brennstoffzelle gerecht wird. Demnach setzt sich diese Arbeit zum Ziel, festzustellen, ob die DWA-Anlage für den zukünftigen vollständig automatisierten Betrieb einsatzbereit ist und in die gesamte Prozesskette eingegliedert werden kann.
In Abbildung 10 ist der Versuchsaufbau zur Druckwechseladsorption (DWA) dargestellt. Bei der DWA-Anlage selbst können die Drucksensoren, die jeweils am Kolonnendeckel montiert sind, und die sieben grünen Thermoelemente am Kolonnenmantel erkannt werden. Vor der DWA-Anlage ist der Schaltkasten mit der integrierten speicherprogrammierbaren Steuerung (SPS) befestigt und gleich daneben sind die beiden Gasanalysegeräte mit drei bzw. fünf messbaren Gaskomponenten aufgestellt. Letzteres ist für Messungen im Volumenprozentbereich mit einem Messfehler von $\pm$1% vom Messbereich geeignet, mit dem 3-Komponentenmessgerät sind CO-Messungen im vol. ppm Bereich möglich, CO_2 und O_2 wiederum in vol.%.
Zu den wesentlichen Anlagenbestandteilen gehören vier gleich aufgebaute Adsorptionskolonnen, ein Pufferbehälter für den Wasserstoff, ein Kompressor, eine Vakuumpumpe und eine Vielzahl an Proportional- und Magnetventilen zur Anlagenschaltung. Das gesamte DWA-Anlagenschema bzw. die Kenndaten der Anlage können aus dem Fließbild in Abbildung 11 entnommen werden.

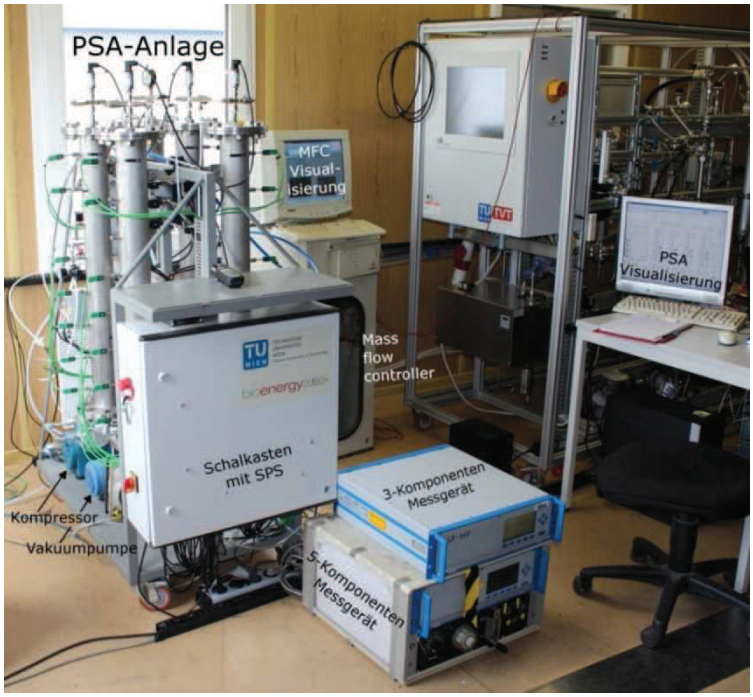

Abbildung 10: Versuchsaufbau in Forschungscontainer im BKW Oberwart.

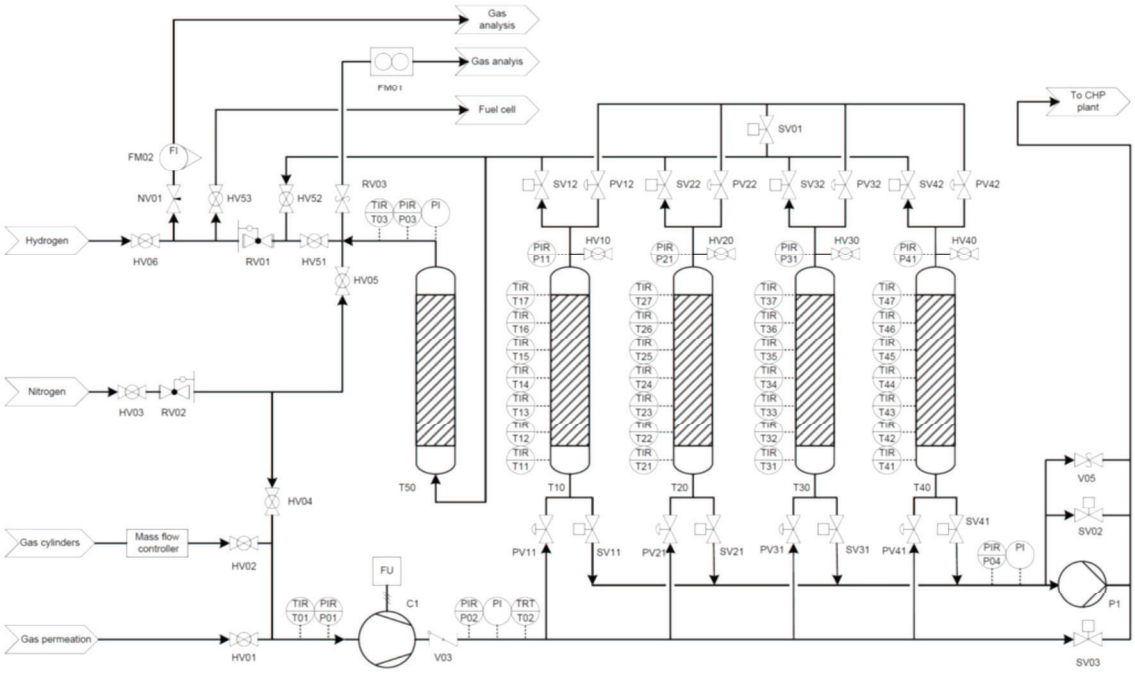

Abbildung 11: Fließbild der DWA Anlage.

Durch die tadellos arbeitende Automatisierung der Anlage konnte der Versuch in Abbildung 12 etwas über 10h gefahren werden. Es wurden insgesamt 13 komplette Durchläufe vollzogen und für die Temperatursensoren 1-3 der Kolonne 2 ist das Temperaturprofil über den gesamten Versuch dargestellt.

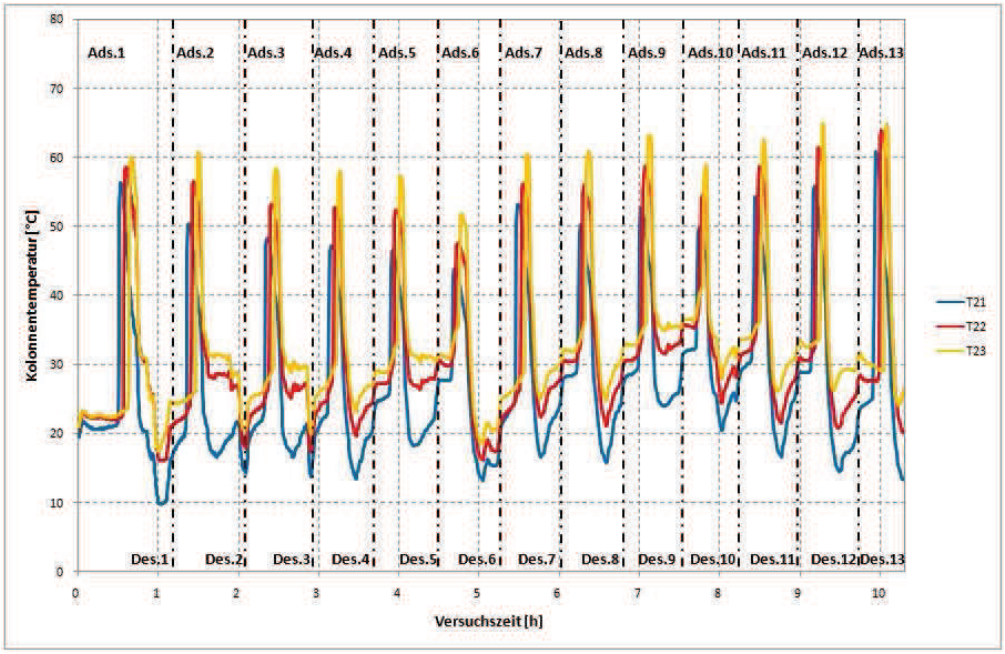

Abbildung 12: Beispiel für Adsorptions- und Desorptionszyklus in Kolonne 2 der DWA.

Mit diesen Ergebnissen konnte ein vollautomatischer Betrieb der DWA erreicht werden, die die erforderliche Qualität des Wasserstoffes für die Brennstoffzelle zu liefern vermag. Damit ist die DWA

soweit ertüchtigt und voll automatisiert (Screenshot in Abbildung 13), dass diese in die gesamte Prozesskette integriert werden kann.

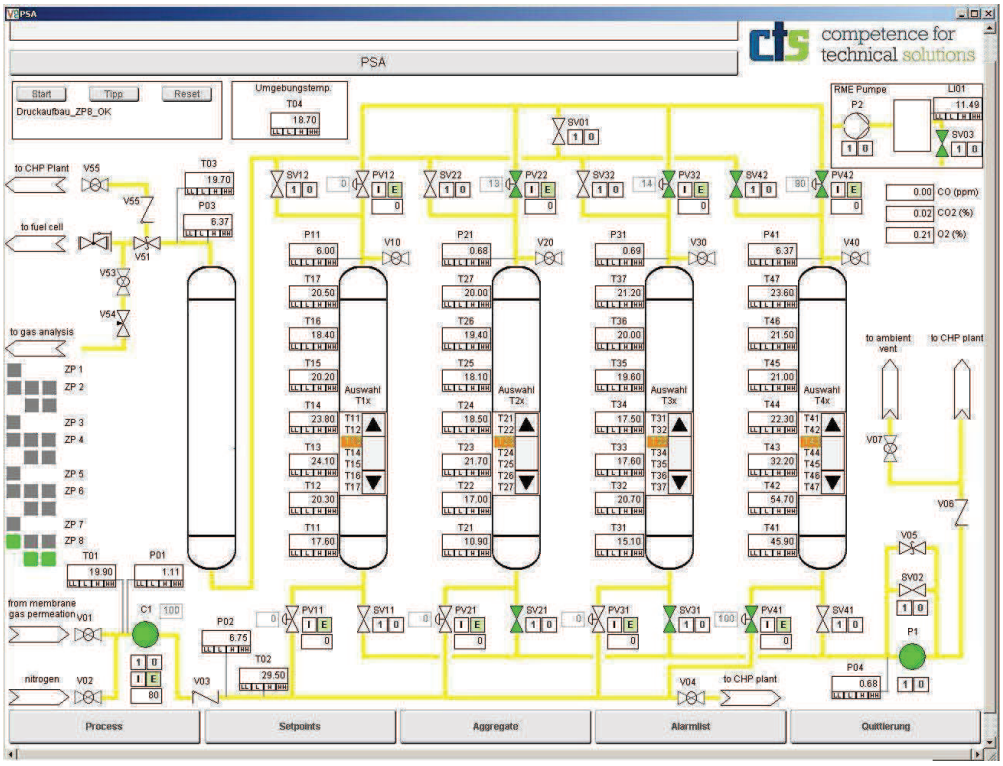

Abbildung 13: DWA Automatisierung Hauptfenster.

3.6.3 Wasser-Gas-Shift-Reaktion (WGS)

Test der WGS-Katalysatoren in der Labor-Kinetik-Apparatur

In einer Labor-Kinetik-Apparatur wurde die WGS-Reaktion mit 2 kommerziell erhältlichen Katalysatoren untersucht. Deren Eigenschaften werden in Tabelle 4 zusammengefasst.

Tabelle 4: Eigenschaften der getesteten WGS-Katalysatoren.

	Zusammensetzung	Aktive Spezies	Trägermaterial	Form
Kat 1	CoO/MoO_3	MoS_2	Al_2O_3	Pellets (⌀ = 3 mm; Länge = 3-10mm
Kat 2	Fe_2O_3/Cr_2O_3	Fe_3O_4	Al_2O_3	Pellets (⌀ = 6 mm; Länge = 3 mm

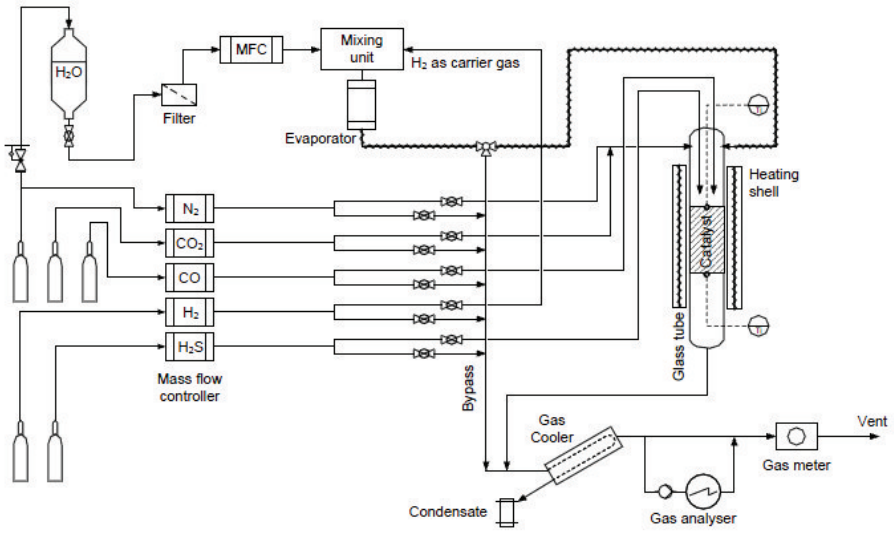

Abbildung 14: Fließbild der Kintetik-Labor-Apparatur (Fail S.,2014).

Abbildung 14 zeigt den Aufbau der Kinetik-Versuche mit den beiden Katalysatoren. Zu deren Untersuchung wurden der Produktgas-Zusammensetzungen ähnliche Gasmischungen mit Hilfe von MFCs über einen Glasreaktor mit einer Festbettschüttung des jeweiligen Katalysators geführt. Zusätzlich wurden für die WGS Reaktion geeignete, eingestellte Dampfmengen zugemischt und Temperaturen eingestellt. Die Ein- und Ausgangsströme wurden dabei chemisch durch ein on-line Analysegerät und einen Balgengaszähler erfasst. Eine Variation des H_2S-Anteils im simulierten Produktgas wurde vorgenommen.

Der Katalysator 1 auf Co/Mo-Basis wurde für saure Shift-Anwendungen entwickelt und ist daher für Gasmischungen geeignet, in denen ein hoher Anteil an H_2S enthalten ist. Seine Aktivität stieg auch wie zu erwarten mit höheren Anteilen an H_2S im Feedgas.

Der Katalysator 2 auf Fe/Cr-Basis ist ein sogenannter Hochtemperatur-WGS-Katalysator, der für gewöhnlich in Kombination mit einem Niedertemperatur-WGS-Katalysator eingesetzt wird. Die Aktivität von Katalysator 2 wurde von höheren H_2S Konzentrationen reversibel herabgesetzt. Dieser mindernde Effekt trat jedoch bei höheren Temperaturen über 320°C in schwächerem Maße auf.

Für beide Katalysatoren wurden Kinetik-Gesetze modelliert. Zusammenfassend war durch die relativ niedrige Konzentration an H_2S im Produktgas die Aktivität des Fe/Cr Katalysators höher und die Effekte einer Katalysatorvergiftung werden bei entsprechend hohen Temperaturen vernachlässigbar. Genauere Ergebnisse dazu können in (Fail S., 2014) gefunden werden.

Die 3 Reaktoren der WGS-Pilotanlage wurden mit Katalysator 1 für 1500 h und mit Katalysator 2 für 800 h betrieben. Für die Kopplungsversuche mit den anderen Prozesseinheiten wurde der Katalysator 2 auf Fe/Cr-Basis eingesetzt.

Optimale Temperatur der WGS-Reaktion

Bei zu niedrigeren Temperaturen ist die Konversion von CO durch die Kinetik der WGS-Reaktion limitiert. Bei zu hohen Temperaturen strebt die WGS-Gleichgewichtsreaktion in Richtung der Edukte. Daher ist es wichtig eine optimale Temperatur zu finden, bei der unter gegebenen Bedingungen die Reaktion mit einer möglichst hohen CO-Konversion abläuft. Einen weiteren wichtiger Faktor für die Wahl der Betriebstemperatur stellt die Abhängigkeit der Langzeit-Stabilität des Katalysators von dieser dar. Für die Pilotanlage, von der eine Fotografie in Abbildung 15 gezeigt wird, wurde eine maximale Gas-Eingangstemperatur in den ersten (linken) Reaktor von 400°C festgelegt.

Abbildung 15: Fotografie des Versuchaufbaus der dreistufigen WGS-Anlage im BKW Oberwart (Fail S.,2014).

In Abbildung 16 wird das Hauptfenster der WGS-Automatisierung gezeigt, mit welcher man diverse Temperaturen und Drücke steuern bzw. messen kann. Zusätzlich kann die Dampfmenge, welche über einen Verdampfer zum Produktgasstrom zugemischt wird eingestellt werden. Die Produktgaszusammensetzung wurde vor und nach jedem Reaktor mit denen in Abschnitt 3.5 beschriebenen Analysemethoden bestimmt.

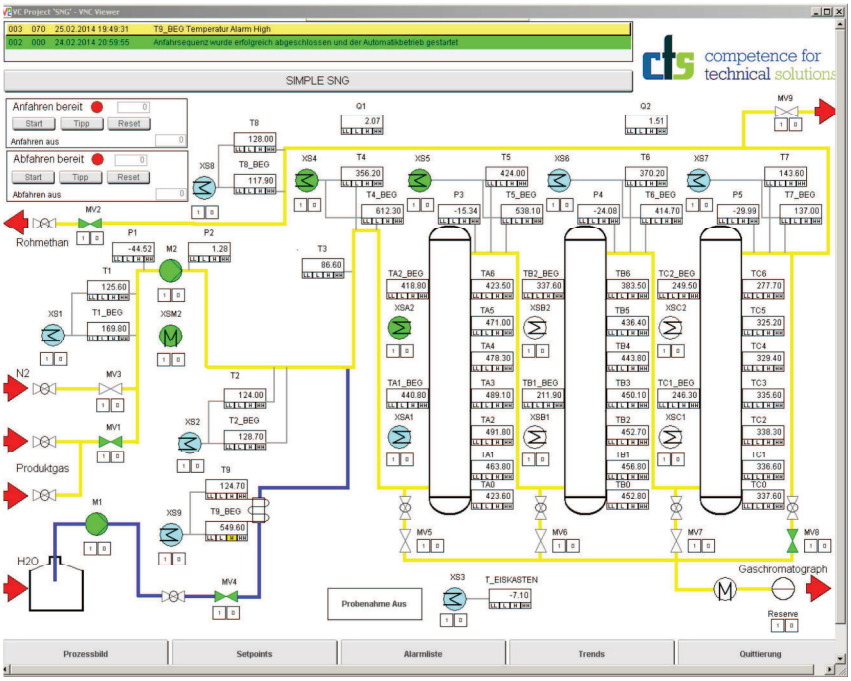

Abbildung 16: WGS-Automatisierung Hauptfenster (Fail S.,2014)

3.6.4 Brennstoffzelle (PEM)

Axane, eine Tochterfirme der Air Liquide hat eine PEM (Polymer Elektrolyt Membran) Brennstoffzelle für den Betrieb mit Wasserstoff aus Biomasse zur Verfügung gestellt. Die Betriebsparameter der Brennstoffzelle können über LabVIEW aufgezeichnet werden. Tabelle 5 zeigt das Datenblatt der PEM Brennstoffzelle.

Tabelle 5: Datenblatt der PEM Brennstoffzelle.

Parameter	Unit	Value
Nominal voltage DC	V	48
Nominal voltage AC	V	230
Minimum power	W	500
Maximum power	W	2500
H_2 quality (ISO 14687)	vol.%	99.99
H_2 operating pressure	mbarg	250 ± 30
H_2 consumption at max power	$NL \cdot min^{-1}$	35.1
H_2 flushing peak flow rate	$NL \cdot min^{-1}$	60

Als Last für die Brennstoffzelle wurde eine simple Kochplatte verwendet. Damit konnten verschiedene Leistungsaufnahmen eingestellt werden. Die PEM Brennstoffzelle mit der Kochplatte ist in Abbildung 17 dargestellt.

Abbildung 17: PEM Brennstoffzelle und Kochplatte.

Für den Betrieb mit Wasserstoff aus Biomasse wurde die Brennstoffzelle zuerst mit Wasserstoff aus Gasflaschen hochgefahren. Nach einer Einlaufphase wurde fließend auf Wasserstoff aus Biomasse umgeschaltet.

3.7 IPSEpro Simulationen

Die beiden Prozessketten mit denen Langzeitversuche durchgeführt wurden, wurden mittels des Prozesssimulationprogrammes IPSEpro simuliert. Es wurden Kennzahlen für die Wasserstoffausbeute sowie den spezifischen Energieverbrauch ermittelt. Dabei wurde zwischen Strom-, Wärme- und Kühlenergie unterschieden.

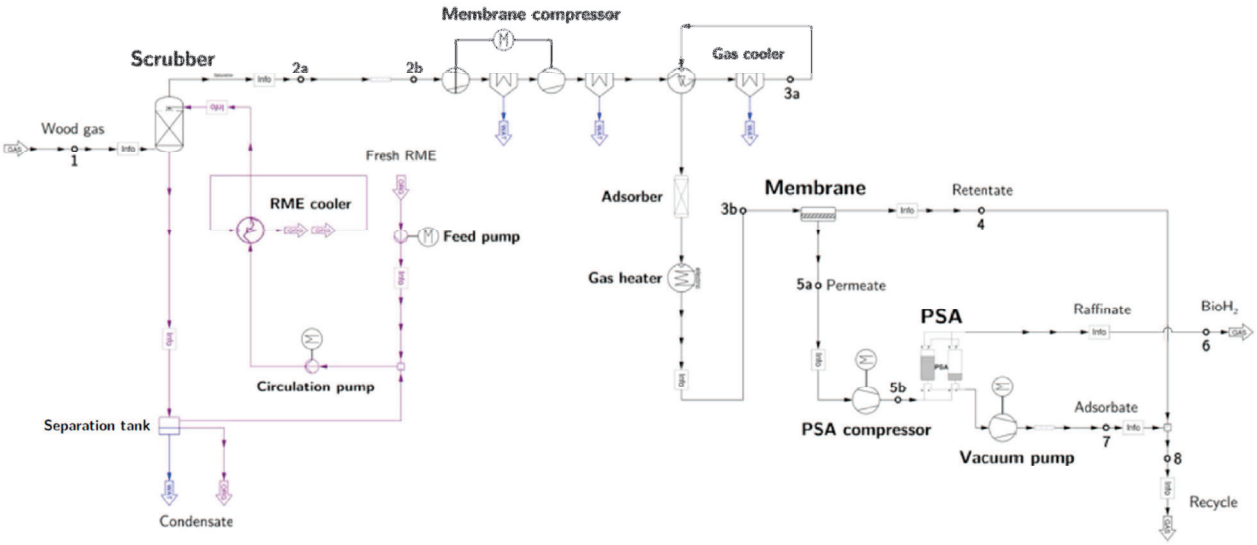

Abbildung 18: Fließbild der IPSEpro Simulation der Prozesskette 1 zur Wasserstofferzeugung aus Biomasse in Oberwart (Hinteregger, 2014).

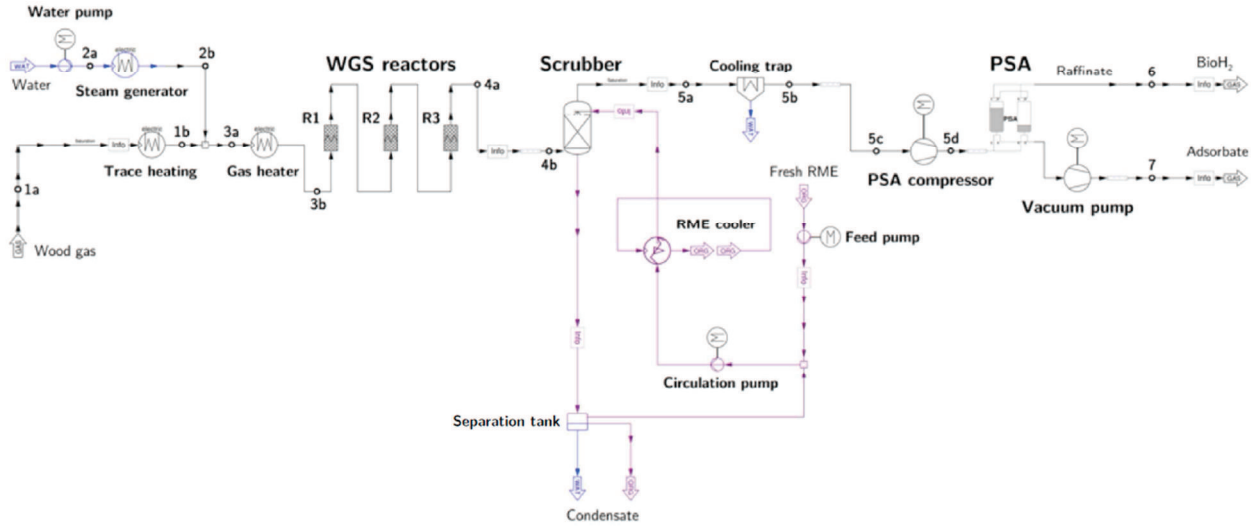

Abbildung 19: Fließbild der IPSEpro Simulation der Prozesskette 2 zur Wasserstofferzeugung aus Biomasse in Oberwart (Hinteregger, 2014).

In Abbildung 18 und Abbildung 19 sind die beiden Fließbilder der IPSEpro Simulation der Prozessketten zur Wasserstoffherstellung dargestellt.

Die Simulation wurde mittels Versuchsdaten aus den Langzeitversuchen mit den beiden Prozessketten durchgeführt. In weiterer Folge wurde aus den Ergebnissen der Simulationen der Prozessketten ein Konzept für den Scale-Up der Versuchsanlage erstellt

3.8 Ergebnisse und Diskussion

In diesem Abschnitt werden die Ergebnisse der Langzeitversuche mit den beiden Prozessketten, der Simulationen und des Konzepts für den Scale-Up dargestellt.

3.8.1 Ergebnisse des Langzeitversuchs mit Prozesskette 1 zur Wasserstofferzeugung aus Biomasse

Eine genaue Zusammenstellung der Ergebnisse zu den Langzeitversuchen mit Prozesskette 1 können in (Diaz, 2013) und (Konlechner, Harasek, Hackel, Sanders, & Bosch, 2015, Anhang) nachgelesen werden.

Abbildung 20: Fotografie der ersten Prozesskette zur Wasserstoffherstellung in Oberwart. Von links nach rechts: PEM Brennstoffzelle, DWA, Membraneinheit mit Kompressor. Der RME Wäscher befindet sich im Stahlbau im Kraftwerk (Diaz, 2013).

Abbildung 20 zeigt eine Fotografie der Konfiguration der Prozesskette 1, wie sie im Forschungscontainer am Standort des Biomassekraftwerks in Oberwart aufgebaut wurde. Sie besteht aus dem RME Gaswäscher im Stahlbau des Kraftwerks, der Membraneinheit, der DWA zur Endreinigung des Holzgases und der PEM Brennstoffzelle.

Tabelle 6: Betriebsbedingungen der einzelnen Stufen der Prozesskette 1 (Diaz, 2013).

Parameter	Value	Units	Comment
Scrubber fresh RME inlet	2.9	L/h	-
Scrubber PG outlet temperature	10 ± 5	°C	Day/night oscillations
Membrane module	M3	-	-
Membrane feed flow rate	3.0	Nm^3/h	Operation at 50 % of compressor power
Membrane pressure	13	bara	-
Membrane temperature	68	°C	Average retentate outlet temperature
Membrane adsorbers	-	-	Adsorbent material from 4th long-term test
Membrane permeate, PSA feed flow rate	0.70	Nm^3/h	-
PSA adsorption pressure	6.50	bara	-
PSA desorption pressure	0.05	bara	-
PSA equalization pressure	4.00	bara	Reduced to 4.00 to increase H_2 recovery
PSA adsorbent	AC1	-	Activated carbon
Adsorption time	380	s	-
Adsorption purge/feed time ratio	0.005	s/s	-

In Tabelle 6 sind die Betriebsbedingungen der einzelnen Prozessschritte aufgeführt. Die Parameter wurden während des 500 h Langzeitversuchs angepasst, um anschließend einen 120 h langen Betrieb der Brennstoffzelle mit Wasserstoff aus Biomasse zu ermöglichen. Während der gesamten Versuchsdauer wurde die Prozesskette zuverlässig mit Holzgas aus dem Biomassekraft Oberwart versorgt. Die Holzgaszusammensetzung des Kraftwerks ist in Abbildung 21 dargestellt.

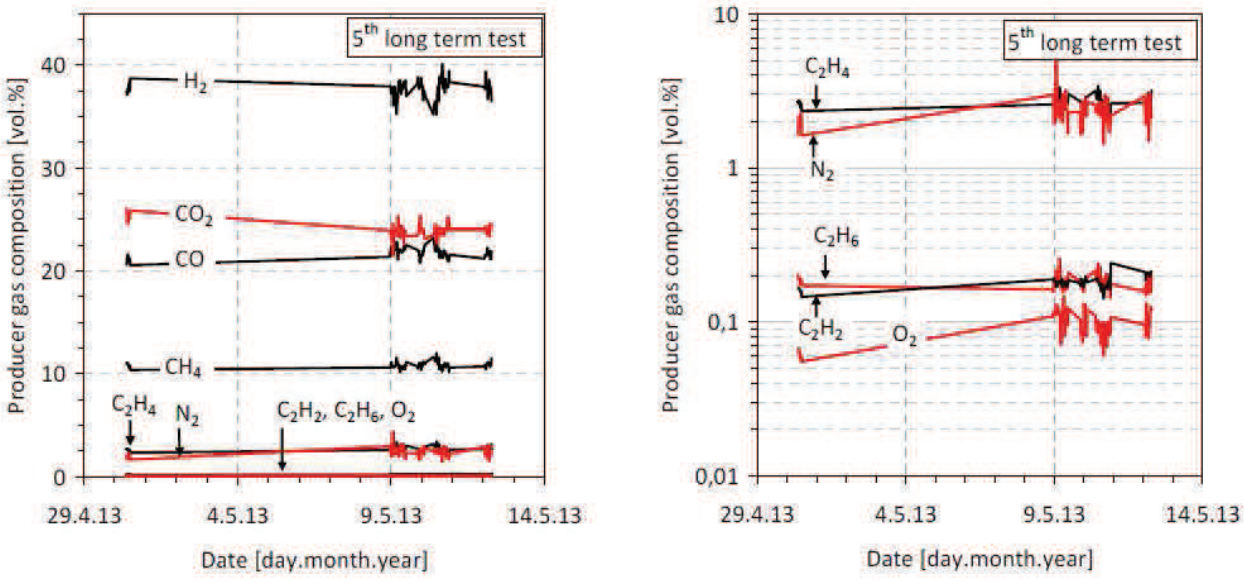

Abbildung 21: Zusammensetzung des Holzgases, welches für den 500h Langzeitversuch für die Prozesskette 1 als Eingangsgasstrom zur Wasserstofferzeugung verwendet wurde (Diaz, 2013).

Das dem Kraftwerk entnommene Holzgas wurde der Prozesskette kontinuierlich zugeführt. Nach der Teerreduzierung und Kondensatabscheidung im RME Gaswäscher wurde das Gas zur Membrananlage und in weiterer Folge zur DWA geleitet.

Tabelle 7: Gaszusammensetzung der Membran Unit und DWA während des Langzeitversuchs mit der Prozesskette 1 (Diaz, 2013).

		Feed	Retentate	Permeate	Adsorbate*	Raffinate
H_2	vol.%	37,4 ± 1	24,2 ± 0,8	72,7 ± 0,9	34,446	99,9517
CO_2	vol.%	22,0 ± 0,6	22,2 ± 0,7	21,7 ± 0,7	52,069	< 0,0005
C_2H_4	vol.%	2,7 ± 0,3	3,5 ± 0,3	0,26 ± 0,03	0,623	< 0,0005
C_2H_6	vol.%	0,19 ± 0,02	0,24 ± 0,02	0,004 ± 0,005	0,009	< 0,0005
C_2H_2	vol.%	0,17 ± 0,01	0,22 ± 0,02	0,08 ± 0,04	0,191	< 0,0005
O_2	vol.%	0,09 ± 0,02	0,17 ± 0,03	0,05 ± 0	0,095	0,0175
N_2	vol.%	2,4 ± 0,5	3,2 ± 0,6	0,29 ± 0,05	0,653	0,0308
CH_4	vol.%	10,8 ± 0,3	14,4 ± 0,4	0,86 ± 0,08	2,063	< 0,0005
CO	vol.%	24,2 ± 0,8	31,8 ± 1	4,1 ± 0,3	9,837	< 0,0005
H_2S	vol.ppm	90,4 ± 10	91,4 ± 10	53,7 ± 8	0,013	< 0,2
COS	vol.ppm	1,7 ± 0,5	2,3 ± 0,6	0,35 ± 0,04	0,000	< 0,2
C_4H_4S	vol.ppm	1,8 ± 0,9	2,8 ± 0,5	0,31 ± 0,5	0,000	< 0,2

Die Gaszusammensetzung entlang der Prozesskette 1 während des Langzeitversuchs ist in Tabelle 7 dargestellt. Man sieht, dass eine Wasserstoffreinheit von > 99,95 vol. % erreicht wurde.

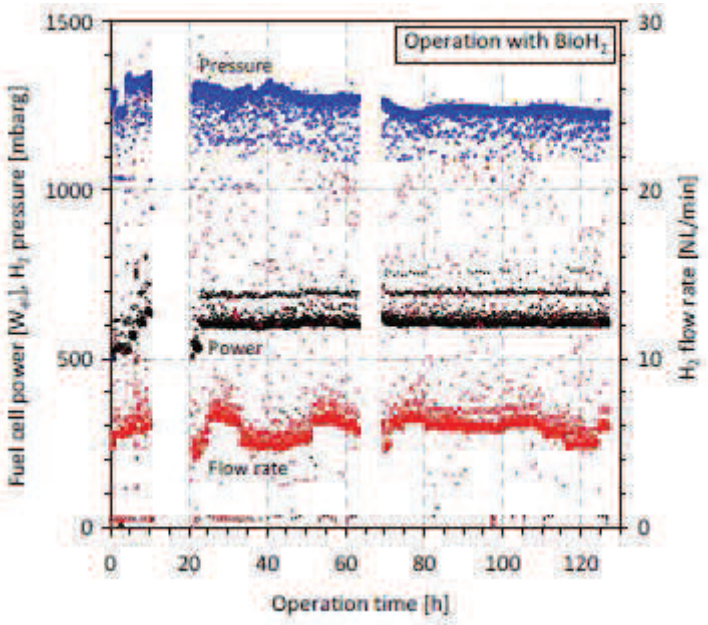

Abbildung 22: Betrieb der PEM Brennstoffzelle mit Wasserstoff aus Biomasse während des Langzeitversuchs mit Prozesskette 1 (Diaz, 2013).

In Abbildung 22 sind der in die PEM Brennstoffzelle eintretende Wasserstoffstrom, sowie dessen Partialdruck und die dabei erzeugte elektrische Leistung dargestellt. Die Prozesskette 1 ermöglichte den problemlosen Betrieb der PEM Brennstoffzelle über 120 h.

3.8.2 Ergebnisse des Langzeitversuchs mit Prozesskette 2 zur Wasserstofferzeugung aus Biomasse

Für den Langzeitversuch mit der Prozesskette 2, der über einen Zeitraum von ca. 250h durchgeführt wurde, wurde folgende Konfiguration gewählt. Sie bestand aus der WGS Unit, dem RME Gaswäscher und der DWA Anlage. Die Betriebsbedingungen der einzelnen Prozessschritte sieht man in Tabelle 8 bis Tabelle 10.

Tabelle 8: Betriebspunkt der dreistufigen WGS Einheit während des Langzeitversuchs mit Prozesskette 2 (Fail S. , et al., 2014).

	value	unit
wood gas in	0.56 ± 0.02	$(m^3_{n\,db})/h$
water addition	0.55 ± 0.02	(kg)/h
T_{in} reactor 1	403 ± 5	°C
T_{in} reactor 2	358 ± 3	°C
T_{in} reactor 3	309 ± 3	°C
pressure	76 ± 7	mbarg
$GHSV_{wet}$	510 ± 5	h^{-1}
$(H_2O)/(CO)$ molar ratio	5 ± 0.2	–
$(H_2O)/C$ molar ratio	2 ± 0.1	–

Tabelle 9: Betriebspunkt des RME Gaswäschers während des Langzeitversuchs mit Prozesskette 2 (Fail S. , et al., 2014).

	solvent	value	unit
T_{in} gas	RME	48.3 ± 2.4	°C
T_{out} gas	RME	5.1 ± 0.2	°C
pressure	RME	58.5 ± 5.8	mbarg
circulation rate	RME	700	L/h
fresh addition	RME	0.5	L/h
T_{out} gas	glycol	0	°C

Tabelle 10: Betriebspunkt der DWA Anlage während des Langzeitversuchs mit Prozesskette 2 (Fail S. , et al., 2014).

	value	unit
adsorption pressure	6.5	bara
desorption pressure	0.1	bara
purge/feed time ratio	5×10^{-3}	–
feed flow rate	0.7 ± 0.04	$(m^3_{n\,db})/h$
feed pressure	1000 ± 17	mbara
adsorption time per column	650	s
equalization pressure	4.5	bara

Auch bei diesem Versuch wurde eine Wasserstoffreinheit erreicht, die für den Betrieb der PEM Brennstoffzelle geeignet war (> 99,97 vol.%).

Abbildung 23 zeigt die Konfiguration der Prozesskette mit den dazugehörigen Messpunkten, an denen die Gaszusammensetzung gemessen wurde. Die Gaszusammensetzung an den einzelnen Messpunkten entlang der Prozesskette ist in Tabelle 11 dargestellt.

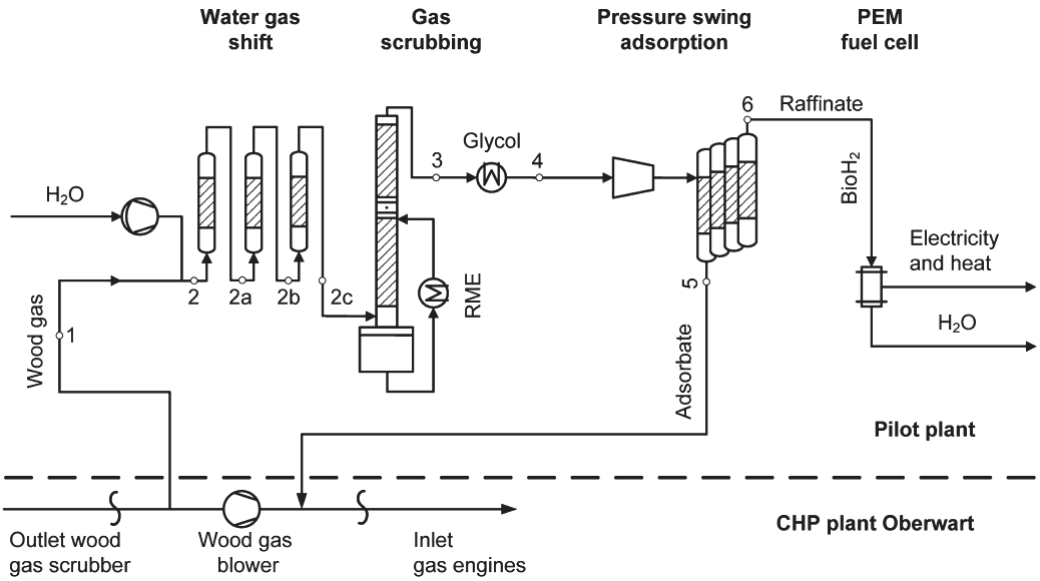

Abbildung 23: Messpunkte für die Gaszusammensetzung entlang der Prozesskette 2 zur Wasserstofferzeugung aus Holzgas (Fail S. , et al., 2014).

Tabelle 11: Gaszusammensetzungen während des Langzeitversuchs mit Prozesskette 2 zur Wasserstofferzeugung aus Holzgas (Fail S. , et al., 2014).

S.pt.	CO_2 (vol $\%_{db}$)	C_2H_4 (vol $\%_{db}$)	C_2H_6 (vol $\%_{db}$)
1	22.7 ± 0.8	2.3 ± 0.3	0.17 ± 0.03
2a	36.9 ± 0.8	1.8 ± 0.1	0.17 ± 0.02
2b	37.0 ± 0.8	1.8 ± 0.1	0.17 ± 0.03
2c	37.1 ± 0.9	1.9 ± 0.2	0.18 ± 0.02
4	36.9 ± 0.2	1.6 ± 0.3	0.14 ± 0.03
5	61.4	2.6	0.23
6	BDL	BDL	BDL
S.pt.	C_2H_2 (vol $\%_{db}$)	O_2 (vol $\%_{db}$)	N_2 (vol $\%_{db}$)
1	0.15 ± 0.02	0.1 ± 0.02	2.3 ± 0.4
2a	0.001 ± 0.001	0.06 ± 0.01	1.8 ± 0.1
2b	BDL	0.08 ± 0.04	2 ± 0.1
2c	BDL	0.07 ± 0.06	1.9 ± 0.3
4	BDL	0.03 ± 0.01	1.5 ± 0.1
5	BDL	0.03	2.6
6	BDL	0.02 ± 0.0003	0.01 ± 0.004
S.pt.	CH_4 (vol $\%_{db}$)	CO (vol $\%_{db}$)	H_2 (vol $\%_{db}$)
1	10.0 ± 0.3	24 ± 1	38.0 ± 1.2
2a	8.2 ± 0.1	1.9 ± 0.3	49.2 ± 0.9
2b	8.1 ± 0.2	1.3 ± 0.2	49.5 ± 0.9
2c	8.2 ± 0.2	1.0 ± 0.1	49.6 ± 0.9
4	8.0 ± 0.2	0.98 ± 0.04	50.9 ± 0.4
5	13.3	1.63	18.2
6	BDL	BDL	99.97 ± 0.004

Auch diese Prozesskonfiguration ermöglichte den Betrieb der PEM Brennstoffzelle, da der erzeugte Wasserstoff über eine ausreichende Reinheit verfügt. Aufgrund des zu kleinen Wasserstoff-volumenstroms, der vom DWA Kompressor vorgegeben wurde, konnte die Brennstoffzelle nur ca. 3h betrieben werden. Danach war der Inhalt des Wasserstoff Pufferspeichers aufgebraucht. Abgesehen davon gibt es keinen Grund, warum die PEM Brennstoffzelle nicht länger mit dem erzeugten Bio-Wasserstoff betrieben hätte werden können. Abbildung 24 zeigt den Betrieb der PEM Brennstoffzelle während des zweiten Langzeitversuchs.

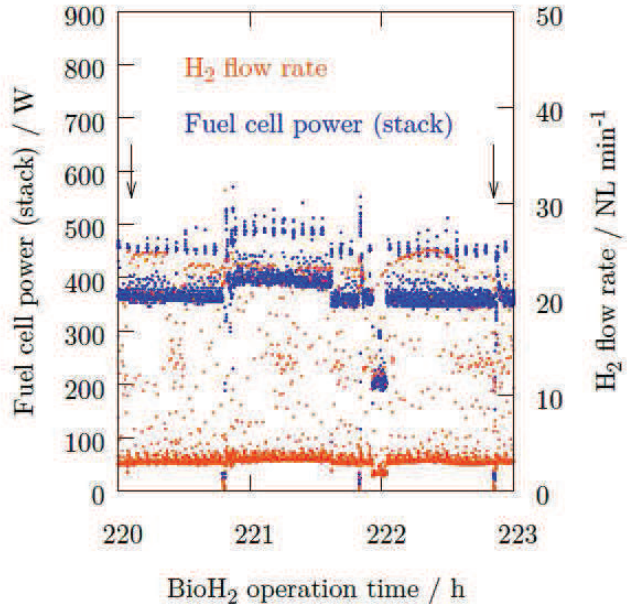

Abbildung 24: Betriebsparameter der PEM Brennstoffzelle während des Langzeitversuchs mit Prozesskette 2 (Kraussler, 2014).

3.8.3 Ergebnisse der IPSEpro Simulationen von Prozesskette 1 und Prozesskette 2

Tabelle 12 zeigt die Simulationsergebnisse der von Prozesskette 1 und 2. Es muss an dieser Stelle erwähnt werden, dass es sich bei diesen Anlagen um Versuchsanlagen handelt. Das wiederrum bedeutet, dass noch Optimierungsbedarf hinsichtlich des Energieverbrauchs der gesamten Prozesskette besteht.

Tabelle 12: Ergebnisse der IPSEpro Simulation der beiden Prozessketten zur Wasserstoffproduktion aus Biomasse (Hinteregger, 2014). SEC=Specific Energy Consumption, SHP=Specific Hydrogen Production

Parameter	Wert		Einheit
	Prozesskette 1 (SCR-MEM-DWA)	Prozesskette 2 (WGS-SCR-DWA)	
H_2 Recovery	39	129	%
LHV Efficiency	12,32	42,18	%
SHP	13,46	45,95	$g_{H2}/kg_{Hackschnitzel}$
SEC Wärme	0,15	2,13	$kWh_{Wärme}/Nm^3_{H2}$
SEC Kühlung	0,57	1,71	$kWh_{Kühlung}/Nm^3_{H2}$
SEC elektrisch	1,12	0,58	kWh_{el}/Nm^3_{H2}

Man sieht, dass die Wasserstoff Ausbeute des im Holzgas enthaltenen Wasserstoffs von Prozesskette 2 etwa drei Mal höher ist, als die von Prozesskette 1. Dies liegt an der WGS Unit, die den Großteil des im Holzgas vorhandenen Kohlenmonoxids mit Wasserdampf in Wasserstoff und Kohlendioxid umwandelt. Daher ist auch die Wasserstoffausbeute bezogen auf die Menge der eingesetzten Biomasse im Fall von Prozesskette 2 höher als bei Prozesskette 1.
Der Wärmebedarf von Prozesskette 1 ist geringer als von Prozesskette 2. Dies ist hauptsächlich der notwendigen Wasserverdampfung der WGS Einheit von Prozesskette 2 geschuldet. Durch die exotherme Reaktion in der WGS Einheit erhöht sich auch der anschließende Kühlbedarf von Prozesskette 2 gegenüber Prozesskette 1.
Der elektrische Energieverbrauch von Prozesskette 2 ist niedriger als der von Prozesskette 1. Dies hat den Grund, dass in Prozesskette 1 zwei Verdichtungsschritte notwendig sind, um Wasserstoff in ausreichender Qualität für die Brennstoffzelle zu erzeugen, jedoch in der Prozesskette 2 das Holzgas nur für die DWA Anlage komprimiert werden muss. Der reine Wasserstoff steht bei beiden Prozessketten mit einem Druck von ca. 6 Bar zur Verfügung.

3.8.4 Konzept eines Scale-Up für eine Anlage zur Wasserstofferzeugung in Oberwart

Basierend auf den Ergebnissen aus 3.8.1 bis 3.8.3 wurde eine Evaluierung eines Scale-ups einer Prozesskette von einer Versuchsanlage zu einer Demonstrationsanlage zur Produktion von Wasserstoff durchgeführt. Der Vergleich der Kennwerte der beiden Prozessketten im Versuchsanlagen-Stadium lässt die Prozesskette 2 lediglich in Hinsicht auf spezifischen Wärme- und Kühlbedarf schlechter abschneiden. Sowohl Wärme- als auch Kühlbedarf können bei geeigneter Integration ins Kraftwerk, durch Abwärmenutzung innerhalb der Prozesskette und durch Scale-Effekte verringert werden. Deswegen wurde die Prozesskette 2 ausgewählt, um diese mit Hilfe der Simulations-Software IPSEpro zur Produktion von 50 Nm³/h Wasserstoff als Demonstrationsanlage auszulegen.

Basis für die Berechnungen waren dabei die experimentellen Ergebnisse der Langzeitversuche. Für die Planung der 50 Nm^3/h Wasserstoffanlage wurde der experimentelle Aufbau dabei in folgenden Punkten modifiziert:

- Das aus dem Kraftwerk entnommene Holzgas wurde vor dem Kraftwerks-Wäscher entnommen. Damit ergeben sich 2 wesentliche Vorteile:

  - Das Gas enthält beim Eintritt in den WGS-Reaktor einen bereits höheren Wassergehalt und somit muss weniger Dampf zusätzlich zugeführt werden, um ein benötigtes Dampf/Trockengas-Verhältnis zu erreichen.
  - Im Gesamtweg von der Biomasse zur Erzeugung von Wasserstoff wird das Gas nur einer Wäsche unterzogen, und ein unnötiges Aufwärmen und Abkühlen des Gases wird vermieden.
- Die WGS-Reaktionswärme wurde zur Überhitzung des in den WGS-Reaktor zugeführten Dampfes benutzt. Der Dampf wurde dabei aus einem überschüssigen Dampfstrom des Kraftwerks entnommen.
- Der aus dem WGS-Reaktor austretende Gasstrom, der aufgrund der exothermen Reaktion aufgeheizt wurde, wurde verwendet, um das in den WGS-Reaktor eintretende Gas aufzuheizen.
- Die Frisch-RME-Menge und RME-Umwälzmenge im Pilotwäscher wurden aufgrund von Erfahrungen angepasst. Die Temperatur des Gasaustritts aus dem Wäscher wurde angehoben, da der DWA-Kompressor bei der Auslegung der Demonstrationsanlage über einen Kondensatabscheider verfügt.
- Der Druck in der DWA wurde aufgrund der geänderten Größenverhältnisse auf 15 bara gesteigert und die Vakuumpumpe entfällt.

Tabelle 13 fasst die wesentlichen Kennwerte der Units bei der Auslegung der Prozesskette auf einen Wasserstoff-output von 50 Nm³/h zusammen.

Tabelle 13: Parameter der Prozess-Units der Demonstrationsanlage.

Parameter	Wert	Einheit
WGS		
Eingang-Gasvolumenstrom	164,4	Nm³/h
Dampf-Massenstrom	36,8	kg/h
Dampf-Parameter	101;1,05	°C;bara
Temperatur Eingang	350	°C
Temperatur Ausgang	300	°C
SCR		
Verhältnis RME/Gas	30	kg_{RME}/kg_{Gas}
Frisch RME-Massenstrom	5	kg/h
Temperatur Gasaustritt	20	°C
Teer Abscheidegrad	97	%
DWA		
H_2-Recovery	80	%
Druck Kompressor-Austritt	15	bara
H_2-Reinheit Raffinat	99,97	$vol.\%_{db.}$
H_2-Raffinatstrom	50	Nm³/h

Aufgrund dieser Auslegung können Energie und Massenbilanzen für die Demonstrationsanlage berechnet werden. Abbildung 25 stellt die Volumenströme der ein- und ausgehenden Gase in die Prozesskette dar. Dabei ist ersichtlich, dass unter den getroffenen Annahmen der Eingangsstrom von 164,4 Nm³/h (139,5 kg/h) feuchtem Holzgas im Zuge der modifizierten Prozesskette 2 in 75,9 Nm³/h (105,2 kg/h) Adsorbat und 50 Nm³/h (4,5 kg/h) hochreinen Wasserstoff aufgetrennt werden können.

Zusätzlich werden aus dem Kraftwerk 36,8 kg/h Wasserdampf entnommen und 57,4 kg/h Kondensat wieder zurückgeleitet und ein RME-Strom von 5 kg/h im Pilot-Gaswäscher eingesetzt bzw. eine Emulsionsphase von 14,1 kg/h zur Brennkammer als Hilfsbrennstoff zurückgeleitet. Zusätzlich werden in Abbildung 25 die Gasvolumenströme des Holzgases an den jeweiligen Entnahme- und Rückgabepunkten eines Betriebs des Kraftwerks Oberwart im Oktober 2013 abgebildet.

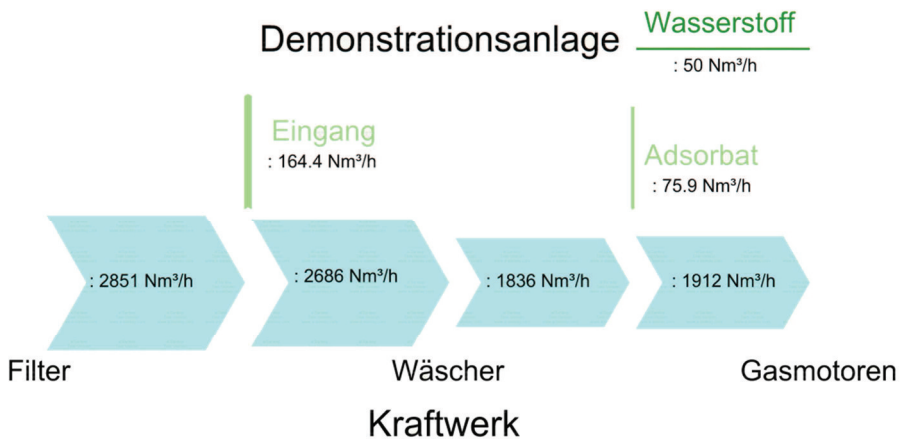

Abbildung 25: Volumenströme der Prozesskette 1 bei Integration in das Kraftwerk Oberwart mit 50 Nm³/h Wasserstoff-Output.

Die bei der Integration der Demonstrationsanlage in das Kraftwerk anfallenden Energieverbräuche werden in Tabelle 14 gelistet. Im rechten Teil werden die sich daraus ergebenden spezifischen Energieverbräuche angeführt.

Tabelle 14: Energieverbrauch der Prozesskette als Demonstrationsanlage.

Bezeichnung	Wert	Einheit	SEC	Wert	Einheit
WGS Gasheizung	6,3	$kW_{Wärme}$	Wärme	0.08	$kWh_{Wärme}/Nm^3_{H2}$
RME Kühlung	54,7	$kW_{Kühlung}$	Kühlung	1.09	$kWh_{Kühlung}/Nm^3_{H2}$
RME Umwälzpumpe	0,4	kW_{el}	elektrisch	0.48	kWh_{el}/Nm^3_{H2}
DWA Kompressor	23,7	kW_{el}			

Mit Hilfe der Kennwerte aus der Tabelle 12 und der Tabelle 14 ist ein Vergleich des Energieverbrauchs der Prozesskette 2 zwischen der Ausführung als Versuchsanlage und als Demonstrationsanlage möglich. Dabei ist erkennbar, dass die getroffenen Maßnahmen zur Reduzierung des Energieverbrauchs und Scale-Effekte die Energieverbräuche extrem reduzieren können. Der spezifische Wärmebedarf wird im Vergleich auf weniger als 4 % gesenkt, die spezifische Kühlenergie um mehr als die Hälfte reduziert und der spezifische Stromverbrauch auf rund 83 % gesenkt.

3.8.5 Weiterführende Untersuchungen an fortschrittlichen Membranprozessen

2-Stufige Membran Verschaltung

Des Weiteren erfolgte auch wie in Abbildung 6 bereits dargestellt eine zweistufige Verschaltung der beiden Membranmodule die zum Ziel hatte Wasserstoffqualität und Ausbeute weiter zu steigern. Die im Zuge der Versuche erhaltenen Ergebnisse sind in Abbildung 26 und Abbildung 27 zusammengefasst. Es ist zu erkennen sowohl Ausbeute als auch Reinheit gesteigert werden konnte und dass generell ein höheres Druckniveau zu besseren Separationsergebnissen führt.

Wasserstoff Konzentration [% (v/v)]

Arbeits Temperatur [°C]		Druckniveau 7 bar(g) Kompressorleistung		Druckniveau 10 bar(g) Kompressorleistung		Druckniveau 13 bar(g) Kompressorleistung	
AL B Stage1	AL A Stage 2	55%	100%	55%	100%	55%	100%
30	30	89,1	89,6	90,7	90,8	91,1	91,6
30	50	86,7	85,8	87,2	87,7	88,4	89,4
30	70			92,2	92,5	92,5	93,8
50	30			86,3	87,9	86,8	88,7
50	50	84,7	85,7	86,6	86,8	86,9	88,4
50	70		87,1		88,7	88,2	90,4
70	30			83,3	83,8	83,5	84,2
70	50	82,2		83,8	83,8	81,8	84,8
70	70				85,6	82,4	86,4

Abbildung 26: Erzielte Wasserstoffkonzentrationen in Abhängigkeit der Betriebsbedingungen während des zweistufigen Versuchsbetriebs (Konlechner, Aufbereitung von Wasserstoff aus der Biomassevergasung mittels Membrantechnologie, 2015).

Wasserstoff Ausbeute [-]

Arbeits Temperatur [°C]		Druckniveau 7 bar(g) Kompressorleistung		Druckniveau 10 bar(g) Kompressorleistung		Druckniveau 13 bar(g) Kompressorleistung	
AL B Stage1	AL A Stage 2	55%	100%	55%	100%	55%	100%
30	30	0,21	0,10	0,31	0,15	0,44	0,21
30	50	0,20	0,11	0,33	0,15	0,51	0,26
30	70			0,36	0,15	0,49	0,22
50	30			0,43	0,22	0,56	0,29
50	50	0,29	0,13	0,46	0,22	0,58	0,33
50	70		0,15		0,24	0,65	0,35
70	30			0,47	0,25	0,62	0,37
70	50	0,32		0,52	0,27	0,66	0,38
70	70				0,28	0,73	0,42

Abbildung 27: Erzielte Wasserstoff Ausbeuten in Abhängigkeit der Betriebsbedingungen während des zweistufigen Versuchsbetriebs (Konlechner, Aufbereitung von Wasserstoff aus der Biomassevergasung mittels Membrantechnologie, 2015).

Revers Selektive Membran

Unter Reversselektiven Membranen versteht man Membranen, bei welchen die zu separierenden Gase als Permeat anfallen und der Wasserstoff auf der Hochdruckseite zurückbleibt. Der wesentliche Vorteil besteht darin das unter anderem schlecht von Wasserstoff zu separierendes Kohlendioxid abgetrennt werden kann. In der durchgeführten Arbeit wurde eine intensive Literaturrecherche zu diesem Thema durchgeführt. Als vielversprechendster Werkstoff stellte sich dabei ein mit Aminogruppen dotiertes Polyvinylalkohol heraus. In Zusammenarbeit mit dem Institut für organische Chemie der technischen Universität wurde aus Basisliteraturdaten ein erstes Flachmodul hergestellt und vermessen (siehe Abbildung 28). Mit diesen Prototypen konnten in der zur Verfügung stehenden Zeit noch keine reproduzierbaren Ergebnisse erzielt werden. Aufbauend auf den gewonnen Ergebnissen ergeben sich jedoch interessante und vielversprechende Möglichkeiten für weitere Arbeiten.

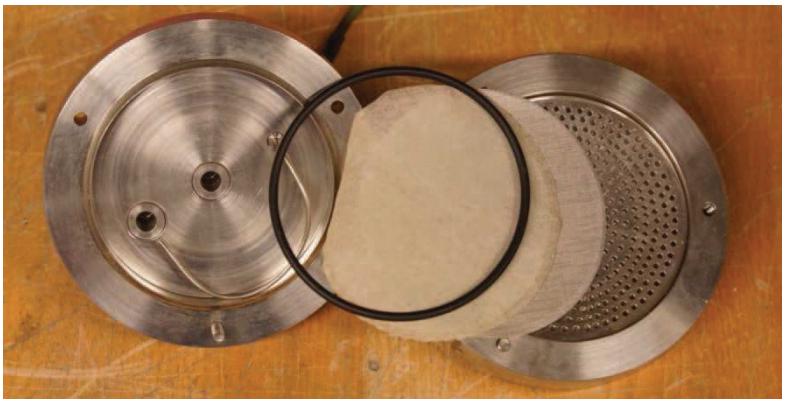

Abbildung 28: H_2 Revers Selektive Membran.

4 Ausblick und Empfehlungen

Während der Langzeitversuche für beide Prozessketten konnte gezeigt werden, dass es möglich ist hochreinen Wasserstoff aus Biomasse zu erzeugen. Dabei spielt das Verfahren der Biomasse Dampfvergasung eine große Rolle. Dieses ermöglicht die Produktion von Holzgas mit hohem Wasserstoffanteil. Für die weitere Aufbereitung und Abtrennung des Wasserstoffs bieten sich verschiedene Prozessschritte an. Bei diesen Versuchen wurden eine WGS Einheit, eine Membraneinheit, ein RME Gaswäscher und eine DWA verwendet. Die beiden Prozessketten konnten jeweils Wasserstoff mit einer Reinheit von > 99,95 vol. % bereitstellen, der den Anforderungen einer PEM Brennstoffzelle genügt hat.

Die Simulationsergbnisse der beiden Prozessketten zeigen, dass die beiden untersuchten Prozessketten Vor- und Nachteile im Hinblick auf den Energieverbrauch aufweisen. Unterschiede gibt es hinsichtlich Wärme-, Kühl-, und Elektrizitätsbedarf. In diesem Zusammenhang und mit dem Hintergrund eines möglichen Scale-Ups muss bei einem solchen Prozess die Integration in den gesamten Kraftwerksprozess berücksichtigt werden.

Das Ziel der nächsten Stufe eines solchen Projektes sollte in jedem Fall den Scale-Up einer der untersuchten Prozessketten beinhalten. Die Größenordnung der produzierten Menge Wasserstoff beim Scale-Up sollte mindestens dem Bedarf einer Wasserstofftankstelle entsprechen. Dies würde eine wirksame Möglichkeit darstellen, um zu zeigen, dass Wasserstoff, produziert aus Biomasse, durchaus eine technische Alternative zur Herstellung aus fossilen Energieträgern sein kann. Ein Alternative wäre die Einspeisung des Wasserstoffes in das in Oberwart vorhandene Erdgasnetz bis zu einem zugelassenen Wert von 4 %.

5 Literaturverzeichnis

Benedikt, F. (2014). *Experimental Evaluation of a Process Chain to Produce Hydrogen from Wood Gas.* Master's thesis, Vienna University of Technology.

Bergamo, I. (2013). *Hydrogen separation and electricity production from biomass steam gasification product gas.* Master's thesis, Vienna University of Technology.

Diaz, N. (2013). *Hydrogen Separation from Producer Gas Generated by Biomass Steam Gasification.* Ph.D. Dissertation, Vienna University of Technology.

Fail, S. et al. (2013). *An experimental approach for the production of pure hydrogen based on wood gasification*. Proceedings ICPS13, Sept. 2013.

Fail, S. (2014). *Biohydrogen Production Based on the Catalyzed Water Gas Shift Reaction in Wood Gas.* Ph.D. Dissertation, Vienna University of Technology.

Fail, S., Diaz, N., Benedikt, F., Kraussler, M., Hinteregger, J., Bosch, K., et al. (2014). Wood Gas *Processing To Generate Pure Hydrogen Suitable for PEM Fuel Cells*. ACS Sustainable Chemistry & Engineering, 2(12), 2690-2698.

Graf, S. (2012). *Experimentelle Optimierung einer Druckwechseladsorptionsanalge zur Wasserstofferzeugung aus Biomasse.* Master's thesis, Vienna University of Technology.

Hinteregger, J. (2014). *Performance Evaluation of Process Chain for the Production of BioH_2 from Wood Gas.* Master's thesis, Vienna University of Technology.

Konlechner, D. (2015). *Aufbereitung von Wasserstoff aus der Biomassevergasung mittels Membrantechnologie.* Ph.D. Dissertation, Vienna University of Technology.

Konlechner, D., Harasek, M., Hackel, M., Sanders, E., Bosch, K. (2015). *Long-term experiment for the separation of green hydrogen from biomass gasification by a polymer membrane.* Filtech 2015.

Kraussler, M. (2014). *PEM Fuel Cell Operation and Applications Using BioH_2* Master's thesis, Vienna University of Technology.

Mayer, T.Makaruk A. Diaz, N., Bosch, K. Miltner, M., Harasek, M. Hofbauer, H. *Efficient Biomass Utilization by Polygeneration Processes- Production of Hydrogen, Electricity and Heat.* Proceedings ICPS10, Sept. 2010.

Mayer, T. (2012). *Über die Aufbereitung biogener Gasen mittels Adsorption.* PhD Dissertation, Vienna University of Technology.

6 Anhang

Im Anhang dieser Arbeit sind die während der Projektarbeit entstandenen Publikationen beigefügt.

Kontaktdaten

ProjektleiterIn:
Univ.Prof. Dipl.-Ing. Dr.techn. Hermann Hofbauer

Institut/Unternehmen:
Technische Universität Wien
Institut für Verfahrenstechnik, Umwelttechnik und technische Biowissenschaften

Kontaktadresse:
Getreidemarkt 9/166
1060 Wien
Tel. +43 (1) 58801-16601
E-mail: hermann.hofbauer@tuwien.ac.at

ACS Sustainable Chemistry & Engineering

Research Article

pubs.acs.org/journal/ascecg

Wood Gas Processing To Generate Pure Hydrogen Suitable for PEM Fuel Cells

Silvester Fail,*[,†] Nicolas Diaz,*[,†,‡] Florian Benedikt,[†] Michael Kraussler,[†] Julian Hinteregger,[†] Klaus Bosch,[§] Marius Hackel,[∥] Reinhard Rauch,[†,‡] and Hermann Hofbauer[†,‡]

[†]Vienna University of Technology, Institute of Chemical Engineering, Getreidemarkt 9/166, Vienna 1060, Austria

[‡]Bioenergy 2020+ GmbH, Inffeldgasse 21b, Graz 8010, Austria

[§]Energie Burgenland AG, Kasernenstrasse 9, Eisenstadt 7000, Austria

[∥]Frankfurt Research and Technology Center (FRTC), Air Liquide, Forschung und Entwicklung GmbH, Gwinnerstrasse 27−33 , Frankfurt 60388, Germany

Supporting Information

ABSTRACT: A test campaign was carried out to generate renewable hydrogen based on wood gas derived from the commercial biomass steam gasification plant in Oberwart, Austria. The implemented process consisted of four operation units: (I) catalyzed water−gas shift (WGS) reaction, (II) gas drying and cleaning in a wet scrubber, (III) hydrogen purification by pressure swing adsorption, and (IV) use of the generated biohydrogen ($BioH_2$) in a proton exchange membrane (PEM) fuel cell. For almost 250 h, a reliable and continuous operation was achieved. A total of 560 ($L_{n\ dry\ basis\ (db)}$)/h of wood gas were extracted to produce 280 ($L_{n\ db}$)/h of $BioH_2$ with a purity of 99.97 vol $\%_{db}$. The catalyzed WGS reaction enabled a hydrogen recovery of 128% $(\dot{n}_{BioH_2})/(\dot{n}_{H_2,wood\ gas})$ over the whole process chain. An extensive chemical analysis of the main gas components and trace components (sulfur, C_xH_y, and ammonia) was carried out. No PEM fuel cell poisons were measured in the generated $BioH_2$. The only detectable impurities in the product were 0.02 vol $\%_{db}$ of O_2 and 0.01 vol $\%_{db}$ of N_2.

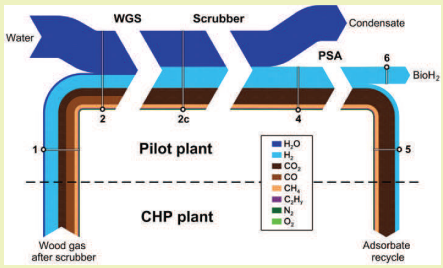

KEYWORDS: *Biohydrogen, Biomass, Gasification, Product gas, Water−gas shift, Gas scrubbing, Pressure swing adsorption, Latex*

INTRODUCTION

Hydrogen is required chiefly for the synthesis of ammonia and methanol as well as for various applications in refineries. In 2007, the world's installed capacity of production was about 65 million tons of hydrogen.[1] Its demand is growing especially because of the usage of heavier and dirtier feedstock in refineries that requires greater amounts of hydrogen for hydrotreating and hydrocracking.[2] Some authors consider a global hydrogen economy as the future perspective to cover the demands for electricity, heat, and transportation.[3,4] This would require a further increase in the production capacity. A total of 96% of the current hydrogen production is directly based on fossil fuels, mainly natural gas (49%).[1]

Considerable research has been carried out in the field of renewable hydrogen production. It can be distinguished between thermochemical, electrochemical, and biological approaches.[5] Especially, the increasing number of power-to-gas concepts, which use the excess electricity from wind power and photovoltaics for the hydrogen production in electrolyzers, should be pointed out.[6] This article deals with hydrogen production via the thermochemical processing of biomass, which is reported to be more costly than the conventional production methods but competitive with the electrolysis of water using renewable electricity.[7,8] Life cycle assessment of gasification-derived biohydrogen shows reduced greenhouse gas emissions compared to steam reforming of natural gas and a low nonrenewable energy demand.[9,10]

The established process chain for biohydrogen ($BioH_2$, here defined as hydrogen generated by or out of biomass) production was operated with a partial flow of wood gas (also product gas, producer gas, syngas, or synthesis gas) derived from the commercial biomass gasification plant in Oberwart, Austria. A total of 8.7 MW of wood chip power (23,000 (t_{wood})/a) is converted to 2.5 MW of electrical power and 3.5 MW of district heat.[11] The flowchart of the gasification power plant Oberwart is illustrated in Figure 1.

The design of this combined heat and power (CHP) plant is based on the well-documented plant in Güssing, Austria.[13] Both plants employ the dual fluidized bed (DFB) steam gasification technology. Wood gas is generated, cooled, filtered, cleaned, and finally burned in gas engines to generate electricity and district heat. Unlike the plant in Güssing, a biomass dryer and an organic rankine cycle (ORC) are employed in the CHP plant Oberwart.[14] The investigated pilot plant for hydrogen production was operated with a partial flow of wood gas extracted after its gas cleaning units. Therefore, particles were

Received: July 9, 2014
Revised: September 11, 2014

dx.doi.org/10.1021/sc500436m | ACS Sustainable Chem. Eng. XXXX, XXX, XXX−XXX

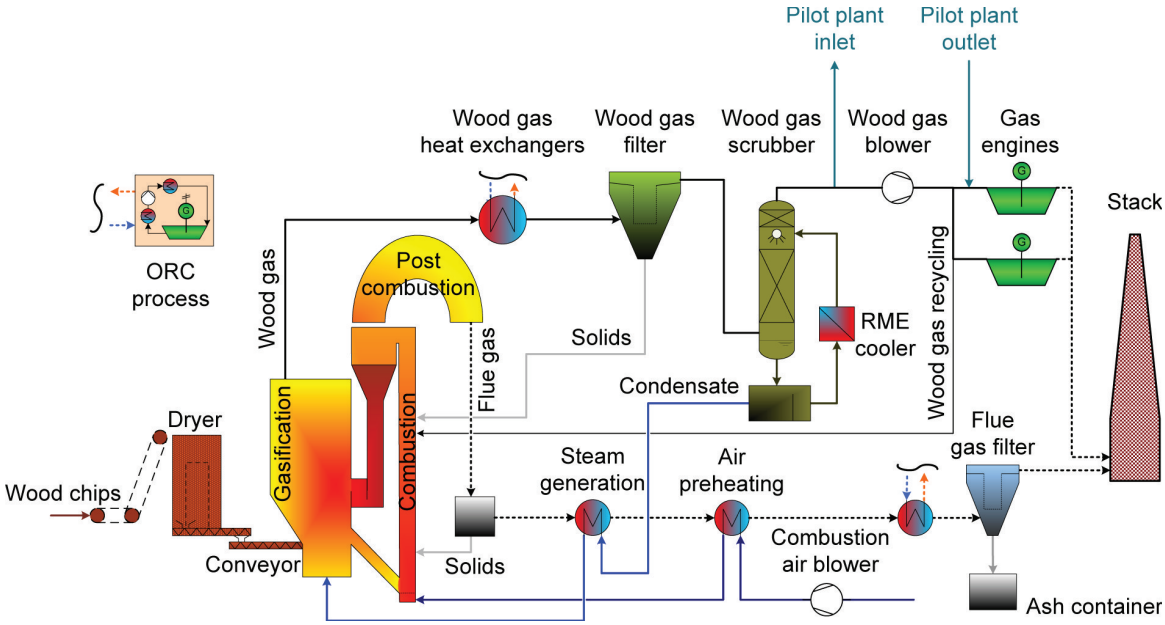

Figure 1. Flowchart of the biomass gasification plant Oberwart including the sampling point of wood gas of the investigated pilot plant. Reprinted with permission from ref 12. Copyright (2013) Nicolas Diaz.

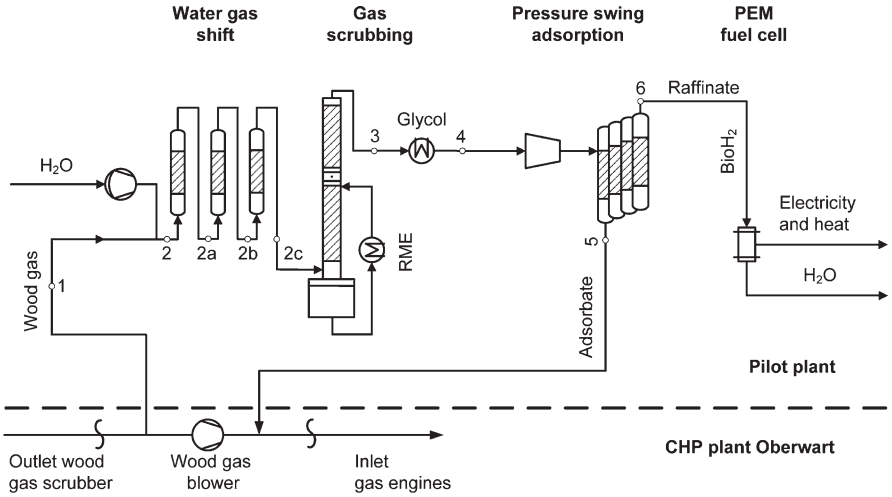

Figure 2. Flowchart of the investigated pilot plant for BioH$_2$ production, including the applied sampling points (1–6) for chemical analysis.

already removed in a baghouse filter, and the majority of the tar was already separated in a gas scrubber operated with rapeseed oil methyl ester (RME). The wood gas extraction point and the point of recycling are plotted in Figure 1 (pilot plant inlet and outlet).

The applied unit operations for wood gas conditioning involved: (I) carbon monoxide conversion via sulfur tolerant catalysis of the water–gas shift (WGS) reaction, (II) gas cleaning in a wet scrubber operated with RME, (III) pressure swing adsorption (PSA) for hydrogen purification, and (IV) application of BioH$_2$ in a proton exchange membrane (PEM) fuel cell.

(I) Catalysis of the WGS reaction (eq 1) is a state of the art technology. A two-stage system with different catalysts is industrially applied in order to produce additional hydrogen by the conversion of carbon monoxide with steam.[15]

$$CO + H_2O \rightleftharpoons H_2 + CO_2 \quad \Delta H_R^0 = -41.1 \frac{kJ}{mol} \tag{1}$$

(II) Wood gas contains traces of ammonia, sulfur components, benzene, toluene, ethylbenzene, and xylene (BTEX), as well as condensable organic compounds (tar). A highly effective approach toward the removal of tar is the absorption in organic solvents (e.g., biodiesel or RME). In parallel, condensing water enables a removal of water-soluble impurities like ammonia and hydrogen sulfide.[16]

(III) The PSA process is based on the physical binding of gas molecules to a solid adsorbent material. The interaction between the gas and the adsorbent depends mainly on the gas component, its partial pressure, the type of adsorbent, and temperature. Hydrogen is a highly volatile compound with a low polarity, and its adsorption capacity on activated carbon is very low.[17]

dx.doi.org/10.1021/sc500436m | ACS Sustainable Chem. Eng. XXXX, XXX, XXX–XXX

(IV) As a demonstration of the high quality of the product, its use in a PEM fuel cell was chosen. The principles of a PEM fuel cell are reviewed in ref 18. In order to meet the requirements of this fuel cell type, the presence of certain wood gas components in the generated $BioH_2$ had to be avoided. In the following, the influence of the relevant wood gas components on a PEM fuel cell are reviewed.

CO is adsorbed on the active surface of the platinum catalyst of a PEM fuel cell and reduces the available area for H_2 oxidation. Concentrations as low as 0.5 to 4.5 vol ppm have been reported to cause performance losses due to a voltage drop that is directly proportional to the CO concentration.[19] CO_2 causes a more pronounced performance loss than inert components like N_2. The reason seems to be the formation of CO, either through the reverse WGS reaction or an electrochemical reduction reaction. Severe performance loss has been reported for CO_2 concentrations of about 20 vol % and higher.[20] H_2S is also adsorbed on the catalyst surface and reduces the area for H_2 oxidation. This mechanism was even observed at concentrations as low as 0.25 vol ppm. In contrast to CO poisoning, the adsorption of H_2S seems to be irreversible.[20] Also carbonyl sulfide (COS) is reported to reduce the active surface of the catalyst.[21] NH_3 is oxidized to NH_4^+ ions, which reduces the proton concentration at the catalyst layer and leads to a reduction of the performance of the anode. After long exposure times, NH_4^+ ions migrate into the proton exchange membrane, resulting in a conductivity loss. These effects have already been observed at ammonia concentrations as low as 1 vol ppm.[20] Inert components like N_2 reduce the partial pressure of H_2, which leads to a potential loss according to the Nernst equation. Apart from this effect, even a high CH_4 concentration shows no negative effects on the performance of a PEM fuel.[22] The O_2 content in the $BioH_2$ needs to be as low as possible in order to avoid the direct formation of water at the anode.[20]

EXPERIMENTAL SECTION

The studied process chain shown in Figure 2 is the third configuration for $BioH_2$ production, which has been tested experimentally at Oberwart. A series of test campaigns, which included a membrane separation unit, were carried out in 2013, and its results have been already published.[12,23]

The current configuration can be seen as a polygeneration concept, aiming at the simultaneous production of H_2, electricity, and district heat. Electricity production can be achieved via combustion of the adsorbate fraction of the PSA unit. The complexity and costs of investment, as well as the operating expense should be kept low, with high overall efficiencies and an acceptable H_2 recovery (H_2 rec) calculated according to the molar flow rate of hydrogen at the inlet and at the outlet of the process chain (eq 2). Therefore, a steam reformer for CH_4 and tar reforming was not desired, although it enables an increased hydrogen yield per biomass input.

$$H_2\text{rec} = \frac{\dot{n}_{H_2,\text{out}}}{\dot{n}_{H_2,\text{in}}} \tag{2}$$

Water−Gas Shift Unit. WGS catalysis was realized in three fixed bed reactors connected in series. A picture of the experimental setup for the catalysis of the WGS reaction is in the Supporting Information. A commercial Fe_2O_3/Cr_2O_3-based catalyst was applied for heterogeneous fixed bed catalysis of the WGS reaction. Prior to the operation of the process chain, the catalyst had been activated according to eq 3 in order to form the catalytically active magnetite (Fe_3O_4). The overall hydrogen demand for this reduction process was negligible (about 1 m_n^3). After the activation of the catalyst, the WGS unit had been commissioned with real wood gas and operated continuously for almost 400 h at an inlet temperature of each reactor of 350 °C. During this conditioning phase, FeS had been formed according to the equilibrium reaction in eq 4. This sulfiding reaction is reversible, and H_2S will be released if the reaction temperature is increased or if the partial pressure of H_2S in the feed is decreased. With respect to the equilibrium constant of the reaction, it can be considered that the loading of FeS is increased by a factor of 6.5 if the temperature is decreased from 400 to 300 °C. FeS is reported to exhibit an activity reduced by 50% compared to magnetite.[15,24]

$$3Fe_2O_3 + H_2 \rightleftharpoons 2Fe_3O_4 + H_2O \quad \Delta H_R^0 = -16.3\frac{\text{kJ}}{\text{mol}} \tag{3}$$

$$Fe_3O_4 + 3H_2S + H_2 \rightleftharpoons 3FeS + 4H_2O \quad \Delta H_R^0 = -75.0\frac{\text{kJ}}{\text{mol}} \tag{4}$$

Steam was added to the wood gas in order to enhance the shift reaction and to prevent carbon formation on the surface of the catalyst.[25] The wood gas flow rate over the WGS unit was set with the rotational speed of the compressor of the PSA unit. The gas at the inlet of each reactor was electrically heated, and the temperature was monitored every 10 cm along the fixed bed. A temperature profile along the three reactors was set, attempting to optimize the overall CO conversion rate. Equilibrium calculations of the WGS reaction have been accomplished using the software HSC. Table 1 summarizes the operating conditions of the WGS unit. In the following, ± denotes the standard deviation of the measured values. The CO conversion rate (X_{CO}) defined in eq 5 was used to describe the performance of the WGS unit. The gas hourly space velocity (GHSV) was calculated using eq 6.

Table 1. Operating Conditions of the WGS Unit

	value	unit
wood gas in	0.56 ± 0.02	$(m^3_{n\ db})/h$
water addition	0.55 ± 0.02	(kg)/h
T_{in} reactor 1	403 ± 5	°C
T_{in} reactor 2	358 ± 3	°C
T_{in} reactor 3	309 ± 3	°C
pressure	76 ± 7	mbarg
$GHSV_{wet}$	170 ± 5	h^{-1}
$(H_2O)/(CO)$ molar ratio	5 ± 0.2	–
$(H_2O)/C$ molar ratio	2 ± 0.1	–

$$X_{CO} = \frac{\dot{n}_{CO,\text{in}} - \dot{n}_{CO,\text{out}}}{\dot{n}_{CO,\text{in}}} \tag{5}$$

$$GHSV = \frac{\dot{V}_{gas}}{V_{catalyst}} \tag{6}$$

Scrubber Unit. The water−gas-shifted gas subsequently entered a wet scrubbing unit in order to be cleaned and dried for PSA operation. A pipe with a length of 22 m was installed to connect the outlet of the WGS unit with the inlet of the scrubber unit. The heat losses over this length resulted in a rather low inlet temperature of the scrubber. A counter current flow of wood gas and organic solvent (RME) was realized over a structured packed column. The RME was cooled with a plate heat exchanger provided with cold ethylene glycol from an external chiller. In order to ensure complete gas drying, a gas washing bottle filled with ethylene glycol cooled to 0 °C was implemented afterward. The operating conditions of the scrubbing unit are listed in Table 2. A detailed description of the scrubber unit is provided in ref 12. Tar components represent a potential risk for the WGS catalyst as they might serve as precursors for the formation of coke.[26] However, the scrubber was placed downstream of the WGS unit in order to avoid an additional energy intensive cycle of condensation and evaporation.

dx.doi.org/10.1021/sc500436m | ACS Sustainable Chem. Eng. XXXX, XXX, XXX−XXX

Table 2. Operating Conditions of the Scrubber Unit

	solvent	value	unit
T_{in} gas	RME	48.3 ± 2.4	°C
T_{out} gas	RME	5.1 ± 0.2	°C
pressure	RME	58.5 ± 5.8	mbarg
circulation rate	RME	700	L/h
fresh addition	RME	0.5	L/h
T_{out} gas	glycol	0	°C

Pressure Swing Adsorption Unit. The cleaned gas was further processed in a PSA unit for H_2 purification. A picture of this setup is in the Supporting Information. The unit consisted of four vessels with a capacity of 4.72 L each. Every reactor was filled with 2.5 kg of activated carbon (Norit, RB2) as the adsorption agent. The volumetric flow rates of PSA feed and raffinate ($BioH_2$) were quantified with diaphragm gas meters enabling an accurate mass balance of the PSA unit. The adsorption pressure was built up with a gas compressor and the desired desorption pressure was achieved using a diaphragm vacuum pump. The PSA unit was operated in a cyclic sequence, which is described in detail in ref . Raffinate was generated during the adsorption step of one vessel carried out over a variable time frame (adsorption time). During the pressure equalization step, the product of one loaded vessel was used to partly repressurize a currently regenerated adsorber. The equalization pressure (in bara) is defined as the value to which the pressure drops in the gas dispensing vessel. The applied adsorption time and equalization pressure for the long-term experiment were estimated in a previous parameter study. During this study, the adsorption time per column was varied between 400 and 800 s, and the equalization pressure was set to the values 4.0 and 4.5 bara. Table 3 summarizes the basic operating conditions of the PSA unit, which were chosen during the continuous long-term operation.

Table 3. Operating Conditions of the PSA Unit

	value	unit
adsorption pressure	6.5	bara
desorption pressure	0.1	bara
purge/feed time ratio	5×10^{-3}	–
feed flow rate	0.7 ± 0.04	$(m^3_{n\ db})/h$
feed pressure	1000 ± 17	mbara
adsorption time per column	650	s
equalization pressure	4.5	bara

Fuel Cell Unit. A proton exchange membrane (PEM) fuel cell from AXANE was operated with the generated $BioH_2$ to demonstrate its quality. A picture of the employed fuel cell is in the Supporting Information. As a benchmark, the PEM fuel cell was also operated with Alphagaz 1 (H_2 purity > 99.999 vol %). Key data of this PEM fuel cell are listed in Table 4 provided by ref 27.

Chemical Analysis and Mass Balance. This section describes the adopted methods of chemical analysis. Extensive analyses of the main gas components, sulfur components, tar, water, BTEX, and ammonia were carried out. The selected sampling points (S.pt.) of the process chain are illustrated in Figure 2. A matrix of the analyzed components at the available sampling points is provided in the Supporting Information. Prior to gas chromatography (GC) analysis, the water-containing sampling streams were dried over two gas washing bottles filled with ethylene glycol, which were connected in series. The flasks were placed in a temperature-controlled cooling box at −3 °C. A flask filled with glass wool was subsequently removing aerosols from the stream. The sampling flow rate was adjusted with a needle valve upstream to a vacuum pump. A gas meter from Kromschröder (BKG2.5T) was used to quantify the volumetric flow rate of the dry sampling gas at ambient pressure. A corresponding increase in weight of the ethylene glycol filled flasks enabled a parallel estimation of the water content. A figure of the sampling line is in the Supporting Information.

Table 4. Key Data of the PEM fuel cell Unit[a]

	value	unit
nominal voltage DC	48	V
nominal voltage AC	230	V
minimum $power_{el}$	500	W
maximum $power_{el}$	2500	W
H_2 quality (ISO 14687)	99.99	vol %
H_2 operating pressure	250 ± 30	mbarg
H_2 consumption at max. power	35.1	L_n/min
H_2 peak consumption	60	L_n/min

[a]Based on ref 27.

The main gas components (CO_2, N_2, CO, O_2, CH_4, C_2H_6, C_2H_4, and C_2H_2) were separated in a combination of two different columns (7′ HayeSep N, 60/80 1/8″ SF and 9′ molecular sieve 13× 45/60, 1/8″ SF) in a GC (Clarus 500) from PerkinElmer. A thermal conductivity detector (TCD) was used for quantification. The sulfur components (H_2S, COS, C_4H_4S, CH_3CH_2SH, and CH_3SH) were separated in a different column (Rt-XL sulfur 1 m.x 0.95 mm OD) and quantified by a flame photometric detector (FPD).

Tar sampling is also illustrated in the Supporting Information. A combination of two cooling boxes was applied. Scrubbing bottles filled with 50 or 100 mL of toluene were applied to dissolve tar components. Three gas washing bottles were placed in an ice bath at 0 °C, and two additional impingers were placed in a temperature-controlled cooling box at −8 °C. For each tar analysis, a sampling stream of 2 L_n/min was taken over a period of 8 h. For detection of the tar components, a GC from PerkinElmer (XL GC) coupled with a mass spectrometer from PerkinElmer (Turbo Mass MS) was used. A detailed description of the applied method for tar analysis can be found in ref 28.

BTEX values were measured by gas chromatography-mass spectrometry (GC-MS, Shimadzu QP2010 Plus) at Vienna University of Technology. Six samples of each relevant point of the process were taken by means of gas sampling bags. For the quantification of NH_3, an absorption method was used. A sample of 1 L_n/min was extracted from the process for 3 h and passed through three gas washing bottles connected in series in a cooling bath at 0 °C. The bottles were filled with 0.05 M H_2SO_4, which solves NH_3 in the form of NH_4^+ ions. NH_4^+ ions were quantified by ion chromatography (Dionex ICS 5000).

It could be considered that the wood gas fed into the pilot plant was saturated with water corresponding to the operation temperature and pressure of the CHP plant scrubber.[16] The water addition upstream of the catalyzed WGS reaction was quantified gravimetrically and monitored with a variable area flow meter. Additionally, the flow rate of condensate formed in the scrubber was quantified volumetrically. The H_2 content in the dry gas was determined via mass balance. Volumetric flow rates of the dry PSA feed and the raffinate were quantified by diaphragm gas meters. The adsorbate flow rate and composition were calculated via mass balance. The flow rate of the wood gas at the inlet of the WGS unit was calculated via mass balance based on the feed flow rate of the PSA and the change of the gas composition according to the WGS reaction.

RESULTS AND DISCUSSION

During the presented long-term experiment, the CHP plant Oberwart was constantly generating an average of 2100 $m^3_{n\ db}$/h of wood gas, of which 350 $m^3_{n\ db}$/h were recycled back into the combustion zone of the DFB reactor. The outlet temperature of the CHP plant scrubber was 35 ± 6 °C. Assuming a relative humidity of 100% at the outlet of this scrubber, a humidity of approximately 5 mol $\%_{wb}$ could be calculated in the feed gas of the experimental setup.[16]

The pilot plant for H_2 production was successfully operated continuously for almost 250 h. This section gives an overview of the performance of each operation unit as well as the results

dx.doi.org/10.1021/sc500436m | ACS Sustainable Chem. Eng. XXXX, XXX, XXX−XXX

of the detailed chemical analysis of the entire process chain. The results of the chemical analysis are presented with respect to the analyzed substance class (main gas components, sulfur components, BTEX components, tar components, and ammonia). Next, the mass balance of the process is presented and visualized in a Sankey diagram. Finally, the issue energy consumption is discussed, and a brief outlook is given.

Water−Gas Shift Unit. The performance of the WGS unit is illustrated in Figure 3, summarizing all three reactors. The

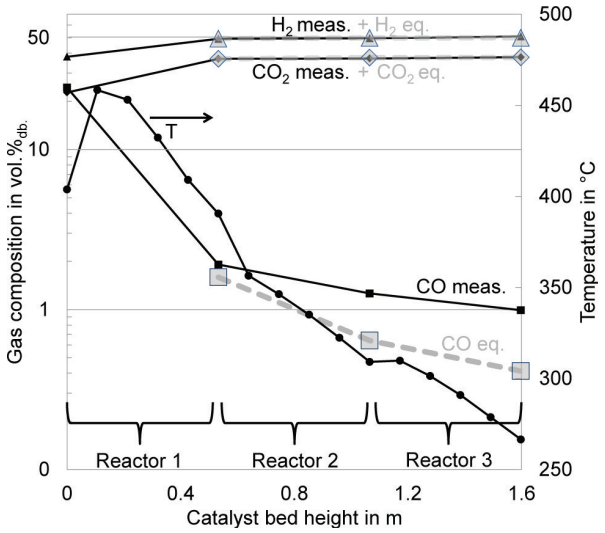

Figure 3. Results of the WGS unit, measured (meas.) and equilibrium (eq) gas composition as well as temperature along the bed height; the sulfidation procedure (eq 4) at the present operating temperature was only completed for reactors 1 and 2 (also see Table 7).

measured gas compositions are plotted on a logarithmic scale and can be compared with the WGS equilibrium at the corresponding outlet temperature of each reactor. Within the first 10 cm of the catalyst bed in the first reactor, the temperature increased by about 60 °C due to the exothermic WGS reaction. The temperature profile demonstrates that the main share of CO was converted within this section of the catalyst bed. Subsequently, the temperature along the bed height decreased due to heat losses. The inlet temperatures of reactors 2 and 3 were steadily lowered in order to harness lower equilibrium CO contents.

At the outlet of the WGS unit, the CO content could be reduced to about 1 vol $\%_{db}$ (also see Table 6), representing a CO conversion rate of 95% and a H_2 recovery of 160% within this unit. The dry volumetric flow rate was increased from 0.56 $m^3_{n\ db}$/h to 0.70 $m^3_{n\ db}$/h, while the H_2O content was lowered from 56 to 45 mol $\%_{wb}$. Low GHSV, low sulfur loads in the feed gas (see Table 7), and the approach of temperature optimization enabled high overall conversion rates.[15] However, especially in reactors 2 and 3 a complete equilibration of the WGS reaction could not be reached. In order to further enhance the CO conversion in these reactors, the temperature should have been set higher. This is demonstrated by an increasing deviation of the equilibrium CO content and the measured CO content. By means of this, the amount of catalyst could have been reduced significantly maintaining the same CO conversion rate. Industrially applied FeO_3/Cr_2O_3-based catalysts are operated at GHSV of 400−1200 h^{-1}.[2]

Scrubber Unit. The scrubber unit was capable of cooling the shifted gas to 0 °C. Hence, it could be assumed that only a negligible amount of H_2O was present at the inlet of the PSA unit. A condensate flow rate of 0.32 L/h was generated in the scrubber, which corresponded to the overall water balance of the process chain. The performance of the scrubber in terms of tar separation and removal of other undesired gas components is shown in Tables 7−10.

Pressure Swing Adsorption Unit. A parameter study of the PSA unit was carried out previous to the long-term experiment. During the study, a steady state operation of the upstream equipment was maintained. The operation parameters adsorption time and equalization pressure were varied, revealing a trade-off between the purity of the product and the H_2 recovery. At a fixed equalization pressure (4.5 bara), the effect of a variation in adsorption time on the content of the impurities is shown in Figure 4. Increasing amounts of contaminants were analyzed at longer adsorption times. Similar results were achieved at an equalization pressure of 4.0 bara.

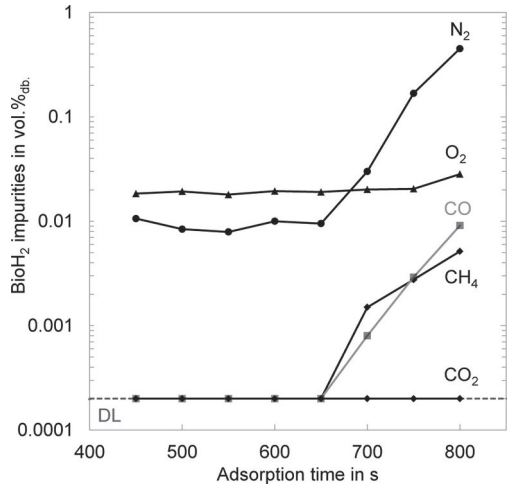

Figure 4. Results of PSA parameter study. $BioH_2$ impurities over adsorption time at an equalization pressure of 4.5 bara; detection limit (DL) = 2 vol ppm.

The influence of varying pressure equalization as well as adsorption time on the H_2 recovery is shown in Figure 5. As shown, the H_2 recovery was improved at lower equalization pressures of the PSA unit.

The aim of this study was to optimize the H_2 recovery provided that the components CO, CO_2, and CH_4 were reduced below the detection limit (BDL, 2 vol ppm_{db}). As a result, the parameters in Table 3 (adsorption time of 650 s and equalization pressure of 4.5 bara) were chosen for the reported steady state operation during the 250 h of continuous experimentation.

Under these fixed conditions, a H_2 purity of 99.97 vol $\%_{db}$ as well as a H_2 recovery of 80.0% were reached. These results are within the range of similar reported PSA systems obtaining H_2 purities up to 99.99 vol $\%_{db}$ and H_2 recoveries between 70% and 85%.[29−33] The volumetric feed flow rate of 0.70 $m^3_{n\ db}$/h was split into an adsorbate fraction of 0.42 $m^3_{n\ db}$/h and a raffinate fraction ($BioH_2$) of 0.28 $m^3_{n\ db}$/h. As shown in Table 6, the only detected impurities in the PSA raffinate were O_2 with 0.02 vol $\%_{db}$ and N_2 with 0.01 vol $\%_{db}$.

dx.doi.org/10.1021/sc500436m | ACS Sustainable Chem. Eng. XXXX, XXX, XXX−XXX

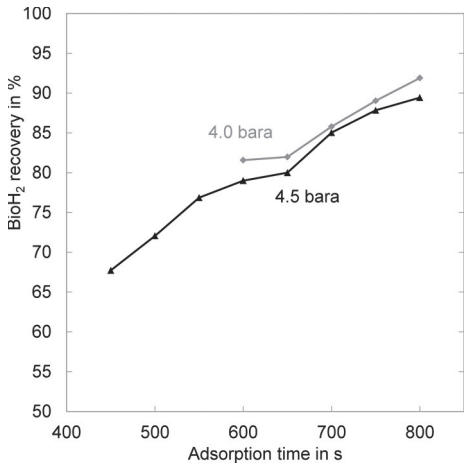

Figure 5. Results of PSA parameter study. $BioH_2$ recovery over adsorption time at an equalization pressure of 4.0 and 4.5 bara.

Fuel Cell Unit. To demonstrate the high purity of the PSA raffinate, the generated $BioH_2$ was fed into a PEM fuel cell (Mobixane from AXANE). The unit was operated flawlessly for over 3 h. The comparison between its operation with the produced $BioH_2$ and Alphagaz 1 H_2 is shown in Table 5.

Table 5. Comparison of PEM fuel Cell Performance with $BioH_2$ and Alphagaz 1

	$BioH_2$	Alphagaz	unit
purity	≥99.97	≥99.999	vol %
$\dot{V}_{H_2}$	0.28 ± 0.01	0.28 ± 0.01	m^3_n/h
p_{Feed}	1268 ± 27	1245 ± 24	mbara
$T_{Fuel\ cell}$	40.5 ± 1.5	36.8 ± 0.9	°C
η_{gross}	53.9 ± 1.0	54.2 ± 1.0	$\%_{LHV\ base}$

It could be demonstrated that there was no significant difference in the fuel cell performance comparing the operation with $BioH_2$ and the operation with Alphagaz 1 in the investigated period. This can be distinguished between the gross electrical efficiency and net electrical efficiency of the fuel cell. In Table 5, the gross electrical efficiencies are presented. The inverter and the peripherals of the fuel cell cause a decrease in its electrical efficiency and account for the net electrical efficiency. A gross electrical efficiency of about 54% was obtained, which is in good accordance to ref 21. The obtained value for the net electrical efficiency was not representative as the unit was operated below its nominal power range. The issue of electrical efficiencies and the setup of this fuel cell are described in detail in refs 12 and 34.

Chemical Analysis and Mass Balance. In this chapter, the evolution of the dry gas composition along the process chain is presented. The results have to be regarded in combination with the corresponding sampling points (S.pt.) illustrated in Figure 2. All results are measured gas compositions, except for the mean adsorbate composition, which was calculated via mass balance (the feed flow rate and the composition of the adsorbate vary strongly as a function of the cyclic PSA operation). Table 6 depicts the evolution of the main gas components on a dry base, detected with the TCD detector of the GC.

In Table 6, the given CO concentrations over the WGS unit represent a CO conversion rate of about 90.5% at the outlet of

Table 6. Results of Analysis of Main Gas Components[a]

S.pt.	CO_2 (vol $\%_{db}$)	C_2H_4 (vol $\%_{db}$)	C_2H_6 (vol $\%_{db}$)
1	22.7 ± 0.8	2.3 ± 0.3	0.17 ± 0.03
2a	36.9 ± 0.8	1.8 ± 0.1	0.17 ± 0.02
2b	37.0 ± 0.8	1.8 ± 0.1	0.17 ± 0.03
2c	37.1 ± 0.9	1.9 ± 0.2	0.18 ± 0.02
4	36.9 ± 0.2	1.6 ± 0.3	0.14 ± 0.03
5	61.4	2.6	0.23
6	BDL	BDL	BDL
S.pt.	C_2H_2 (vol $\%_{db}$)	O_2 (vol $\%_{db}$)	N_2 (vol $\%_{db}$)
1	0.15 ± 0.02	0.1 ± 0.02	2.3 ± 0.4
2a	0.001 ± 0.001	0.06 ± 0.01	1.8 ± 0.1
2b	BDL	0.08 ± 0.04	2 ± 0.1
2c	BDL	0.07 ± 0.06	1.9 ± 0.3
4	BDL	0.03 ± 0.01	1.5 ± 0.1
5	BDL	0.03	2.6
6	BDL	0.02 ± 0.0003	0.01 ± 0.004
S.pt.	CH_4 (vol $\%_{db}$)	CO (vol $\%_{db}$)	H_2 (vol $\%_{db}$)
1	10.0 ± 0.3	24 ± 1	38.0 ± 1.2
2a	8.2 ± 0.1	1.9 ± 0.3	49.2 ± 0.9
2b	8.1 ± 0.2	1.3 ± 0.2	49.5 ± 0.9
2c	8.2 ± 0.2	1.0 ± 0.1	49.6 ± 0.9
4	8.0 ± 0.2	0.98 ± 0.04	50.9 ± 0.4
5	13.3	1.63	18.2
6	BDL	BDL	99.97 ± 0.004

[a]Sampling points (S.pt.) are illustrated in Figure 2; BDL = below detection limit, DL = 2 vol ppm_{db}; adsorbate composition (5) was calculated via mass balance.

the first reactor ($GHSV_{wb}$ 510 h^{-1}) and a CO conversion rate of about 93.5% at the outlet of the second reactor ($GHSV_{wb}$ 255 h^{-1}). At the outlet of the last reactor ($GHSV_{wb}$ 170 h^{-1}), an overall CO conversion rate of about 95% was reached. The H_2 content was increased from 38 vol $\%_{db}$ to about 50 vol $\%_{db}$. The simultaneous increase in the dry gas flow rate by 25% led to a general dilution effect. C_2H_2 was totally hydrogenated to C_2H_4 and could not be detected at the outlet of the WGS unit. C_2H_4 was assumed to be partly hydrogenated to C_2H_6. The overall mass balance of the C_2H_y components was approaching 98%. The slightly higher content of H_2 in the PSA feed (4) compared to the outlet of the WGS unit (2c) could be explained by the low solubility of hydrogen in water as well as by the removal of a series of gas components in the scrubber unit (e.g., benzene and ammonia). It is also shown that O_2 and N_2 were the only detectable impurities that were fed into the fuel cell. O_2 is reported to be tolerated up to 500 vol ppm, and N_2 has only dilution effects on the PEM fuel cell.[20]

The evolution of the sulfur components along the process is provided in Table 7.

Table 7. Results of Analysis of Sulfur Components[a]

S.pt.	H_2S (vol ppm_{db})	COS (vol ppm_{db})	C_4H_4S (vol ppm_{db})
1	59 ± 10	1.0 ± 0.1	7.2 ± 3.1
2a	49 ± 4	BDL	2.0 ± 0.7
2b	50 ± 3	BDL	1.0 ± 0.5
2c	4 ± 1	BDL	1.0 ± 0.6
4	2.5 ± 0.3	BDL	0.3 ± 0.01
5	0.4 ± 0.3	BDL	0.5 ± 0.3
6	BDL	BDL	BDL

[a]DL = 0.3 vol ppm_{db}.

dx.doi.org/10.1021/sc500436m | ACS Sustainable Chem. Eng. XXXX, XXX, XXX−XXX

As proved by constant H_2S concentrations, the catalyst sulfidation was completed in the first two reactors, where the main CO conversion took place. However, only 4 vol ppm_{db} of H_2S was measured after the third reactor, which shows an incomplete sulfidation of this stage during the presented study. Compared to the conditioning of the catalyst (carried out before the test run, 400 h of operation at 350 °C), the last reactor was now operated at a lower temperature level, which provided a favorable condition for an enhanced catalyst sulfidation.[35] The WGS unit was basically designed for higher GHSV than applied during the operation of the process chain. In more recent experiments, the same conversion rate of 95% could be achieved with the completely sulfided catalyst (same concentration of H_2S at the inlet and outlet) at $GHSV_{wb}$ of about 500 h^{-1} and slightly higher operating temperatures.

COS was not detected at the outlet of the WGS unit, which could be explained by the reactions shown in eqs 7 and 8. The decrease in thiophene (C_4H_4S) along the WGS unit is suggested to be due to the reaction of thiophene hydrogenolysis in eq 9.[15] Less C_4H_4S and H_2S could be detected after gas scrubbing. The organic C_4H_4S was assumed to dissolve in the RME, whereas the H_2S dissolved in the condensate. Table 7 also indicates that a fraction of the H_2S present in the feed was captured in the PSA unit. However, previous experiments at the PSA unit showed a complete desorption of H_2S from the activated charcoal at higher sulfur loads in the PSA feed.[12] The rather low sulfur load in the adsorbate was explained by adsorption effects of the used gas sampling bag.

$$H_2 + COS \rightleftharpoons H_2S + CO \quad \Delta H_R^0 = 10.9 \frac{kJ}{mol} \tag{7}$$

$$H_2O + COS \rightleftharpoons H_2S + CO_2 \quad \Delta H_R^0 = -30.3 \frac{kJ}{mol} \tag{8}$$

$$C_4H_4S + 4H_2 \rightleftharpoons C_4H_{10} + H_2S \quad \Delta H_R^0 = -261.2 \frac{kJ}{mol} \tag{9}$$

Analyses of BTEX are shown in Table 8. In the WGS unit, no significant change in the content of benzene, toluene, and xylene could be observed, apart from a dilution effect due to an increased volumetric gas flow rate. The hydrogenation of styrene (Table 9) was assumed to be responsible for the formation of the ethylbenzene as a side reaction in the WGS unit. The scrubber unit removed the majority of the BTEX compounds. Only benzene and toluene could be detected at the inlet of the PSA unit. Analysis of the PSA raffinate and adsorbate suggests a complete adsorption and subsequent desorption of these compounds from the activated carbon.

Table 8. Results of Analysis of Benzene (B), Toluene (T), Ethylbenzene (E), and Xylene (X)[a]

S.pt.	B	T	E	X
1	3296 ± 36	201 ± 5	1.3 ± 0.6	1.1 ± 0.6
2c	2850 ± 54	176 ± 6	33 ± 12	2.2 ± 0.9
4	536 ± 5	17 ± 2	BDL	1.2 ± 0.6
5	641 ± 13	21 ± 1	BDL	BDL
6	BDL	BDL	BDL	BDL

[a]BTEX, in vol ppm_{db}; DL = 1 vol ppm_{db}.

The results of the tar analysis in Table 9 are based on three continuous long-term samples. Therefore, no standard deviations can be given. As a side reaction in the WGS unit, styrene and indene were probably hydrogenated to form ethylbenzene (Table 8) and indane (not analyzed). Furthermore, a hydrogenation of phenylacetylene to ethylbenzene as well as a hydrogenation of acenaphthylene to acenaphthene could be assumed. Besides the frequently observed dilution effect, naphthalene as the predominant tar component was probably not affected in the WGS unit. In the scrubbing unit, all measured tar components except naphthalene could be removed to below the detection limit.

Table 9. Results of Analysis of Tar Components (one continuous sample)[a]

	S.pt.		
tar component	1 ($mg/m^3_{n\ db}$)	2c ($mg/m^3_{n\ db}$)	3 ($mg/m^3_{n\ db}$)
naphthalene	1139	824	2
styrene	247	BDL	BDL
indene	191	9	BDL
phenylacetylene	25	BDL	BDL
mesitylene	BDL	4	BDL
benzofuran	2	BDL	BDL
1-benzothiophene	2	BDL	BDL
2-methylnaphthalene	5	4	BDL
1-methylnaphthalene	3	2	BDL
biphenyl	1	BDL	BDL
acenaphthylene	13	BDL	BDL
acenaphthene	2	7	BDL
anthracene	2	4	BDL
flouranthene	1	3	BDL
pyrene	1	3	BDL

[a]DL = 1 $mg/m^3_{n\ db}$.

The results of the NH_3 analysis in Table 10 are also based on one continuous sample per sampling point. Therefore, no standard deviations can be given. Apart from the dilution effect in the WGS unit, no influence of the catalyst on the NH_3 was observed. In the scrubbing unit, the amount of NH_3 was reduced below the detection limit. Hence, there was no NH_3 present at the inlet of the PSA unit.

Table 10. Results of Analysis of NH_3 (one continuous sample)[a]

S.pt.	NH_3 (vol ppm_{db})
1	954
2c	740
3	1
4	BDL

[a]DL = 1 vol ppm_{db}.

Summing up, the aim of this polygeneration approach was to minimize its complexity at acceptable H_2 recoveries. The process used one single compression step and worked flawlessly for 250 h. The obtained flow rates and water contents over the process chain are summarized in Table 11. The global mass balance of the established process is also illustrated by means of the Sankey diagram in Figure 6. The width of the arrows is shown proportionally to the molar flow of each component.

The diagram shows that more H_2 could be separated in the PSA unit than H_2 was present in the wood gas feed. The overall hydrogen recovery of 128% was enabled by the production of additional H_2 in the WGS unit (recoveries of the single process

Table 11. Mass balance and H_2O Content over the Process Chain[a]

S.pt.	description	Flow rate ($m^3_{n\ wb}$)/h	H_2O (vol $\%_{wb}$)
1	raw gas	0.60	5.21
2	WGS in	1.28	55.82
2c	WGS out	1.28	45.46
3	RME out	0.71	0.84
4	PSA in	0.70	0
5	adsorbate	0.28	0
6	$BioH_2$	0.42	0

[a]Water considered as an ideal gas at standard conditions.

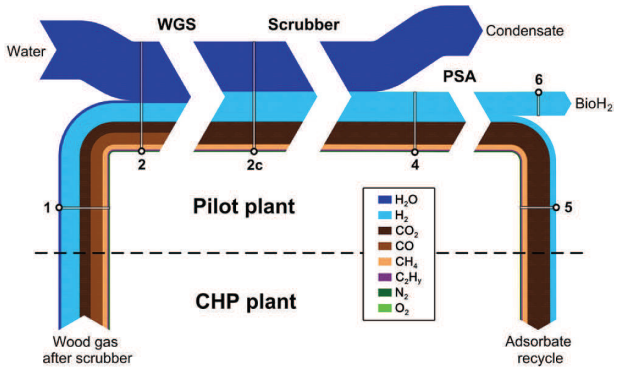

Figure 6. Sankey diagram of the process chain. The width of the arrows is shown proportionally to the molar flow of each component, including sampling points of chemical analysis.

steps: 160% in the WGS unit, 100% in the gas scrubber, and 80% in PSA unit).

A total of 0.56 $m^3_{n\ db}$/h of dry wood gas was extracted after the scrubber of the CHP plant Oberwart. Catalysis of the WGS reaction caused an increase in the dry volumetric flow rate to 0.70 $m^3_{n\ db}$/h, decreasing the CO content from about 24 to 1 vol $\%_{db}$. In the PSA unit, the feed was split into 0.42 $m^3_{n\ db}$/h of adsorbate and 0.28 $m^3_{n\ db}$/h of raffinate. The only detectable impurities in the PSA raffinate were O_2 (0.02 vol $\%_{db}$) and N_2 (0.01 vol $\%_{db}$). This gas composition enabled the operation of a PEM fuel cell.

Within this working group, a master thesis was carried out to evaluate the presented process chain in terms of energy consumption.[36] It was distinguished between the electricity demand for pumps and compressors, the heating demand, and the cooling demand. A specific energy demand of 0.57 (kW h_{el})/(m^3_n $BioH_2$), 1.71 (kW h_{cool})/(m^3_n $BioH_2$), and 2.12 (kW h_{heat})/(m^3_n $BioH_2$) was calculated by means of the process simulation software IPSEpro (LHV of H_2: 3 kWh/m^3_n. In order to reduce the heat demand for steam production, wood gas for $BioH_2$ production should be extracted upstream of the scrubber of the CHP plant. A water content of already 35 mol $\%_{wb}$ can be estimated at this point of the process.[14] In this case, the catalyst of the WGS unit would have to face a considerably higher load of impurities. Future experimental work will cover the long-term stability of the catalyst in combination with this tar-rich wood gas. Apart from this, an adsorption tube will be installed in the feed of the fuel cell in order to reduce the detection limit of impurities in the $BioH_2$.

A positive overall assessment will provide the basis for an upscale of the process to a capacity of about 50 $m^3_{n\ db}$/h $BioH_2$.

■ ASSOCIATED CONTENT

Supporting Information

Pictures of the CHP plant Oberwart, installed WGS unit, PSA unit, and PEM fuel cell. Matrix of the analyzed components and the available sampling points, as well as a flowchart of the sampling line for chemical analysis. This material is available free of charge via the Internet at http://pubs.acs.org.

■ AUTHOR INFORMATION

Corresponding Authors

*E-mail: silvester.fail@gmail.com (S.F.).
*E-mail: nicolas.diaz@gmx.at (N.D.).

Notes

The authors declare no competing financial interest.

■ ACKNOWLEDGMENTS

The authors thank the project partners: Energie Burgenland, Air Liquide, Binder Industrieanlagenbau and CTS. The company Clariant is gratefully acknowledged for providing the WGS catalyst. Especially, the CHP plant Oberwart is thanked for providing a unique working environment and a stable supply of wood gas. The long-term conditioning of the WGS catalyst could only be achieved with the help of Matthias Binder. Christian Jordan is thanked for his commitment related to BTEX analysis. Nicolas Diaz received financial support from Conicyt-Becas Chile. Several research projects collaborated to realize the presented process chain: "Polygeneration 2" (Bioenergy2020+), "Green H_2" (FFG), and "Simple SNG" (FFG). Bioenergy2020+ is funded within the Austrian COMET program managed by the Austrian Research Promotion Agency (FFG). The financial support of the funding association FFG and the Austrian Climate and Energy Fund is gratefully acknowledged.

■ NOMENCLATURE

Abbreviations and Acronyms

a: year (anno)
BDL: below detection limit
$BioH_2$: biohydrogen, hydrogen produced by or out of biomass
BTEX: benzene, toluene, ethylbenzene, xylene
CHP: combined heat and power
C_xH_y: hydrocarbons
DFB: dual fluidized bed
DL: detection limit
FPD: flame photometric detector
GC: gas chromatography
GHSV: gas hourly space velocity
LHV: lower heating value
L: liter
mol: molar
ORC: organic rankine cycle
PEM: proton exchange membrane
PSA: pressure swing adsorption
RME: rapeseed oil methyl ester
S.pt: sampling point
TCD: thermal conductivity detector
t: ton
vol: volumetric
WGS: water−gas shift

Indices

cool: cooling

db: dry base
el: electric
eq: equilibrium
heat: heating
in: inlet
meas: measured
n: standard conditions (0 °C and atmospheric pressure)
out: outlet
rec: recovery
wb: wet base

Symbols

ΔH_R^0: Standard enthalpy of reaction in (kJ)/(mol) (at 0 °C and 1 bar)
$\eta_{\text{el gross}}$: Gross electrical efficiency, dimensionless
$\dot{n}$: molar flow rate in (mol)/h
$\dot{V}$: Volumetric flow rate in (m_n^3)/h
X_{CO}: CO conversion rate, dimensionless

REFERENCES

(1) *Hydrogen Production and Distribution*; Energy Technology Essentials; International Energy Agency: Paris, 2007.
(2) Liu, K.; Song, C.; Subramani, V. *Hydrogen and Syngas Production and Purification Technologies*; Wiley, NewYork, 2010; pp 14−17, 313.
(3) Dunn, S. Hydrogen futures: Toward a sustainable energy system. *Int. J. Hydrogen Energy* **2002**, *27*, 235−264.
(4) Hefner, R. A. The age of energy gases. *Int. J. Hydrogen Energy* **2002**, *27*, 1−9.
(5) Chaubey, R.; Sahu, S.; James, O. O.; Maity, S. A review on development of industrial processes and emerging techniques for production of hydrogen from renewable and sustainable sources. *Renewable Sustainable Energy Rev.* **2013**, *23*, 443−462.
(6) Gahleitner, G. Hydrogen from renewable electricity: An international review of power-to-gas pilot plants for stationary applications. *Int. J. Hydrogen Energy* **2013**, *38*, 2039−2061.
(7) Abbasi, T.; Abbasi, S. Renewable hydrogen production: Prospects and challenges. *Renewable Sustainable Energy Rev.* **2011**, *15*, 3034−3040.
(8) Tock, L.; Maréchal, F. Co-production of hydrogen and electricity from lignocellulosic biomass: Process design and thermo-economic optimization. *Energy* **2012**, *45*, 339−349.
(9) Moreno, J.; Dufour, J. Life cycle assessment of hydrogen production from biomass gasification. Evaluation of different Spanish feedstocks. *Int. J. Hydrogen Energy* **2013**, *38*, 7616−7622.
(10) Susmozas, A.; Iribarren, D.; Dufour, J. Life-cycle performance of indirect biomass gasification as a green alternative to steam methane reforming for hydrogen production. *Int. J. Hydrogen Energy* **2013**, *38*, 9961−9972.
(11) *Booklet Biomassevergasungskraft Oberwart*; Energie Burgenland: Eisenstadt , Austria2014.
(12) Diaz, N. Hydrogen Separation from Producer Gas Generated by Biomass Steam Gasification. Ph.D. Thesis, Vienna University of Technology, 2013.
(13) Hofbauer, H.; Rauch, R.; Bosch, K.; Koch, R.; Aicherning, C. In *Biomass CHP Plant Güssing, A Success Story*; Bridgwater, A., Ed.; CPL Press: Berks, U.K., 2003; pp 527−536.
(14) Kotik, J. Über den Einsatz von Kraft-Wärme-Kopplungsanlagen auf Basis der Wirbelschicht-Dampfvergasung fester Biomasse am Beispiel des Biomassekraftwerks Oberwart. Ph.D. Thesis, Technische Universität Wien, 2010.
(15) Twigg, M. V. *Catalyst Handbook*, 2nd ed.; Manson Publishing: Singapore, 1989; pp 200−201, 283−288, 302−306, Chapter 6.
(16) Pröll, T.; Siefert, I. G.; Friedl, A.; Hofbauer, H. Removal of NH_3 from biomass gasification producer gas by water condensing in an organic solvent scrubber. *Ind. Eng. Chem. Res.* **2005**, *44*, 1576−1584.
(17) Ruthven, D. M. *Pressure Swing Adsorption*; VCH: Weinheim, 1994; pp 235−238.
(18) *Fuel Cell Handbook*; U.S. Department of Energy: Washington, DC, 2004.
(19) Benesch, R.; Jacksier, T. Hydrogen and Material Quality Issues for PEM Fuel Cells. Vehicle Power and Propulsion, 2005 IEEE Conference, 2005; pp 646−651.
(20) Besancon, B. M.; Hasanov, V.; Imbault-Lastapis, R.; Benesch, R.; Barrio, M.; Mlnvik, M. J. Hydrogen quality from decarbonized fossil fuels to fuel cells. *Int. J. Hydrogen Energy* **2009**, *34*, 2350−2360.
(21) Kurzweil, P. In *Brennstoffzellentechnik*; Fister, M., Ed.; Springer Vieweg: Weinheim, Germany, 2013; pp 87, 98.
(22) Blessing, I.; Gardner, C.; Ternan, M. Separation of hydrogen from a hydrogen/methane mixture using a PEM fuel cell. *Int. J. Hydrogen Energy* **2007**, *32*, 908−914.
(23) Fail, S.; Diaz, N.; Konlechner, D.; Hackel, M.; Sanders, E.; Rauch, R.; Harasek, M.; Bosch, K.; Schwenninger, F.; Zapletal, P.; Schee, Z.; Hofbauer, H. An Experimental Approach for the Production of Pure Hydrogen Based on Wood Gasification, Proceedings of the International Conference for Polygeneration Strategies (ICPS), 2013.
(24) Hla, S. S.; AMorpeth, L.; Sun, Y.; Duffy, G.; Ilyushechkin, A.; Roberts, D.; Edwards, J. A CeO_2-La_2O_3-based Cu catalyst for the processing of coal-derived syngases via high-temperature water gas shift reaction. *Fuel* **2013**, *114*, 178−186.
(25) Shiratori, Y.; Ijichi, T.; Oshima, T.; Sasaki, K. Internal reforming SOFC running on biogas. *Int. J. Hydrogen Energy* **2010**, *35*, 7905−7912.
(26) Bartholomew, C. H. Mechanisms of catalyst deactivation. *Appl. Catal., A* **2001**, *212*, 17 − 60, Catalyst Deactivation.
(27) Moine, S. *Mobixane Operation Manual*; Axane Fuel Cell Systems: Sassenage, France, 2009.
(28) Wolfesberger, U.; Aigner, I.; Hofbauer, H. Tar content and composition in producer gas of fluidized bed gasification of wood-influence of temperature and pressure. *Environ. Prog. Sustainable Energy* **2009**, *28*, 372−379.
(29) Yang, J.; Hana, S.; Chob, C.; Lee, C.-H.; Lee, H. Bulk separation of hydrogen mixtures by a one-column PSA process. *Sep. Purif. Technol.* **1995**, *5*, 239−249.
(30) Ribeiro, A. M.; Grande, C. A.; Lopes, F. V.; Loureiro, J. M.; Rodrigues, A. E. A parametric study of layered bed PSA for hydrogen purification. *Chem. Eng. Sci.* **2008**, *63*, 5258−5273.
(31) Park, J.-H.; Kim, J.-N.; Cho, S.-H. Performance analysis of four-bed H_2 PSA process using layered beds. *AIChE J.* **2000**, *46*, 790−802.
(32) Ahn, S.; You, Y.-W.; Lee, D.-G.; Kimb, K.-H.; Oh, M.; Lee, C.-H. Layered two- and four-bed PSA processes for H_2 recovery from coal gas. *Chem. Eng. Sci.* **2012**, *68*, 413−423.
(33) Lopes, F. V.; Grande, C. A.; Rodrigues, A. E. Activated carbon for hydrogen purification by pressure swing adsorption: Multi-component breakthrough curves and {PSA} performance. *Chem. Eng. Sci.* **2011**, *66*, 303−317.
(34) Kraussler, M. PEM Fuel Cell Operation and Applications Using BioH_2. Master of Science Thesis, Vienna University of Technology, 2014.
(35) Morpeth, L.; Sun, Y.; Hla, S. S.; French, D.; Duffy, G.; Edwards, J. Effect of H_2S on the performance of $La_{0.7}Ce_{0.2}FeO_3$ perovskite catalyst for high temperature water-gas shift reaction. *Int. J. Hydrogen Energy* **2012**, *37*, 1475−1481.
(36) Hinteregger, J. Performance Evaluation of Process Chains for the Production of BioH_2 from Wood Gas. Master of Science Thesis, Vienna University of Technology, 2014.

Long-term experiment for the separation of “green” hydrogen from biomass gasification by a polymer membrane

Dipl.-Ing. David Konlechner*, Ass. Prof. Dipl.-Ing. Dr. Michael Harasek, Univ. Prof. Dipl.-Ing. Dr. Hermann Hofbauer
Vienna University of Technology, Institute of Chemical Engineering
Getreidemarkt 9/166 – A-1060 Vienna – Austria

Dr.-Ing. Marius Hackel
Air Liquide Forschung und Entwicklung GmbH, Frankfurt Research & Technology Center (FRTC), Gwinnerstrasse 27-33 - D-60388 Frankfurt am Main – Germany

Dr. Ed Sanders
Delaware Research and Technology Center
200 GBC Drive – Newark – DE-19702 – USA

Dr. Klaus Bosch
Energie Burgenland AG
Kasernenstraße 9 – A-7000 Eisenstadt – Austria

ABSTRACT

Hydrogen is seen as an important part of a lasting energy mix for the future. The Institute of Chemical Engineering at the Vienna University of Technology is operating an experimental setup for the separation of sustainable hydrogen from product gas of an industrial biomass gasification plant located at Oberwart, Austria. The overall concept follows the polygeneration concept which has the aim to produce valuable products on an economic basis and to utilize remaining by-products, for example in a gas engine. With the installed experimental process chain hydrogen is upgraded to fuel cell quality. The current paper has its focus on the membrane separation step which is a key step within the implemented process chain. The overall goal of the research work is to develop the basics for a simple industrially feasible CO_2 neutral hydrogen production process using biomass as raw material.

Gas permeation is a state of art technology which shows its performance in various applicable fields. The novel approach is now its application for the hydrogen separation from renewable resources. At the current case, product gas from an industrial biomass gasification plant is taken for the experiments. Within the executed work, the long-term reliability of the process and the used membrane material is evaluated. Therefore, the pressure of the pretreated gas is increased to 13 barg by a piston compressor. By using a single-stage polymer membrane module provided by Air Liquide™ it is possible to increase the hydrogen concentration from 35-40 %(v/v) up to 80 %(v/v). The experimental setup is operated at stable process conditions for about 20 days without interruption. Within that period no decrease of the performance is seen.

KEYWORDS

Biomass Gasification. Gas Permeation. Hollow Fiber Membrane. Hydrogen. Membrane Separation. Polymeric Membrane

Introduction

Hydrogen, especially when it is produced by using renewable resources, is expected as an important "green" energy carrier of the future (Miltner, Wukovits et al. 2010; Lee 2014). The Vienna University of Technology's Institute of Chemical Engineering has pushed the biomass gasification process technology from lab to industrial scale over the last decade (Kramreiter, Url et al. 2008; Kern, Pfeifer et al. 2013) and has now the possibility to produce hydrogen rich product gas from sustainable biomass. By the thermal biomass steam gasification in a dual fluidized bed it is possible to reach different hydrogen concentrations depending on the process parameters and bed materials (35-45 vol% standard method, 67-75 vol% AER-gas method) (Koppatz, Pfeifer et al. 2009). This gasification technology is proven on an industrial scale and therefore it is logical to consider it as a promising technology for the sustainable production of hydrogen.

It is obvious to apply the polygeneration concept to this process and its further development. The idea behind this strategy is to separate valuable gas components or parts of it at a justifiable and economic approach and use the remaining gas for heat or electricity production. This opens various possibilities and enables the use of different technologies as unit operations. Even if the current work has its focus on membrane technology and the separation of hydrogen by this technology, beside it is very important to give a brief overview on the gas source, pretreatment, and final use of hydrogen.

Figure 1 shows the principle flow diagram of the 8MW biomass gasification plant owned and operated by Energie Burgenland, located at Oberwart, Austria. The pilot plant in Figure 2 uses pre-treated gas directly from this plant and feeds the off gas back to the plant. The position of the connections between plant and pilot plant can also be seen at Figure 1.

Next to hydrogen (H_2) production methane (CH_4), carbon monoxide (CO) and carbon dioxide (CO_2) are produced as main gas components within the gasification process. There are additional gases present but just at minor concentrations. In the current work a principle check about their possible effects to the membrane performance is executed. Table 1 summarizes the average gas composition produced in the plant, including the mentioned trace components for reference.

Table 1: Average inlet gas composition (Pérez 2013) SD … standard deviation

Gas	Concentration %(v/v) d.b.	SD %(v/v) d.b.
H_2	38	2
CO	24	1
CO_2	22	1
CH_4	10	1
C_2H_2	0.20	0.02
C_2H_4	2.7	0.3
C_2H_6	0.20	0.02
C_3H_6	0.06	0.01
N_2	2.4	0.6
O_2	0.08	0.02
H_2O	12	2

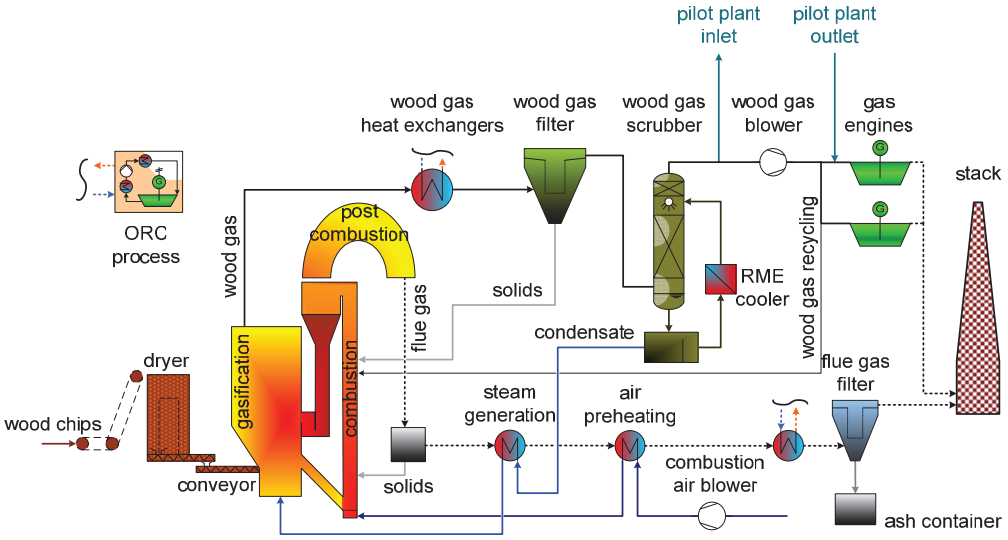

Figure 1: Gasification process (Fail, Diaz et al. 2013)

The experimental process chain is operated with feed streams up to 6 Nm³/h. Dust free and at a first RME scrubber prewashed gas from the plant is taken as a gas source. In Figure 2 the process flow diagram of the experimental process chain is illustrated. The product gas from the plant is fed to an additional chilled RME scrubber which is operated at a low temperature of about 4°C. This cleaning step lowers the tar and water concentration at the gas stream with tolerable effort and guarantees a gas quality which allows executing a membrane separation step. A compressor takes the purified gas from the second scrubber and increases the pressure up to 13 barg. The pressurized gas passes zinc oxide (ZnO) and activated carbon adsorbers before it is fed to the membrane module. The adsorbers act as control filters and it is an aim of the ongoing research to check if they can be removed for further simplification of the process. The second gas chiller is for removing the last water traces from the stream and a standard component of the membrane test setup.

Following the pretreatment steps the gas separation process takes place in the membrane module. Hydrogen has the strongest tendency to permeate through the membrane material and is enriched at permeate side at set pressure level. Methane and carbon monoxide have a low tendency for permeation and almost remain totally at the retentate side still pressurized. The carbon dioxide's ability to permeate is in between these two boundaries. The tendency to permeate is less than the one of hydrogen but still present and therefore a certain amount of carbon dioxide is found at the permeate side.

The methane, carbon monoxide, and carbon dioxide enriched retentate is directly fed back to the industrial plant. The hydrogen enriched permeate is fed to a pressure swing adsorption (PSA) unit for a final precise purification step with the aim to reach fuel cell quality. The remaining CO traces are critical for the installed fuel cell and must finally be below 10 ppm. The PSA unit has the capabilities to do so and electricity is generated from "bio hydrogen" at the installed Axane™ fuel cell.

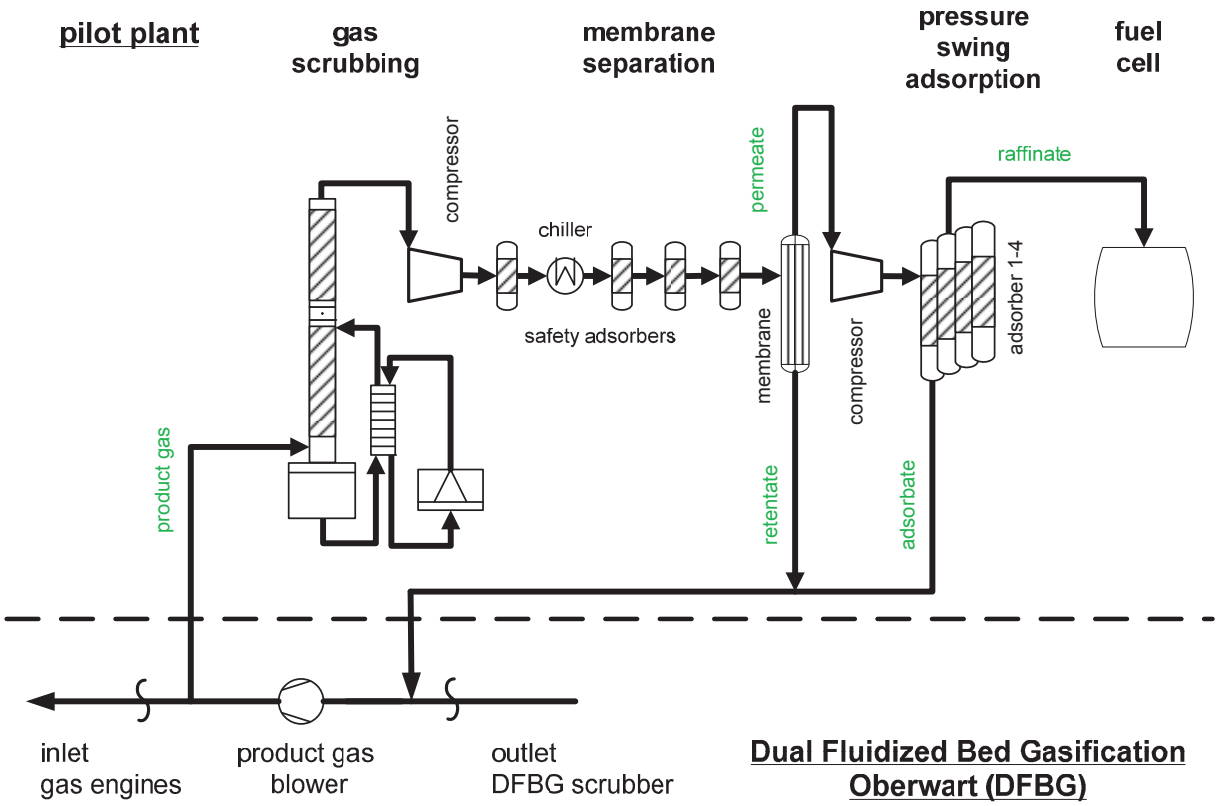

Figure 2: Experimental process chain at the DFBG plant Oberwart

Within the installed pilot plant the possibility to purify the product gas up to fuel cell quality is demonstrated. The stable and continuous operation of the process chain, with focus on possible aging effects of the different equipment, is an important aspect during executed research work.

The idea is to find a setup which allows operating each unit at ideal process conditions in terms of the economic situation. Unused components of the source gas fed back and are utilized in a gas engine for electricity production. The membrane can easily handle bigger volume flows and act as an effective pre-cleaning step to reduce the load of the PSA afterwards. By optimizing each stage it should be possible to generate sustainable hydrogen with purities according to fuel cell specification. Finally, the aim is to reduce the effort and find an economically reliable solution.

Experimental Setup

Within the whole process chain the membrane test rig is in principle a closed unit. It can be operated as a standalone experimental setup. Inside the battery limits a compressor, gas pretreatment, gas temperature control, process analysis, process control, and process data monitoring are implemented. Figure 3 shows the entire membrane test setup at an early project stage and Figure 4 gives a detailed view at the process analysis and insolated membrane module.
In Figure 5 a more detailed flow sheet of the membrane test rig itself can be seen. It also gives an overview about the installed measurement systems.

Figure 3: Full setup of the membrane test unit

Figure 4: Photo of analytic equipment and an insulated membrane module at the membrane test unit

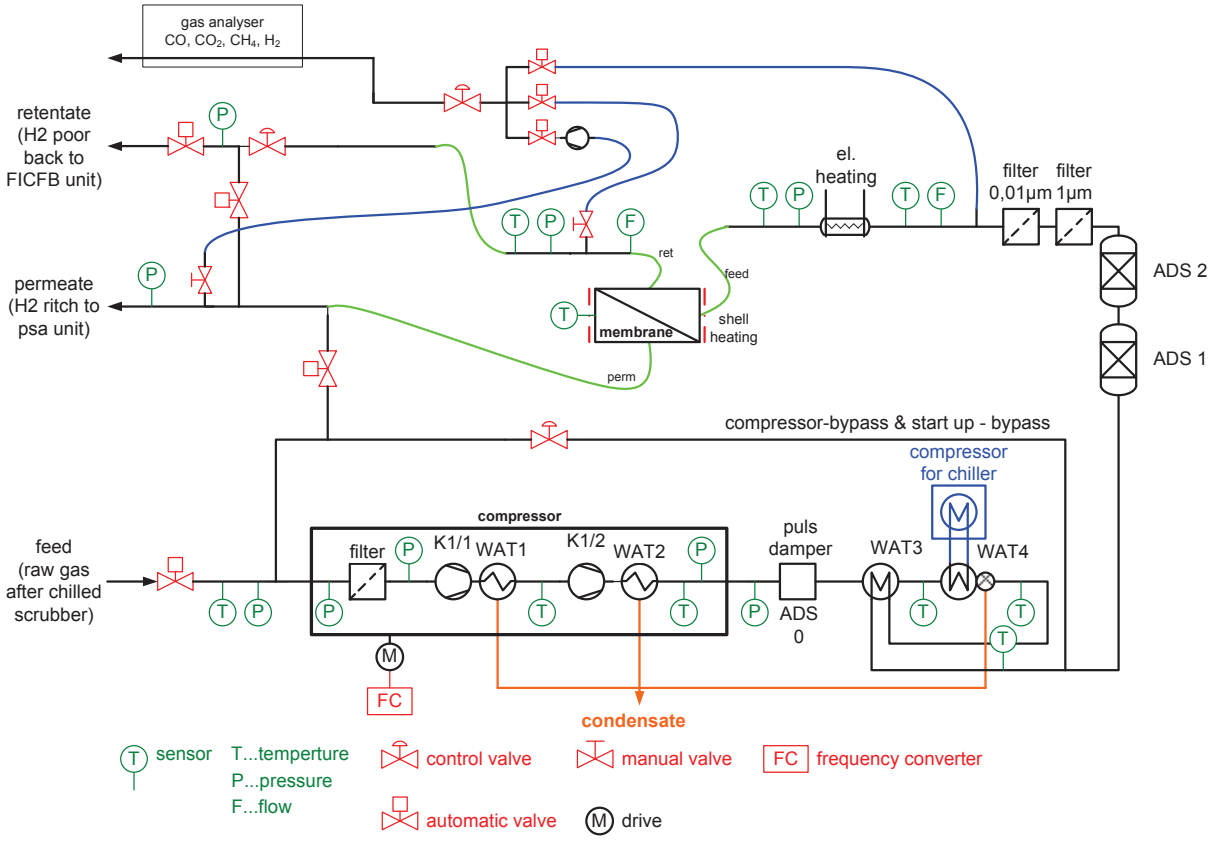

Figure 5: Process flow diagram of the membrane test setup

Compressor

To generate the pressure difference required for the gas permeation process an oil free VTEGX 80/40 LM L compressor obtained from Haug Kompressoren AG is used. It is a two stage system with a 50 to 100 % frequency controlled drive. Feed flows to the membrane below 50 % of the design capacity are possible in case of bypass operation. This guarantees a maximum flexibility. The design flow is 6 Nm³/h and a maximum pressure of 16 barg can be reached. The

compressor has a certificate for operation in Ex-Zone 1. Temperature and pressures are monitored at different positions and a Donaldson candle filter finally protects the compressor from dust or droplets.

Gas Cooling

An EGK 10 sample gas cooler from Sicom Prozeß- und Umwelttechnik GmbH is installed downstream the compressor. In this stage the pressurized process gas is cooled down to 4 °C to condensate the remaining water to protect the membrane from droplets. The condensed water is discharged from the pressurized system by an automatic condensate drain.

Adsorber (ADS) and Filter

To protect the membrane from harmful substances and guarantee ideal process conditions different cleaning steps are foreseen. The ADS 0 positioned directly after the compressor is filled with ZnO granulate to remove sulphuric components from the gas stream. The above mentioned gas cooler is located between ADS 0 and ADS 1. The two following adsorbers are filled with special treated activated carbon granulate. ADS 1 contains Donau Carbon Desorex Pi50K which is a specially treated activated carbon for the removal of benzene, toluene, and xylene (BTX) components. ADS 2 contains a Donau Carbon Desorex K47P which is a phosphoric acid impregnated activated carbon to remove ammonia (NH_3) from the gas stream. After the adsorber there are two Donaldson cartridge filters with a porosity of 1 µm and 0.01 µm installed to remove the dust particles emitted by the adsorber.

Gas Heating

To be able to run the experiments at different temperature levels and at constant conditions an electrical gas heater is installed upstream the membrane module. The gas preheater is built by Elmess Thermosystem-technik GmbH and has a rated power of 500 W. Pressures up to 16 barg and temperatures up to 300 °C could be handled with this system. It is used to set the feed gas temperature to a certain constant level to be able to check the membrane performance at different temperature levels.

Membrane Module

The core part of the test unit is a specialized MEDAL™ hollow fiber membrane from Air Liquide™. The module is built in a way that the gas feed as well as retentate release are located shell side. The installed hollow fibers are blocked at one side and the permeate pressure level is present inside the fibers. The partial pressure difference is the driving force for the separation task. Some components like hydrogen permeate better trough the fibers than others which is the key effect of membrane separation. As a result, the gas stream with the enriched hydrogen concentration leaves the membrane module at the pore side of the fibers as permeate. To be able to guarantee stable temperature conditions a shell heating as well as insulation are installed. Figure 6 shows a sketch of the membrane module. It is installed vertically at the test rig.

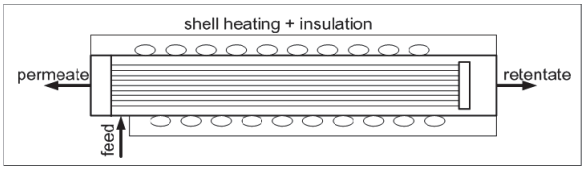

Figure 6: Sketch of the installed membrane module

Gas Analysis

To analyze the gas streams online the extractive gas analyzer GMS 800 obtained from Sick AG is installed. The GMS 800 includes a non dispersive infrared sensor (NDIR) as well as a thermal conductivity detector (TCD) and is able to measure H_2, CO, CO_2, and CH_4 continuously in a range from 0 to 100 %(v/v). The measuring accuracy is +/- 1 % of the measuring range of each component which leads in the present case to an absolute tolerance of +/- 1 %(v/v) for each component.

Figure 5 illustrates the three-sample-point implemented in the system which allows an alternating measurement of feed, permeate and retentate stream. Finally, this manageable monitoring possibility generates a solid fundament for balancing the process. The sampling points are located upstream and after the flow meters. This setup allows continuous measurement without influencing the measured flows at the membrane by taking samples.

Flow Measurement

To measure the volume flows in the system there are two RGV G16 rotary gas meters from Elster-Instromet installed. The flow meters measure the operating gas flow of the feed and the retentate gas stream. Permeate gas flow is calculated from the difference of feed and retentate flow. Temperature and pressure of the streams are continuously measured. Based on that data the normal volume flows are calculated and stored directly at the database of the Programmable Logic Controller (PLC) system. Based on an internal validation procedure of the rotary gas meters at experimental conditions the accuracy is in the range of 0 to -5 %.

PLC and HMI

As for other experimental setups realized at the Vienna University of Technology, Institute of Chemical Engineering, Research Group of Thermal Process Engineering – Computational Fluid Dynamics (Makaruk and Harasek 2009) the PLC type RX3i provided by GE Fanuc is used to control and record all measured process data at this test rig. GE's platform Cimplicity is used as an HMI system for controlling all functions. During critical phases in the experiments a data collection rate of one data set per second can be used. For long-term experiments as in the present case, the sampling frequency is reduced to one set per minute.

Experiment and Results

Within the executed long-term experiment the membrane unit was operated continuously for 465 hours. Figure 7 shows the main process parameter membrane temperature, system pressure feed side, feed flow and permeate flow. It demonstrates the smooth operation of the system based on the collected measurement data. The average values of process conditions including some basic statistical information were calculated and summarized in Table 2

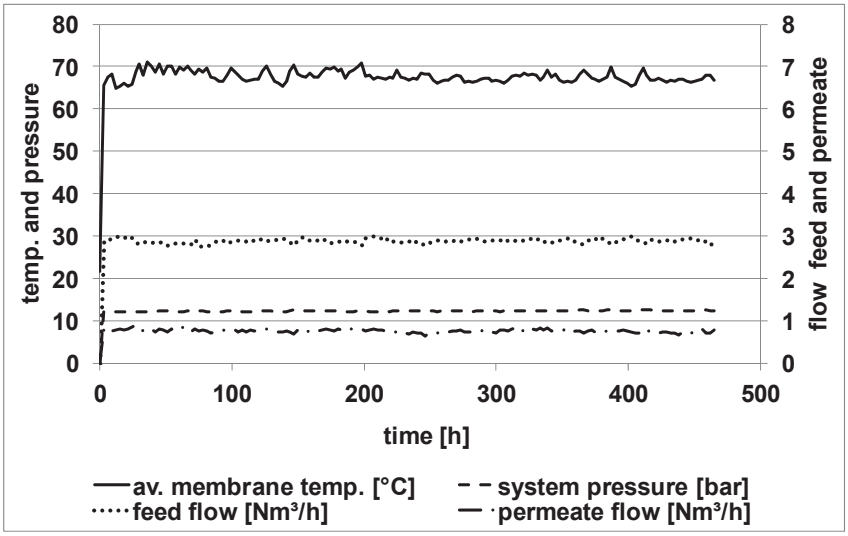

Figure 7: Graph of operation parameters of the long-term experiment

Table 2: Data of the operation parameters of the long-term experiment

	average value	max	min	standard deviation	average error
av. membrane temp. [°C]	67.6	71.1	64.9	1.3	0.10
system pressure [bar]	12.3	12.6	12.1	0.1	0.01
feed flow [Nm³/h]	2.9	3.0	2.8	0.1	0.00
permeate flow [Nm³/h]	0.8	0.9	0.6	0.0	0.00

Within the first operation days the safety absorbers were saturated and so no precision cleaned gas was fed to the membrane module. An important result of the executed long-term test is that no effects like aging or even a performance decrease of the membrane can be detected.

During the experiment an alternating measurement of the gas composition of the different process streams feed, permeate, and retentate is executed. There are only minor fluctuations in the results and therefore the average values for the total experiment period can be calculated easily. The fluctuations itself are determined by periodic variations at the feed gas composition from the plant which take place during normal operation. So it has to be pointed out that the experiments took place in an industrial environment which on the one hand increases variations of measured values but on the other hand has a big impact to the practical relevance of received data.

Figure 8 summarizes the measured gas compositions at the different process streams. It can be seen that the hydrogen concentration could be doubled by the use of just one membrane stage. The concentration of methane and carbon monoxide is strongly reduced in the permeate which demonstrates the good selectivity of these gases in relation to hydrogen. For carbon dioxide there is

just a minor concentration decrease measured which is a result of the lower selectivity for H_2/CO_2 of the used membrane material.

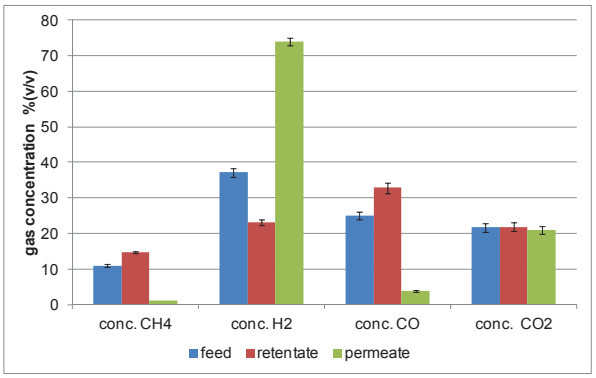

Figure 8: Gas composition at different process streams

The Sankey diagram shown in Figure 9 summarizes gas concentrations and flows at the membrane module. It strikingly points out that the received permeate mainly consists of hydrogen and carbon dioxide. The diagram highlights that the permeate stream contains 53 %(v/v) of the hydrogen which was fed into the membrane. It is a very good value for a one-stage operation, but it can be seen that there is space for improvement and optimization.

Based on the measured data it was possible to close the balance of the system and check how accurate it fits. Table 3 summarizes the balance data of the main gas components and the trace gasses. It can be seen that the balance for single main gasses closes very well and the errors are in the range of only 1% of the feed stream.

The “rest” which is also mentioned in Table 3 is the sum of the trace gasses which have a low permeation rate through the membrane. Within the executed experiment there is no focus on those components. The calculated error for the “rest” is high in relation to the main gas components. The reason is that the amount of this trace gases is small, no direct measurement takes place and so finally the tolerances of used analytical equipment have more impact on the calculated values of the trace gas stream.

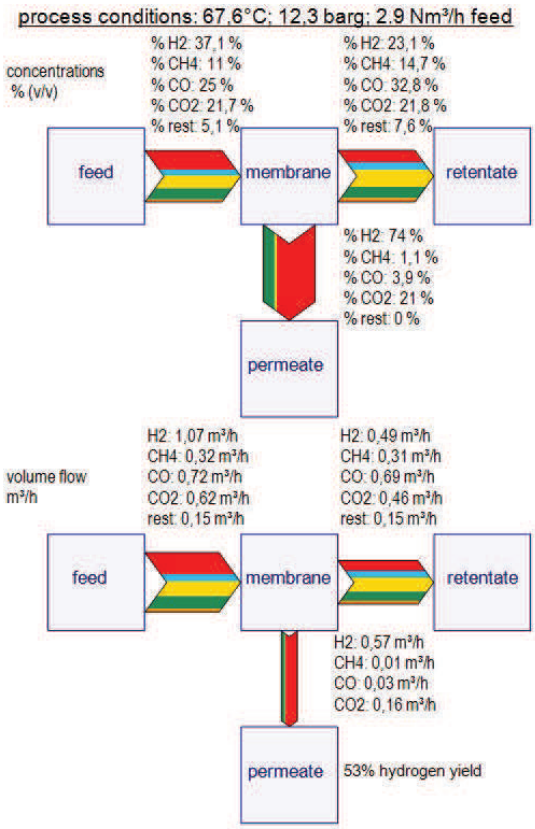

Figure 9: Sankey diagrams of gas composition and flows

In Table 3 the yields for the main gases are indicated. Hydrogen has the biggest yield which can be even improved during further optimization. Carbon dioxide also has a significant yield. This is an undesirable effect and it has to be reduced during further development. The yields for methane and carbon monoxide are small and a desired result. It indicates that the main portion of these gases remain at the retentate side of the membrane and are separated from hydrogen.

Table 3: Balance check and yields for the single gases

	CH_4	H_2	CO	CO_2	rest
feed [m³/h]	0.317	1.068	0.721	0.624	0.148
retentate [m³/h]	0.310	0.489	0.693	0.461	0.160
permeate [m³/h]	0.009	0.565	0.030	0.160	0.000
difference [m³/h]	-0.006	0.014	-0.002	0.003	-0.013
difference [%]	-0.59	1.32	-0.29	0.43	-8.70
yield [%]	2.7	52.9	4.1	25.7	0.0

Based on the available data it is possible to determine the membrane performance based on real, mixed gas data. Therefore, the module permeances for the main components methane, hydrogen, carbon monoxide, and carbon dioxide are calculated. The equation below is used.

$$P_{Module\ x} = \frac{J_x}{\Delta p_x}$$

Wherein $P_{Module\ x}$ [Nm^3_x/(h bara)] is the permeance of a single pure gas component, J_x is the volume flow [Nm³/h] of the gas component x and Δp_x [bara] is the partial pressure difference for the single gas. Table 4 summarizes the permeances for methane, hydrogen, carbon monoxide, and carbon dioxide

By putting the permeances in relation to each other it is possible to calculate the selectivity (α) [-] of different gas combinations.

$$\alpha_{x,y} = \frac{P_x}{P_y}$$

The selectivity is an important indication of membrane performance. Table 5 summarizes determined permeances during the long-term experiment.

Conclusion

Within the 465 hours continuous operation without interruption it has been demonstrated that the entire test setup as well as the membrane unit itself is a robust system. Precision cleaning adsorbers for the gas are fully loaded within the first period of the experiment and the membrane is operated practically without the cleaning system.

Table 4: Pure gas permeances during long-term experiment

	CH_4	H_2	CO	CO_2
Permeances [Nm^3_x/(h bara)]	0.006	0.134	0.009	0.060

Table 5: Membrane selectivity during long-term experiment

Selectivity [-]	CH_4	CO	CO_2	H_2
CH_4	1.0	1.5	10.2	22.8
CO		1.0	6.7	14.9
CO_2			1.0	2.2
H_2				1.0

No performance decrease or any other negative effects were detected and so precision cleaning seems not to be necessary and will be skipped during ongoing experiments. It has been demonstrated that the one-stage membrane process can be used as a reliable pre-conditioning process. The requirements of further separation steps are reduced drastically.

The results obtained up to now are promising and further experiments will be executed. Through different parameter variation experiments the detailed influence of the flow, pressure and temperature for the membrane performance will be evaluated and optimal operation condition has to be found. It is planned to install a second membrane stage and implement a recycle stream to increase hydrogen purity and yield as far as possible. Within the further operation of the membrane unit the performance will be monitored and it will be checked if aging effects take place.

Acknowledgements

The authors would like to thank all project partners and the funding agencies for their assistance and the possibility to execute this work.
Especially:

- Austrian Research Promotion Agency (FFG) for financially supporting the research project *Wasserstoff aus Biomasse zur CO_2-neutralen, effizienten und dezentralen Strom- und Wärmeerzeugung* ("Decentral Green H_2")(Project-Number: 834584).

- Air Liquide Forschung und Entwicklung GmbH. Frankfurt Research & Technology Center (FRTC) and Delaware Research and Technology Center for providing specialized industrial membranes
- CHP-Oberwart and Energie Burgenland for being the host of the experiments and great assistance during every day experimental business
- Martin Miltner and Aleksander Makaruk who are responsible for the backbone of the membrane test rig and its automation systems.
- Silvester Fail and Nicolas Diaz for operation other parts of the process chain and for guaranteeing continuous gas supply

References

Fail, S., M. Diaz, et al. (2013). An Experimental Approach for the Production of Pure Hydrogen Based on Wood Gasification. ICPS 2013, Vienna.

Kern, S., C. Pfeifer, et al. (2013). "Gasification of wood in a dual fluidized bed gasifier: Influence of fuel feeding on process performance." Chemical Engineering Science **90**(0): 284-298.

Koppatz, S., C. Pfeifer, et al. (2009). "H2 rich product gas by steam gasification of biomass with in situ CO2 absorption in a dual fluidized bed system of 8 MW fuel input." Fuel Processing Technology **90**(7–8): 914-921.

Kramreiter, R., M. Url, et al. (2008). "Experimental investigation of a 125 kW twin-fire fixed bed gasification pilot plant and comparison to the results of a 2 MW combined heat and power plant (CHP)." Fuel Processing Technology **89**(1): 90-102.

Lee, D.-H. (2014). "Development and environmental impact of hydrogen supply chain in Japan: Assessment by the CGE-LCA method in Japan with a discussion of the importance of biohydrogen." International Journal of Hydrogen Energy(0).

Makaruk, A. and M. Harasek (2009). "Numerical algorithm for modelling multicomponent multipermeator systems." Journal of Membrane Science **344**(1–2): 258-265.

Miltner, A., W. Wukovits, et al. (2010). "Renewable hydrogen production: a technical evaluation based on process simulation." Journal of Cleaner Production **18, Supplement 1**(0): S51-S62.

Pérez, N. F. D. (2013). Hydrogen separation from producer gas generatad by biomass steam gasification. Doktors der technischen Wissenschaften Dissertation, Vienna University of Technology.

An Experimental Approach for the Production of Pure Hydrogen Based on Wood Gasification

S. Fail[1] and N. Diaz[1, 2], D. Konlechner[1], M. Hackel[3], E. Sanders[4], R. Rauch[1, 2], M. Harasek[1], K. Bosch[5], F. Schwenninger[5], P. Zapletal[6], Z. Schee[6] and H. Hofbauer[1, 2].

1. Vienna University of Technology, Institute of Chemical Engineering, Vienna, Austria.
2. Bioenergy 2020+ GmbH, Güssing, Austria.
3. AIR LIQUIDE™ Forschung und Entwicklung GmbH, Frankfurt Research and Technology Center(FRTC), Germany.
4. AIR LIQUIDE™ America, Delaware Research and Technology Center (DRTC), USA.
5. Energie Burgenland AG. , Eisenstadt, Austria.
6. Technical University of Ostrava, Department of Power Engineering, ENET, Ostrava, Czech Republic.

Abstract

In this experimental work, a unique process chain for hydrogen production based on biomass gasification has been investigated. For almost 100 hours, a pilot plant was operated continuously with 2 Nm³/h of dry product gas, derived from dual fluidized bed steam gasification at the combined heat and power plant in Oberwart, Austria. The implemented process chain consisted of four operation units: (1) sulfur resistant catalysis of the water gas shift reaction, (2) gas drying and cleaning in a chilled rapeseed methyl ester scrubber, (3) hydrogen enrichment via membrane separation and (4) generation of pure hydrogen by means of pressure swing adsorption. High hydrogen yields of all operational units were achieved, resulting in an overall hydrogen recovery of almost 70% (42g/kg dry biomass). The purity of hydrogen was above 99.85%vol.

1. Introduction

More than 100 million Nm³/h of hydrogen are currently produced worldwide. By far the most important application of hydrogen is the production of ammonia (50%), followed by various applications in refineries (22%) and the synthesis of methanol (14%) [1]. 96% of this hydrogen production is directly based on fossil fuels, 49% are derived from natural gas, 29% from liquid hydrocarbons and 18% from coal. The remaining 4% are generated as a by-product from electrolysis and other processes [2]. Large scale production of hydrogen is usually achieved by means of thermochemical oxidative processing of the mentioned fossil fuels. The most important industrial process for hydrogen production is steam reforming of hydrocarbons, especially methane. Besides, catalytic partial oxidation of hydrocarbons and coal gasification are carried out for the generation of hydrogen rich gases [3, 4].

Since the invention of the Haber-Bosch process the hydrogen demand for ammonia production has been rising continuously [5]. Also the consumption of hydrogen in refineries is increasing, as heavy crudes are making up a steadily increasing proportion in refineries. This leads to a reduction of internally produced hydrogen required for hydroprocessing techniques. Finally, upcoming processing of oil sands, gas-to-liquid approaches and the synthesis of liquid hydrocarbons based on coal gasification increase the hydrogen demand in refineries [2].

The growing hydrogen demand, the dependency on fossil fuels with limited long-term availability, considerable amounts of greenhouse gas emissions due to hydrogen production, as well as the on-going discussion about the replacement of fossil fuels by “green” hydrogen led to

numerous research activities aiming for a renewable production of hydrogen. These approaches can broadly be divided into electrochemical approaches, biological processes and thermochemical conversion of biomass (gasification or pyrolysis) [6, 4, 7]. This article addresses the production of H_2 via thermal biomass gasification.

The established routes for hydrogen production based on coal gasification cannot be applied directly for hydrogen production based on biomass gasification. From an economic point of view it is very difficult to predict the availability and the price of biomass for future energy production [8]. From a technological view, different structures and another chemical composition of biomass in contrast to coal have to be faced. This also results in a different composition of gasified biomass and gasified coal [9]. Anyway, coal or biomass gasification is assumed to be the cheapest way of hydrogen generation when natural gas prices are high [3, 7]. A promising technology for hydrogen production from aqueous biomass suspensions is gasification in supercritical water [10, 11]. For solid biomass however, the dual fluidized bed (DFB) steam gasification seems to be an appropriate technology, generating a high calorific gas mixture poor in nitrogen. In the following this gas mixture is referred to as product gas, whereas in literature it is also named synthesis gas or syngas. Especially when applying the sorption enhanced reforming (SER) concept, a hydrogen-rich product gas can be produced [12, 13, 14].

Pure hydrogen based on biomass gasification can only be obtained by means of further processing of the product gas. Different configurations for hydrogen production based on biomass gasification are suggested in literature [15, 16, 17]. Most of the reported work on biomass based hydrogen production is process evaluation by means of simulation. Little experimental data of a complete process chain can be found in the open literature.

In this work, the process chain in Figure 1 is suggested for hydrogen production based on biomass gasification. Regarding an upscale of this experimental approach, this configuration should be considered as a polygeneration concept, aiming the simultaneous production of hydrogen, electricity and district heat. It is not the main purpose to maximize hydrogen yields per biomass input, but to achieve high overall efficiencies and thus economic benefits.

The process chain involves:

(1) CO conversion via sulfur resistant catalysis of the water gas shift (WGS) reaction;

(2) Gas drying and cleaning in a chilled rapeseed methyl ester (RME) scrubber;

(3) Hydrogen enrichment via membrane separation and

(4) Final generation of pure hydrogen by means of pressure swing adsorption (PSA).

(1) Prior to the application of gas cleaning and gas separation techniques, the catalysis of the water gas shift (WGS) reaction (a) was applied in order to produce additional H_2 from the conversion of CO.

(a) $$CO + H_2O \leftrightarrow CO_2 + H_2$$
$$\Delta H^0 = -41.1 kJ/mol$$

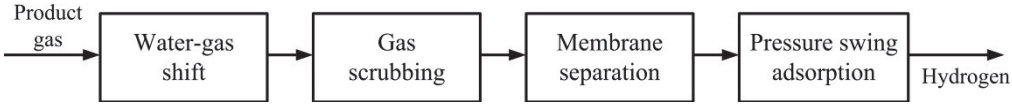

Figure 1: implemented process chain for the production of pure hydrogen starting from product gas based on DFB steam gasification of wood chips.

The surplus of hydrogen was also thought to increase the efficiencies of the subsequent operation units, resulting in higher overall hydrogen yields. Especially, an enhanced efficiency of the pressure swing adsorption unit was expected, as the adsorption of carbon monoxide on activated charcoal is inferior to the adsorption of carbon dioxide [18]. Catalysis of the WGS-reaction is a well-established key technology in industrial hydrogen production based on steam reforming of hydrocarbons. It is normally carried out in a two stage system with a desulfurized feed. A high temperature (HT) stage employing a Fe_2O_3/Cr_2O_3 based catalyst is usually followed by a low temperature (LT) stage with a Cu/Zn based catalyst. Especially the applied catalysts for LT catalysis are vulnerable to sulfur poisoning [19, 20]. At low temperatures the reaction rates diminish and the reaction becomes kinetically controlled [3]. As organic and inorganic sulfur components are present in the biomass-derived product gas, a CoO/MoO_3 based catalyst has been chosen for the suggested process chain in Figure 1. These catalysts require sulfur to be present in the product gas and are resistant to sulfur poisoning. For activation a sulphidation of the catalyst has to be performed in order to create MoS_2 as an active species. During sulphidation, also Co_9S_8 crystallites are formed which are said to act as promotor for the MoS_2 [21].

(2) Product gas from biomass gasification contains NH_3, H_2S and high molecular weight organic compounds (tars) which must be removed prior to further gas utilization. A highly effective approach toward the removal of tars is absorption in organic solvents. As a secondary effect, condensation of water takes place in the scrubber, allowing the removal of water-soluble gaseous trace components such as NH_3 and H_2S from the gas stream. Both Austrian DFB gasification power plants (Güssing and Oberwart) employ gas scrubbing in rapeseed methyl ester (RME) prior to gas utilization in gas engines. Lowering the scrubbing temperature and increasing the amount of fresh solvent enhances the separation efficiency for tars with low boiling point, NH_3 and H_2S [22, 23, 24], respectively.

(3) Membranes are barriers which, by their physical nature, enable components to permeate selectively across them. For polymer membranes, gas separation is explained via a solution-diffusion mechanism. Separation is a product of solubility and mobility through a solid barrier [25]. Polymer membrane technology is a commercially viable separation process and especially efficient for the separation of CO_2, CH_4 (natural gas sweetening, biogas upgrading, and enhanced oil recovery [26]) and for hydrogen separation from gaseous mixtures consisting of nitrogen, carbon monoxide, or hydrocarbons [25]. It is also used for N_2 generation from compressed air. Providing an operation with a suitable feed composition on an appropriate scale, membrane-related processes are a promising technology for the production of high-purity hydrogen [25]. In the context of this work, a membrane was implemented to increase the efficiency of the subsequent PSA unit.

(4) The PSA process is based on physical binding of gas molecules to an adsorbent material. The forces acting between the gas molecules and the adsorbent material depend on the gas component, type of adsorbent material, partial pressure of the gas component and operating temperature. Highly volatile components with low polarity, such as hydrogen, are practically non-adsorbable in contrast to CO, CO_2, hydrocarbons and water vapor. Consequently, these impurities can be adsorbed from a

hydrogen-containing stream and high purity hydrogen is recovered [27]. Major commercial PSA processes include H_2 and CO_2 recovery, air separation, landfill gas separation and separation of hydrocarbons. The largest PSA processes are generally found in petroleum refineries. In a typical hydrogen purification process the product purity is commonly 99.995%vol. or higher [27].

The presented process chain was operated with real product gas from the commercial biomass steam gasification process in Oberwart, Austria (Figure 2). The equipment was placed in laboratory containers next to this combined heat and power (CHP) plant. The design of the CHP plant is based on the well documented biomass gasification plant in Güssing, Austria [28]. It is the second commercial plant implementing the innovative dual fluidized bed (DFB) steam gasification technology, proved first of its kind in Güssing, Austria. In both plants a high calorific gas mixture poor in nitrogen is produced, which is cleaned by means of filters and scrubbers and subsequently burned in gas engines generating electricity and district heat. In comparison to Güssing, several modifications have been implemented in Oberwart. The main differences are an installed biomass dryer and an organic rankine cycle (ORC) process in order to increase the electric efficiency. Generally, these modifications follow the suggestions for improvement given in the final report of the "Big power" project [29]. Only few publications dealing with the CHP plant in Oberwart can be found in literature [30, 31, 32].

Starting from the chilled gas scrubber, a simplified configuration of the process chain in Figure 1 has already been operated for more than 1000 hours. This process will be subject to future publications. The scope of this 100 hours lasting experiment was to study the influence of a preliminary WGS unit on the overall performance of the process chain. The project also disposes of a 2.5kW Mobixane® fuel cell from AXANE™. The investigation of this fuel cell will also be subject to future publication.

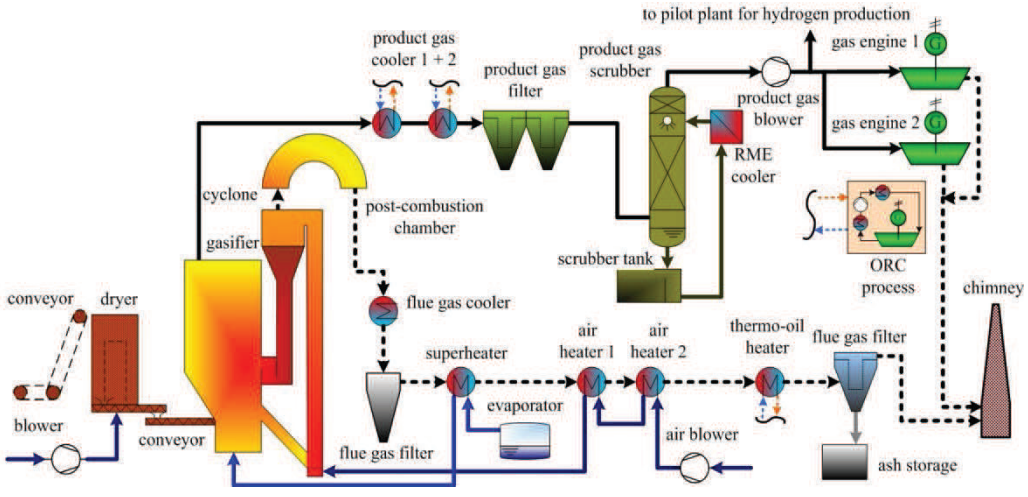

Figure 2: design of the combined heat and power plant in Oberwart (Austria), the process is based on dual fluidized bed steam gasification of biomass.

2. Concept and methodology

The product gas fed into the pilot plant was extracted after gas cleaning of the CHP plant Oberwart [31]. On the one hand, particles have been removed in industrial baghouse filters. On the other hand, the majority of heavy tars present in the product gas have been separated in a gas scrubber [22, 23]. Also, it can be considered that the product gas exits the RME-scrubber with an equilibrium humidity corresponding to its temperature and pressure at the outlet [24]. During experimentation, product gas left the RME scrubber of the CHP plant with a temperature of about 44°C, resulting in an average water content of 10%wt. in the product gas being fed into the pilot plant. With approximately 40% H_2, 24% CO, 21% CO_2 and 10% CH_4 the dry gas composition was typical for DFB biomass steam gasification. The detailed composition can be found in Table 6. Figure 3 presents an extended flow chart of the studied process chain described first in Figure 1. In terms of a polygeneration concept, the side streams produced in the membrane permeation unit (retentate) and in the PSA unit (adsorbate) were fed back into the CHP plant. After analysis, also the PSA raffinate, composed of almost pure hydrogen, was recycled to the power plant.

2.1. WGS unit

High temperature WGS catalysis at about 375°C has been realized in three fixed bed reactors. A commercial CoO/MoO_3 based catalyst was implemented. Prior to product gas admission, the catalyst was activated by sulphidation.
The product gas was extracted from the power plant with a heated and flow controlled membrane pump (Figure 3). Before entering the catalyst bed, steam had to be added to enhance the water gas shift reaction and to prevent coking at the surface of the catalyst [33, 34]. Therefore, a peristaltic pump was used to feed water into an evaporator generating process steam. The flow rate of water could be

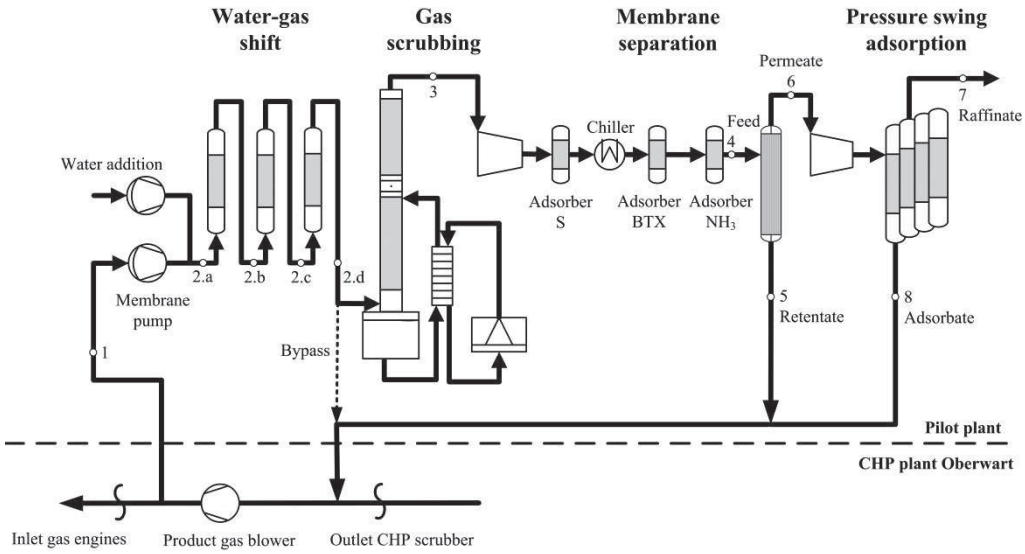

Figure 3: flow chart of the applied process chain for hydrogen production based on wood gasification, the test rigs have been operated with about 2Nm³/h of dry product gas from the CHP plant Oberwart, Austria.

adjusted by rotation speed control. A flow meter was used to control the actual flow rate of added water. Subsequently, the steam loaded gas was heated up to the desired reaction temperature and introduced into the three fixed bed reactors connected in series. Process control was achieved by several thermocouples and pressure sensors distributed over the system. Catalyst temperature inside the reactors was monitored every 10cm along the fixed bed. Gas hourly space velocity (GHSV) and the steam to carbon monoxide ratio (S/CO) were adjusted by choosing an appropriate combination of rotation speeds of both pumps.

The GHSV over the catalyst could be calculated according to a water balance over the WGS unit. The water content at the inlet was measured gravimetrically (condensation of water in cooled impinger bottles filled with glycol and subsequent quantification of dry gas in a gas meter) and was also validated by calculating the equilibrium steam content of the product gas at the outlet of the CHP scrubber. The water content at the outlet of the WGS reactors was measured gravimetrically, allowing a closure of the water balance and the total molar balance over this unit.

Table 1 provides the reaction conditions of the WGS unit.

Table 1: Operation conditions of the WGS unit.

WGS unit	Value	Units
Flow rate wet gas	4.6 ± 0.2	Nm³/h
GHSV wet basis	565 ± 20	h^{-1}
Water content inlet	58 ± 2	% mol.
H_2O/CO	6 ± 0.4	-
Pressure	100 ± 25	mbar(g)
Temp. reactor 1	385 ± 17	°C
Temp. reactor 2	385 ± 7	°C
Temp. reactor 3	330 ± 6	°C

The CO conversion rate (X_{CO}) defined in equation (b) was used as a characteristic factor for the evaluation of the performance of the WGS catalysis.

(b) $$X_{CO} = \frac{\dot{n}_{CO\ in} - \dot{n}_{CO\ out}}{\dot{n}_{CO\ in}}$$

2.2. Scrubber unit

The water gas (WG) shifted gas subsequently entered a cleaning and cooling stage. A chilled gas scrubber operated with rapeseed methyl ester (RME) was employed for gas drying and absorption of tars and ammonia from the gas stream. This gas scrubber was operated at lower temperatures than the RME scrubber from the CHP plant Oberwart. A countercurrent flow of the gaseous and liquid phase over a structured packed column (Sulzer Mellapak®) has been implemented, cooling down the gas stream and therefore condensing the majority of the process water. The flow of RME was arranged in a circuit. A centrifugal pump continuously charged the packed column with cooled RME. Cooling of RME was achieved in an external plate heat exchanger. Ethylene glycol was used as coolant liquid, which in turn was cooled in an external chiller (HAAKE Phoenix II C41P). For safety reasons, the chilled RME scrubber was connected in bypass processing only a partial flow of the WG shifted gas (Figure 3, Table 1, Table 2). Table 2 summarizes the steady state operation conditions of the chilled gas scrubber.

Table 2: Operation conditions of the chilled RME scrubber.

Scrubber unit	Value	Units
Flow rate (dry)	0.97 ± 0.01	Nm³/h
Temp. gas inlet	67 ± 1	°C
Temp. gas outlet	21 ± 1	°C
Mean pressure	35 ± 4	mbar(g)
RME circulation	700	L/h
Fresh RME input	1.5	L/h

2.3. Membrane permeation unit

After preliminary evaluation of three different membranes, a polymer based membrane module from Air Liquide™ was chosen for further enrichment of hydrogen in the gas mixture.
Entering the membrane unit, the pre-dried feed from the chilled RME scrubber was initially compressed to 13 bars (find Figure 3). After compression, H_2S present in the feed was removed on zinc oxide granulate. Subsequently, a heat exchanger cooled the gas down to 4°C in order to condense the remaining water. Two additional adsorbents have been used to remove undesired trace components. Activated charcoal has been implemented to adsorb residual tar components as well as benzene, toluene and xylenes (BTX). Activated carbon impregnated with phosphoric acid was used to remove NH_3. A particle filter was applied to prevent particles from entering the membrane module. Hydrogen preferentially permeated the membrane resulting in enhanced hydrogen concentrations in the low pressure permeate. Methane and carbon monoxide were accumulated in the high pressure retentate. The permeate was further used for final processing of pure hydrogen in the PSA unit. The retentate was expanded and recycled to the CHP plant. All relevant process parameters have been measured continuously and registered automatically at low time scale. A series of thermocouples and pressure sensors were implemented to control the process. Gas meters were used to quantify the flow rates of feed and retentate. For process control, the main gas components were measured continuously via non-dispersive infrared (NDIR) for CO, CO_2 and CH_4 and a thermal conductivity sensor for quantification of H_2. The process conditions shown in Table 3 were chosen for membrane separation.

Table 3: Operation conditions of the membrane permeation unit.

Membrane unit	Value	Units
Feed flow rate	0.97 ± 0.09	Nm³/h
Feed pressure	12.0 ± 0.1	bar(g)
Temp. module	25 ± 5	°C

2.4. PSA unit

The membrane permeate was further processed by a pressure swing adsorption unit for hydrogen purification. The desired adsorption pressure was built up with a gas compressor (KNF® PM 25821-186). The unit was equipped with four 4.72L adsorber vessels, each filled with 2.5kg of activated charcoal (Norit RB2®). Desorption under vacuum was achieved using a diaphragm vacuum pump (Pfeiffer® MVP020-3AC). At the bottom, each vessel was connected to one control valve leading to the gas compressor (for feeding the vessel while adsorption) and one solenoid valve leading to the vacuum pump (for regeneration of adsorbent by desorption). At the top, each vessel was connected with one solenoid valve leading to a buffer vessel (for gas production) and one control valve leading to the other three absorbers (for pressure equalization and repressurization). A constant adsorption pressure was achieved by means of a back pressure valve situated at the exit of the buffer vessel.

Product purity and recovery were used to define the performance of the studied PSA system. These characteristic values are strongly dependent on the operation conditions. Table 4 summarizes the chosen operation parameters for pressure swing adsorption in the reported experiment. The cyclic operation of the four adsorbers is summarized in Figure 7 in the annex.

Table 4: Operation conditions of the PSA unit.

PSA unit	Value	Units
Adsorption pressure	6.5	bar(a)
Adsorption time/cycle	12.0	min
Desorption pressure	0.15	bar(a)
Equalization pressure	5.0	bar(a)
Purge/feed time ratio	$5 \cdot 10^{-3}$	-
Feed flow rate	0.40 ± 0.08	Nm^3/h
Feed pressure	1.03 ± 0.01	bar(a)
Cyclic operation	Figure 7 in the annex	

The hydrogen recovery of each operation unit was calculated according to the equation given in (c).

$$H_{2_{Recovery}} = \frac{\dot{n}_{H2\ out}}{\dot{n}_{H2\_in}} \quad \text{(c)}$$

In the case of the membrane permeation unit, the outlet was considered as the hydrogen flow in the permeate. For the PSA unit the referred outlet was the molar flow of the generated raffinate.

2.5. Analytics

As described in Table 5, an exhaustive analysis of all streams has been carried out in order to present a complete characterization of the entire process chain. The sampling points are also plotted in Figure 3.

Table 5: Gas sampling points and employed analytical techniques.

Nr.	Name	GC	GC/MS	HPIC
1	WGS entry dry	✓	✓	✓
2.b 2.c 2.d	WGS exit reactor 1(b), 2(c), 3(d)	✓ ✓ ✓	✓	✓
3	Scrubber exit	-	✓	✓
4	Membrane feed after adsorbers	✓	✓	✓
5	Membrane retentate	✓	✓	✓
6	Membrane permeate	✓	✓	✓
7	PSA raffinate	✓	✓	✓
8	PSA adsorbate	-	-	-

A Clarus 500® gas chromatograph from Perkin Elmer® was used on site to analyze the main gas components as well as the present organic and inorganic sulfur impurities at the sampling points 1 to 7. A thermal conductivity detector (TCD) was employed to detect CO, CO_2, CH_4, C_2H_2, C_2H_4, C_2H_6, CH_4, N_2 and O_2. An additional flame photometric detector (FPD) enabled the detection of the sulfur components H_2S, COS, CH_3SH, CH_3CH_2SH and C_4H_4S. Benzene, toluene and xylenes (BTX) were quantified by gas chromatography–mass spectrometry (GC-MS, Shimadzu QP2010 Plus®) from samples of the points 1 to 7 taken in sampling bags. The BTX analysis was carried out at the Vienna University of Technology directly after sampling. An absorption method was used for quantification of NH_3. For 30 min, a sampling stream of 3 NL/min was taken from the process and passed through three impinger bottles which were arranged in a cooling bath at 0 °C. The impinger bottles were filled with 0.05 M H_2SO_4, which solves NH_3 in the form of NH_4^+ ions.

Subsequently NH_4^+ was detected by ion chromatography (Dionex ICS 5000®). Sampling for tar analysis was performed by means of impinger bottles filled with toluene. A gas chromatograph from Perkin Elmer® (XL GC®) coupled with a mass spectrometer from Perkin Elmer® (Turbo Mass MS®) was used subsequently to measure the content of 50 different tar species. A detailed description of the applied method for tar analysis can be found in [35]. Data reconciliation was carried out by applying the process simulation software IPSEpro®. The software was provided with all available gas concentrations from GC analysis and the measured flow rates from membrane feed and retentate. The permeate flow rate was calculated by closing the mass balance over the membrane unit. The data reconciliation entailed small deviations of the measured values and the presented results in chapter 3. Equilibrium calculations for WGS catalysis have been accomplished using the chemistry software HSC® minimizing the Gibbs free energy.

3. Results and discussion

Table 6 depicts the mean gas concentrations over 100 hours of operation. Each sampling point of the process chain is defined in Table 5 and Figure 3. All dry gas compositions, except for adsorbate gas from the PSA unit, have been analyzed by means of gas phase chromatography. The presented data are partly reconciled, closing the mass balances of the entire process chain. Besides, a comprehensive analysis of the sulfur components was carried out (Table 7). Sulfur measurements have not been reconciled and are plotted with the corresponding standard deviations. BTX analyses are shown in Table 8. Analysis of ammonia is presented in Table 9.

Table 6: Gas concentrations (dry) along the process chain, * Reconciled data, ** Calculated data from mass balance, below detection limit (BDL) : <0.0001%vol.

Component	Unit	H_2	CO	CO_2	CH_4	C_2H_2	C_2H_4	C_2H_6	N_2	O_2
1. Raw PG	%vol.	39.73	23.58	21.38	9.94	0.13	2.47	0.21	2.43	0.15
2d. WGS exit	%vol.*	49.99	5.63	32	8.13	BDL	2.13	0.4	1.7	0.03
5. Retentate	%vol.*	31.8	9.33	38.49	13.67	BDL	3.19	0.67	2.82	0.04
6. Permeate	%vol.*	76.08	0.3	22.67	0.17	BDL	0.06	0.01	0.08	0.09
7. Raffinate	%vol.	99.85	0.001	0.01	0.001	BDL	BDL	BDL	0.09	0.052
8. Adsorbate	%vol.**	37.76	0.78	59.27	0.44	BDL	0.03	0.01	0.131	0.002

Table 7: Measured concentrations of sulfur components along the process chain, below detection limit (BDL) : <0.2ppm$_v$, n/a*: not available, measurement was carried out during tar analysis over toluene filled impinger bottles, thiophene (C_4H_4S) is strongly absorbed in toluene.

Component	Unit	H_2S	C_4H_4S	COS	MeSH	EtSH
1. Raw PG	ppm$_v$	96 ± 7	9 ± 2	1.8 ± 0.4	BDL	BDL
2d. WGS exit	ppm$_v$	94 ± 7	19 ± 3	0.4 ± 0.1	BDL	BDL
3. Scrubber exit	ppm$_v$	80 ± 7	n/a*	0.3 ± 0.1	BDL	BDL
4. Membrane feed	ppm$_v$	BDL	0.2 ± 0.5	0.4 ± 0.1	BDL	BDL
5. Retentate	ppm$_v$	BDL	3 ± 1	0.9 ± 0.1	BDL	BDL
6. Permeate	ppm$_v$	BDL	BDL	BDL	BDL	BDL
7. Raffinate	ppm$_v$	BDL	BDL	BDL	BDL	BDL

Table 8: BTX analysis over the process chain, benzene (Ben.), toluene (Tol.), xylenes (Xyl.), BDL: <1ppm$_v$.

Component	Unit	Ben.	Tol.	Xyl.
1. Raw PG	ppm$_v$	6183	388	15
2d. WGS exit	ppm$_v$	5728	388	107
3. Scrubber exit	ppm$_v$	5009	162	14
6. Permeate	ppm$_v$	288	28	7
7. Raffinate	ppm$_v$	BDL	BDL	BDL

Table 9: Ammonia (NH_3) analysis along the process chain, BDL: <0.3ppm$_v$.

Component	Unit	NH_3
1. Raw PG	ppm$_v$	1460 ± 200
2d. WGS exit	ppm$_v$	1010 ± 70
3. Scrubber exit	ppm$_v$	2.3 ± 0.6
4. Membrane feed	ppm$_v$	BDL
7. Raffinate	ppm$_v$	BDL

Tar analysis was carried out at three different sampling points of the process chain. The corresponding results are stated in Table 10.

Table 10: Tar composition (dry base) in the raw product gas (1), the outlet of the WGS unit (2d), and the exit of the chilled scrubber (3).

	1	2.d	3
	mg/ Nm^3	mg/ Nm^3	mg/ Nm^3
Total gravimetric tar	19	24	13
Total GC/MS tar	4625	3211	116
Naphtalene	3376	2923	81
1H-Indene	462	48	4
Styrene	456	3	3
Acenaphtylene	150	2	2
Phenylacetylene	43	0	0
2-Methylnaphthalene	31	28	2
Biphenyl	19	18	1
1-Methylnaphthalene	18	13	2
Benzofuran	14	7	4
Flourene	7	6	2
Dibenzofuran	7	6	2
Anthracene	6	6	0
Acenaphtene	5	104	1
Phenanthrene	5	5	0
Quinoline	5	4	0
Phenol	5	5	0
1-Benzothiophene	5	3	0
Pyrene	4	4	0
Flouranthene	4	3	0
Isoquinoline	3	3	0
Mesitylene	0	19	0

3.1. WGS unit

Figure 4 illustrates the effect of temperature on the equilibrium gas composition of the gas mixture entering the WGS reactors (Table 6). Only the equilibration of the WGS-reaction was taken into consideration. For simplification, all components not taking part in the WGS reaction were summarized as an unreactive species ("no WGS"). In this graph, the achieved gas composition after the WGS unit is plotted at the outlet temperature of the last reactor (330°C).

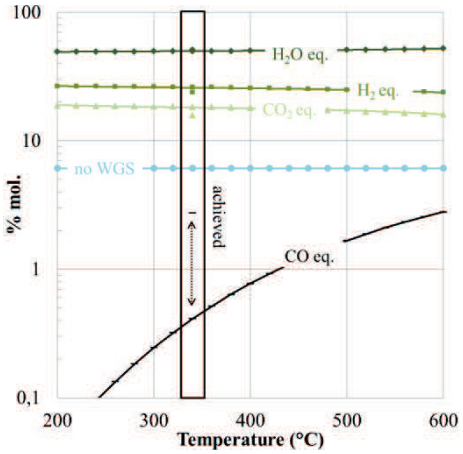

Figure 4: Temperature dependence of the WGS equilibrium of the wet gas entering the WGS unit; logarithmic scale; the achieved composition at the exit of the WGS unit was plotted at the outlet temperature of the last reactor.

The WGS-reaction is moderately exothermic (ΔH^0 = -41.1kJ/mol), which leads to higher equilibrium concentrations of the reactants at elevated temperatures. Regarding the performance of the WGS unit, the CO content was lowered from ~24%vol. to ~6%vol. in the dry gas, representing a CO conversion rate of about 72% and an equilibration of the WGS-reaction up to 75% ($\dot{n}_{CO_{out}} / \dot{n}_{CO_{out\_eq}}$). At the same time the water content was lowered from 58%mol. to 51%mol. and due to hydrogen production, the dry flow rate was increased from 1.92Nm³/h to 2.26Nm³/h. The observed conversion rate seems to be low, as it is reported in literature that Co-Mo catalysts are capable of reducing the CO content in a feed gas derived from coal gasification to less than 1% [20]. In this experiment the WGS reaction was carried out at a GHSV (wet basis) of about $600h^{-1}$ which is in the range of operation of commercial high temperature WGS reactors employing Fe_2O_3/Cr_2O_3 catalysts ($400\text{-}1200h^{-1}$) [3]. Co-Mo

catalysts are said to be more active than Fe_2O_3/Cr_2O_3 catalysts [3] but less active than copper based catalysts applied for low temperature WGS catalysis [20]. These catalysts are usually operated at GHSV of 4800 to 24000h^{-1}, pressures between 5 and 27bar and temperatures between 250 and 300°C [3]. In [36, 37, 38] commercially available Fe-Cr catalysts and a commercial Co-Mo catalyst for hydrogen production have been investigated in a synthetic coal derived product gas. For the Co-Mo catalyst, high H_2S concentrations in the feed were found to enhance the conversion of CO. In the studied range from 330ppm_w to 2670ppm_w H_2S in the dry gas, the activity of the catalyst increased strongly [38]. In the present experiment the H_2S content in the feed of the WGS unit was below 170ppm_w in the dry gas. On the other hand, it is reported in literature that the CO conversion rate increases linearly with an increase in total pressure [37]. Pressure does not have a significant influence on the equilibrium of the WGS reaction but on kinetics [3]. With respect to these articles, the rather low conversion rate during this experiment could be explained by low H_2S concentrations in the feed (<100ppm_v in the dry gas), as well as the low operation pressure (~100mbar(g)).
During experimentation of the coupled process chain, samples were taken after each reactor of the WGS unit. This allowed an investigation of the dependence of the CO conversion ratio on the GHSV. These results are illustrated in Figure 5.

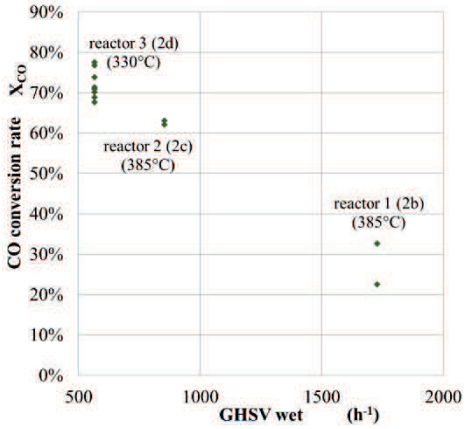

Figure 5: CO conversion rate (X_{CO}) depending on GHSV wet (h^{-1}).

Besides the catalysis of the WGS-reaction, a complete hydrogenation of acetylene as well as a partly hydrogenation of ethylene were observed. Regarding the influence of the WGS catalyst on the composition of the sulfur components, a reduction of the COS content at the reactor outlet was observed. This could be explained by the reactions (d) and (e) [39].

(d) $H_2S + CO \leftrightarrow COS + H_2$
(e) $H_2S + CO_2 \leftrightarrow COS + H_2O$

Furthermore, an increase in thiophene at the exit of the WGS unit was observed. The production could not be explained by the reaction of thiophene hydrogenolysis (f). The equilibrium of this reaction in the present gas mixture is strongly on the side of butane production [20].

(f) $C_4H_4S + 4H_2 \leftrightarrow C_4H_{10} + H_2S$

Therefore, thiophene is suggested to be generated from a conversion of furan [40] (not analyzed) or other tars in the presence of H_2S. Regarding the BTX analysis, an increase in xylene content was observed over the WGS unit. In the WGS unit the detected GC/MS tar

content was lowered from 4.6 to 3.2 g/Nm³. Especially significant reductions of styrene and indene were observed. Acenaphthylene was hydrogenated to acenaphthene. Also, mesitylene could be detected after WGS catalysis, although it was not present in feed.

3.2. Scrubber unit

The WGS unit and the RME scrubber have been connected via 15m of trace heated stainless steel pipes. Due to controlled heat losses the WG-shifted gas, leaving the last reactor with 330°C, entered the scrubber with a temperature of 67°C. Gas temperature as well as the content of BTX and tars at the outlet, were characteristic for the performance of the scrubber. In the course of the experiment, the chiller turned out to be not suitable for the coupled process chain. Due to the high water content of the gas entering the scrubber unit (~51%) and the high enthalpy of water condensation, the targeted exit temperature of 5°C could not be reached. Tars were reduced from a total of 3211mg/m^3 to 116mg/m^3. Also at the exit of the scrubber, naphthalene turned out to be the most important tar component. High removal levels were accomplished for toluene and xylenes. However, benzene was not removed significantly. This could be explained with the low amount of fresh RME added and the relatively high operation temperature in the scrubber (above the melting point of benzene). Finally, the frequently reported efficient removal of ammonia by means of the condensed water in the scrubber could be observed [22, 23, 24].

3.3. Membrane unit

H_2S could not be detected in the feed of the membrane and was, therefore, removed efficiently with the employed ZnO adsorber. Also, the phosphoric acid impregnated activated carbon reduced the NH_3 content in the membrane feed below the limit of detection. The only impurities which could still be detected in the feed of the membrane were less than 1ppm of thiophene and carbonyl sulfide and BTX components.
0.97Nm³/h of dry gas were further processed in the membrane unit. At the present operation conditions (12bar(g) and ambient temperature), the feed was separated according to Table 11.

Table 11: Partition of the membrane feed in the applied module.

Permeate flow rate	0.40 ± 0.08	Nm³/h
Retentate flow rate	0.57 ± 0.06	Nm³/h

The hydrogen content in the permeate could be enriched up to 76%vol. Especially the low CO content of 0.3%vol. in this gas mixture was representing a good condition for the subsequent pressure swing adsorption.

3.4. PSA unit

During the experiment, analysis of the main gas components at the outlet of the PSA unit was carried out continuously for almost 10 hours. The measured raffinate composition as a function of time is illustrated in Figure 6.

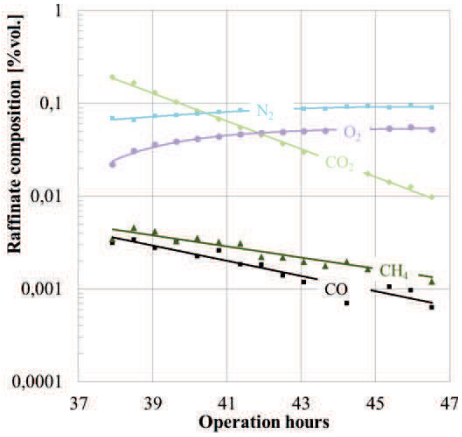

Figure 6: Continuous analysis of the raffinate composition at the exit of the PSA unit.

The increasing purity of the generated hydrogen flow could be explained by time-demanding flushing of the analytical sampling line. During this experiment an equilibration of the composition could not be achieved. The reported impurities in Table 6 are equivalent to the gas composition at the end of the continuous analysis in Figure 6, even though the content of undesired components (CO, CO_2 and CH_4) was probably lower as reported here. This assumption is also confirmed by more recent experiments, where the detection limit of CO, CO_2 and CH_4 could be reached with an improved analytical sampling line.

With the presented PSA unit, a hydrogen purity of 99.85%vol. as well as a hydrogen recovery of 76% could be achieved. This is within the range of similar PSA systems reporting hydrogen purity up to 99.99%vol. and hydrogen recoveries between 70 and 85% [41, 42, 43, 44].

No traces of sulfur compounds, benzene, toluene, xylenes or ammonia were detected in the raffinate (Table 7, Table 8 and Table 9).

The most important impurities were 0.09%vol. of N_2 and 0.05%vol. of O_2 (Table 6). These components have already been contained in the feed gas and were not removed completely over the entire process chain. N_2 and O_2 in the product could have been removed in applying a multiple adsorbent bed involving a layer of zeolite with an enhanced capacity for these gases [43].

To facilitate the desorption process, only a single layer of activated carbon was preferred to a mixed bed with zeolite. Activated carbon has relatively moderate strengths of adsorption for the relevant gases, whereas CO_2 is adsorbed almost irreversibly on zeolite [18].

3.5. Hydrogen recovery

Table 12 gives an overview of the achieved hydrogen recoveries of each operation unit.

Table 12: Overview of the hydrogen recoveries of each operation unit.

Component	Unit	H_2 recovery
WGS unit	-	1.38
Scrubber unit	-	1
Membrane unit	-	0.66
PSA unit	-	0.76
Overall	-	0.69

Based on cold gas efficiency, low heating values and the stated wood composition (19%wt. water content) by Wilk et al. [45] an overall hydrogen yield for the presented process chain of 42g/kg of dry biomass was calculated. Toonssen et al. simulated hydrogen production based on five different commercial or pilot scale gasification systems. Among various sceneries a hydrogen yield of 96g/kg of dry biomass was calculated for a 10 MW DFB steam gasification power plant including low temperature gas cleaning, reforming of hydrocarbons, two step WGS catalysis and a PSA process [15]. Comparable hydrogen yields are also presented by [46]. The next chapter

demonstrates a series of possible improvements of the presented configuration. A further approximation to simulated hydrogen yields in literature is feasible and desired. Anyway, values in the order of magnitude of 100g/kg of dry biomass are not possible due to the absence of a steam reforming unit.

4. Conclusion and Outlook

The accomplished hydrogen yield of about 70% over the entire process chain was a satisfactory result. Also the purity of the generated hydrogen came up to the expectations. During the reported 100h of operation including WGS catalysis, the raffinate did not meet the high standards from ISO 14687 and SAE J2719. Anyway it can be considered, that the operation of a proton exchange membrane (PEM) fuel cell is viable. N_2 as the most important impurity is only reported to entail a dilution effect. O_2 should be tolerated up to 500ppm$_v$ [47].

With respect to the numerous operational units and their interactions it is apparent that the investigated process chain still has a big potential of optimization. A series of desirable improvements have been discovered during the presented experiment and isolated test runs of the single operation units. For instance, the catalysis of the WGS reaction has not yet been optimized for the presented process chain. It turned out that conversion rates at these GHSV would have been enhanced at more elevated operation temperatures. Especially it is favorable to operate the first WGS reactor near maximum temperature of the catalyst. High initial conversion rates would have been achieved due to the great influence of temperature on reaction kinetics. Temperature level in the subsequent reactors should be decreased deliberately, in order to benefit from the low equilibrium CO contents at reduced temperatures. Also, the operation of the gas scrubber could be improved by lower operation temperatures.

The membrane permeation unit with a reconciled recovery of about 66% has been operated at conditions which turned out to be suitable for direct processing of product gas. For the WG shifted gas however, the optimum operation conditions are likely to be different. Therefore it is assumed, that also the hydrogen yield of the membrane unit can still be increased by adjusting the process parameters. Further improvements of the membrane separation unit could also include a multi-stage process with more than one membrane. Moreover it would be desirable to introduce a reverse selective membrane which could reduce the number of essential compression steps [48]. The implemented gas cleaning stages upstream the module were designed very carefully to avoid damage of the polymer membrane. With respect to an industrial application of similar approaches, present experiments are investigating the reduction of these measures to a minimum operating expense.

Especially, for the operation with water gas shifted feed, also more optimization work is necessary for the PSA system. The goal is to achieve hydrogen purities which allow an operation of the available PEM fuel cell from AXANE^{TM}. At the same time, the hydrogen yield of the PSA unit has to be maximized.

An overall hydrogen yield of 80% for the complete process chain could already be achieved in another test run with an incomplete characterization of the entire process chain.

5. Acknowledgements

The authors would like to thank all project partners involved. Especially we want to thank the research and

development division from AIR Liquide™. Furthermore we would like to thank the CHP-Oberwart and Energie Burgenland® for a stable supply of product gas and operation resources. Automation was carried out by cts® (competence for technical solutions) and the working group from Michael Harasek (Vienna University of Technology). Manufacturing was supported by Jörg Artner and Binder Industrieanlagenbau®. The coupling of both test rigs could only be achieved with the help of Michael Weitzer. Also, we would like to thank Ivan Bergamo, Martin Miltner, Aleksander Makaruk and Christian Jordan for their collaboration. Nicolas Diaz received financial support from Conicyt-Becas Chile. Bioenergy2020+ is funded within the Austrian COMET program managed by the Austrian Research Promotion Agency (FFG). The financial support of the funding association FFG and the Austrian Climate and Energy Fund is gratefully acknowledged.

6. References

[1] A. DÜKER, Hydrogen-Production and Application in Industry, in *Presentation Süd-Chemie*, Süd-Chemie AG, 2011.

[2] B. M. BIZZARI, S. N., Chemical Industries Newsletter CEH Marketing Research Report Abstract- Hydrogen, Technical report, SRI Consulting, 2007.

[3] V. S. LIU, K; CHUNSHAN SONG, *Hydrogen and Syngas Production and Purification Technologies*, Wiley, 2010.

[4] IEA, Hydrogen Production and Distribution, International Energy Agency - Energy Technology Essentials, 2007.

[5] C. FRANCESCO, D. KRAMER, and L. APODACA, Nitrogen (fixed) - ammonia statistics, 2010.

[6] R. CHAUBEY, S. SAHU, O. O. JAMES, and S. MAITY, *Renewable and Sustainable Energy Reviews* **23**, 443 (2013).

[7] M. NI, D. Y. LEUNG, M. K. LEUNG, and K. SUMATHY, *Fuel Processing Technology* **87**, 461 (2006).

[8] M. HOOGWIJK, A. FAAIJ, R. VAN DEN BROEK, G. BERNDES, D. GIELEN, and W. TURKENBURG, *Biomass and Bioenergy* **25**, 119 (2003).

[9] S. KERN, C. PFEIFER, and H. HOFBAUER, Dual fluidized bed steam gasification of coal and biomass: influence of the state of pyrolysis on the process performance, in *Clean Coal Conference*, 2013.

[10] Y. MATSUMURA, T. MINOWA, and B. POTIC, *Biomass and Bioenergy* **29**, 269 (2005).

[11] Y. CALZAVARA, C. JOUSSOT-DUBIEN, G. BOISSONNET, and S. SARRADE, *Energy Conversion and Management* **46**, 615 (2005).

[12] C. PFEIFER, B. PUCHNER, and H. HOFBAUER, *International Journal of Chemical Reactor Engineering* **5**, 1542 (2007).

[13] S. KOPPATZ, C. PFEIFER, R. RAUCH, H. HOFBAUER, T. MARQUARD-MOELLENSTEDT, and M. SPECHT, *Fuel Processing Technology* **90**, 914 (2009).

[14] T. PRÖLL and H. HOFBAUER, *Fuel Processing Technology* **89**, 1207 (2008).

[15] R. TOONSSEN, N. WOUDSTRA, and A. H. VERKOOIJEN, *International Journal of Hydrogen Energy* **33**, 4074 (2008).

[16] M. STEINBERG and H. CHENG, *International Journal of Hydrogen Energy* **14**, 797 (1989).

[17] S. MUELLER, M. STIDL, T. PROELL, R. RAUCH, and H. HOFBAUER, *Biomass Conversion and Biorefinery* **1**, 55 (2011).

[18] S. SIRCAR, T. GOLDEN, and M. RAO, *Carbon* **34**, 1 (1996).
[19] I. N. J. CHORKENDORFF, *Concepts of Modern Catalyis and Kinetics*, Wiley-VCH, 3rd reprint 2013 edition, 2013.
[20] M. V. TWIGG, *Catalyst Handbook-Chapter 6: The Water-gas Shift Reaction*, Manson Publishing, 1989.
[21] M. BRUNE, *Verfahren zur Entschwefelung von flüssigen handelsüblichen Brennstoffen*, Scientific Publishing, 2009.
[22] H. HOFBAUER, , R. RAUCH, and K. BOSCH, Zwischenbericht Wäscher, Report for Renewable Energy Network Austria 12, Technische Universität Wien, Insitut für Verfahrens-, Brennstoff- und Umwelttechnik, 2000.
[23] H. HOFBAUER, R. RAUCH, K. BOSCH, and I. G. SIEFERT, Produktgasreinigung Lösungsmittel - Wäscher, Report for Renewable Energy Network Austria 34, Technische Universität Wien, Insitut für Verfahrenstechnik, Umwelttechnik und technischen Biowissenschaften, 2002.
[24] T. PRÖLL, I. G. SIEFERT, A. FRIEDL, and H. HOFBAUER, *Industrial & Engineering Chemistry Research* **44**, 1576 (2005).
[25] S. ADHIKARI and S. FERNANDO, *Industrial & Engineering Chemistry Research* **45**, 875 (2006).
[26] Y. ZHANG, J. SUNARSO, S. LIU, and R. WANG, *International Journal of Greenhouse Gas Control* **12**, 84 (2013).
[27] D. M. RUTHVEN, *Pressure Swing Adsorption*, VCH, 1994.
[28] H. HOFBAUER, R. RAUCH, K. BOSCH, R. KOCH., and C. AICHERNING, *Biomass CHP Plant Güssing – A Success Story*, CPL Press, 2003.
[29] E. KURKELA and M. KURKELA, Advanced Biomass Gasification for High-Efficiency Power, Publishable Final Activity Report of BiGPower Project, Technical report, VTT, TUV, Kokemäen Kaasutin, Carbona, RPT, MEL, Norta, GEJ, MTU, BKG, CERTH, TKK, Clear Edge, 2009.
[30] F. KIRNBAUER, J. KOTIK, and H. HOFBAUER, Investigations on inorganic matter in DFB biomass steam-gasification plants in Güssing/Austria and Oberwart/Austria, in *19th European Biomass Conference and Exhibition*, p. 6, 2011.
[31] J. KOTIK, *Über den Einsatz von Kraft-Wärme-Kopplungsanlagen auf Basis der Wirbelschicht-Dampfvergasung fester Biomasse am Beispiel des Biomassekraftwerks Oberwart ausgeführt*, PhD thesis, Technische Universität Wien, 2010.
[32] H. HELLSMARK and S. JACOBSSON, *Energy Policy* **37**, 5597 (2009).
[33] Y. SHIRATORI, T. IJICHI, T. OSHIMA, and K. SASAKI, *International Journal of Hydrogen Energy* **35**, 7905 (2010).
[34] E. XUE, M. O'KEEFFE, and J. ROSS, *Catalysis Today* **30**, 107 (1996).
[35] U. WOLFESBERGER, I. AIGNER, and H. HOFBAUER, *Environmental Progress & Sustainable Energy* **28**, 372 (2009).
[36] S. S. HLA, D. PARK, G. DUFFY, J. EDWARDS, D. ROBERTS, A. ILYUSHECHKIN, L. MORPETH, and T. NGUYEN, *Chemical Engineering Journal* **146**, 148 (2009).
[37] S. S. HLA, G. DUFFY, L. MORPETH, A. COUSINS, D. ROBERTS, and J. EDWARDS, *Catalysis Communications* **11**, 272 (2009).
[38] S. S. HLA, G. DUFFY, L. MORPETH, A. COUSINS, D. ROBERTS, and J. EDWARDS, *International Journal of Hydrogen Energy* **36**, 6638 (2011).
[39] L. LI and D. L. KING, *Catalysis Today* **116**, 537 (2006).
[40] Q. LI, Y. XU, C. LIU, and J. KIM, *Catal Lett* **122**, 354–358 (2008).

[41] J. YANG, S. HANA, C. CHOB, C.-H. LEE, and H. LEE, *Separations Technology* **5**, 239 (1995).
[42] S. AHN, Y.-W. YOU, D.-G. LEE, K.-H. KIMB, M. OH, and C.-H. LEE, *Chemical Engineering Science* **68**, 413 (2012).
[43] A. M. RIBEIRO, C. A. GRANDE, F. V. LOPES, J. M. LOUREIRO, and A. E. RODRIGUES, *Chemical Engineering Science* **63**, 5258 (2008).
[44] J.-H. PARK, J.-N. KIM, and S.-H. CHO, *AIChE Journal* **46**, 790 (2000).
[45] V. WILK, H. KITZLER, S. KOPPATZ, C. PFEIFER, and H. HOFBAUER, Gasification of residues and waste wood in a dual fluidised bed steam gasifier, in *ICPS Leipzig*, 2010.
[46] S. MÜLLER, *Hydrogen from Biomass for Industry - Industrial Application of Hydrogen Production Based on Dual Fluid Gasification*, PhD thesis, Vienna University of Technology, 2013.
[47] B. M. BESANCON, V. HASANOV, R. IMBAULT-LASTAPIS, R. BENESCH, M. BARRIO, and M. J. MØLNVIK, *International Journal of Hydrogen Energy* **34**, 2350 (2009).
[48] C. H. LAU, P. LI, F. LI, T.-S. CHUNG, and D. R. PAUL, *Progress in Polymer Science* **38**, 740 (2013).

7. Annex

PSA automation

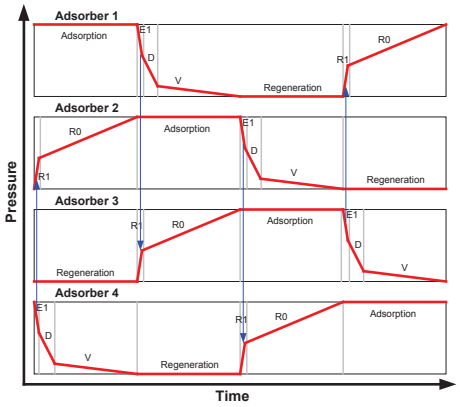

Figure 7: Cyclic sequence steps of the PSA test rig.

The pressure swing adsorption unit in the pilot plant was equipped with an automation system to control the cyclic operation of the adsorbers. Figure 7 illustrates the cyclic sequence of the PSA, which considers the following seven steps:

(1) Adsorption at high pressure, with raffinate withdrawal to repressurize the next bed.
(2) Pressure equalization (E1), cocurrent depressurization.
(3) Dump step (D), countercurrent depressurization of the adsorber to produce the tail gas.
(4) Vacuum (Regeneration), countercurrent regeneration of the bed by desorption at low pressure with.
(5) Purging (Regeneration), countercurrent regeneration of the bed at low pressure with highly pure hydrogen from the adsorption step.
(6) First repressurization (R1), countercurrent repressurization carried out by using pure hydrogen from the adsorber presently under depressurization (pressure equalization step).
(7) Final repressurization (R0), countercurrent repressurization is carried out with a split stream from the hydrogen product line until the required pressure level is reached.

Efficient Biomass Utilization by Polygeneration Processes- Production of Hydrogen, Electricity and Heat

Tamara Mayer[1], *Aleksander Makaruk*[2], *Nicolas Diaz*[1], *Klaus Bosch*[1], *Martin Miltner*[2], *Michael Harasek*[2] *and Hermann Hofbauer*[2]

1. Bioenergy 2020+ GmbH, Wienerstraße 49, 7540 Güssing
2. Institute of Chemical Engineering, Vienna University of Technology, Getreidemarkt 9/166, 1060 Wien

tamara.mayer@bioenergy2020.eu

ABSTRACT
A polygeneration process is about to be implemented at the biomass gasification plant in Oberwart, Austria. Apart from conventional heat and electricity production, product gas obtained from gasification of wood chips is used for production of hydrogen. A membrane separation process was chosen for this application. Meeting the requirements of robustness and simplicity are additional benefits of this technology. Simulation results show the gas compositions of both permeate and retentate stream as a function of different membrane stage-cuts. Basically high hydrogen content in the permeate stream can be achieved, but only with the drawback of low stage-cuts. Moreover, the trade-off between hydrogen purity and hydrogen recovery as well as the influence of the operating pressure on the purity are illustrated.

Keywords: polygeneration, biomass, gasification, membrane, hydrogen

1 INTRODUCTION

Polygeneration represents one appropriate concept towards an efficient utilization of resources for energy generation and fuels production. With regard to the limited availability of renewable resources, among them especially biomass resources, efficiency in terms of consumption and utilization becomes a vital.
Polygeneration is defined as production of at least three different products, which in case of gasification typically are heat, electricity and biofuels [1].

Based on the concept of polygeneration, the fundamental idea of this project is to produce heat, electricity and hydrogen from product gas obtained from biomass gasification. Thereby, the overall aim is to develop economic feasible process configurations. This could be achieved on the one hand by realizing a polygeneration concept and as a consequence gaining more than one product. On the other hand process chains should be created which meet the requirements of both robustness and simplicity.

As illustrated in figure 1, the gasification process uses solid biomass as feedstock and produces gas. The produced gas undergoes gas cleaning and is processed further for production of heat and electricity. In addition, a slip stream is taken after the gas cleaning step. The slip stream passes an additional cleaning step, which is necessary for further gas processing. Afterwards, the gas is compressed and finally it is led to the separation unit. For the separation (enrichment) of hydrogen from the product gas a membrane separation process

is applied. The membrane splits the feed gas into two main gas streams, a low-pressure permeate and a high-pressure retentate stream. The permeate stream is mainly composed of hydrogen. The retentate stream (off-gas stream) contains components which remained at the feed-side of the membrane. In order to avoid any losses, the off-gas is recycled and utilized for heat and electricity production.

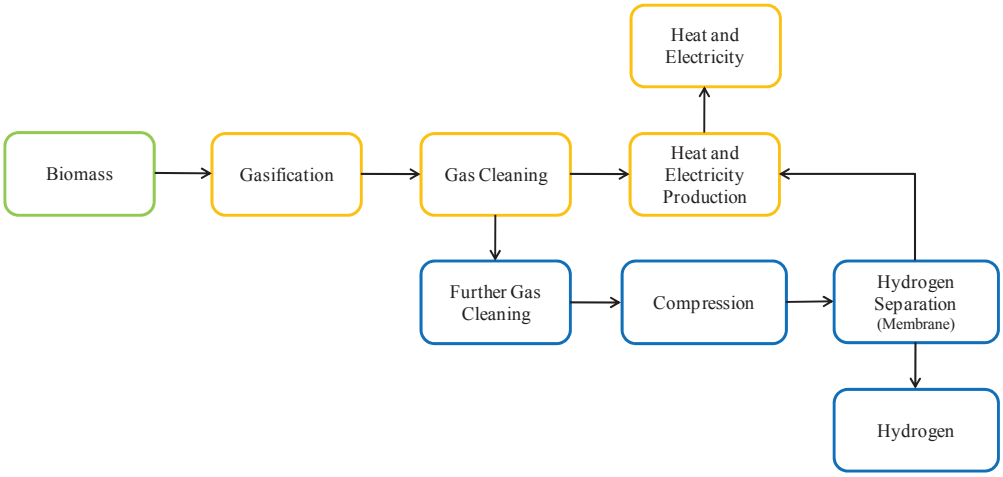

Figure 1. Flow sheet of polygeneration process

2 DESCRIPTION OF THE POLYGENERATION PROCESS

The polygeneration concept described above is being implemented at the biomass gasification plant located in Oberwart, Austria. The gas produced in this plant was commonly used to produce heat and electricity, but in order to improve energy utilization and simultaneously meet the requirements of the polygeneration idea, a hydrogen production process is about to be put into operation.

2.1 Heat and Electricity Production

Figure 2 shows a simplified process flow sheet of the CHP plant Oberwart. Solid wet biomass (wood chips) is used as feedstock for the gasification process. The biomass is dried before it is fed into the gasifier. The gasification process is based on the dual fluidized bed technology. Accordingly, one fluidized bed is dedicated for a gasification process (fluidization with steam) whereas the other fluidized bed (fluidization with air) performs a combustion process. Combustion is necessary for generating heat which is transferred through a circulating bed material to the gasification reactor in order to maintain the endothermic gasification process. Corresponding to the concept of two fluidized beds, two different gas streams are produced. In case of the gasification reactor product gas is obtained and in case of the combustion reactor it is flue gas.

Each of these two gases undergoes a certain gas treatment. The flue gas passes a gas cooler and a gas filter where particulate matter is separated. Afterwards it is led to the chimney.
Treatment of the product gas obtained from gasification also includes cooling, filtering and additional scrubbing. Within the product gas scrubber, which is operated with biodiesel (rape seed methyl ester), removal of water and tars takes place. By undergoing this treatment, the product gas gets conditioned for its further application in the gas engine.

A typical composition of the product gas at this stage of the process is given in table 1. Furthermore, the product gas contains apart from tars, trace components. Among them are nitrogen-, sulphur- and chlorine compounds.

Table 1. Typical composition of product gas from biomass steam gasification in a dual fluidized bed gasifier after internal gas cleaning (Data from Güssing gasifier) [2]

main components	value	unit
H_2	35…45	vol% (dry)
CO	19…23	vol% (dry)
CO_2	20…24	vol% (dry)
CH_4	7…10	vol% (dry)
C_xH_y	2.5…4	vol% (dry)
N_2	0.7…2	vol% (dry)

The product gas is used as a fuel in a gas engine for electricity and heat production. The off-gas (flue gas) from the gas engine passes an oxidation-catalyst and a cooler and is finally led to the chimney.
Moreover, additional electricity can be produced by an ORC (Organic Rankine Cycle), which is also implemented at the plant. Heat from both flue gas and producer gas contributes to the operation of the ORC.
In case of gas engine failure the product gas can optionally be fired in a district heating boiler.

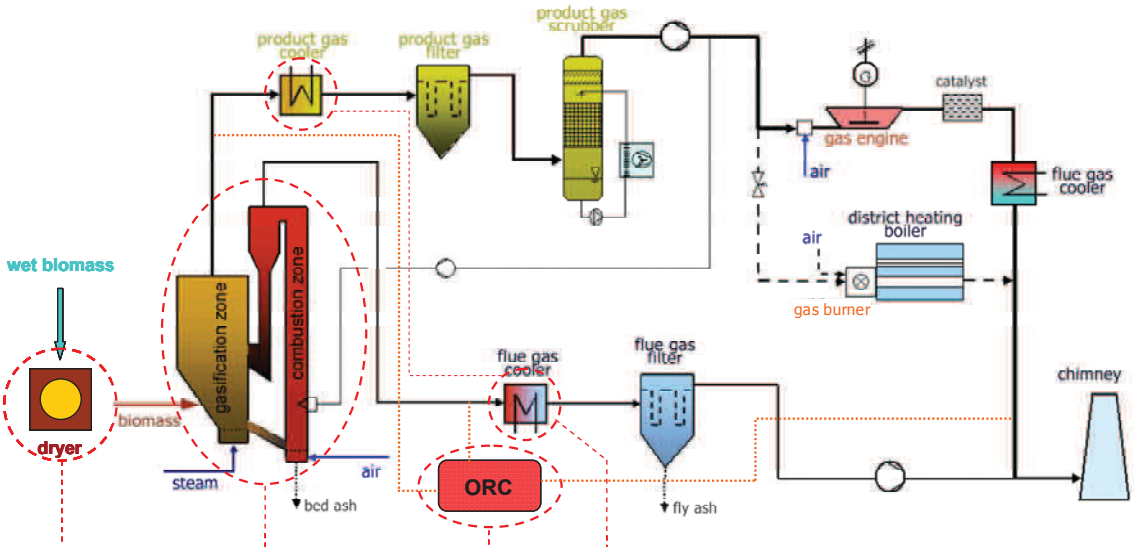

Figure 2. Simplified flow sheet of CHP plant Oberwart [3]

2.2 Hydrogen Production

For hydrogen production, a slip stream of the product gas is taken after the product gas scrubber. A membrane separation technology was chosen for separating hydrogen from the product gas. This separation technology is considered to be well suited for this application and it meets the requirements of robustness as well as simplicity.

Since the membrane has more stringent requirements with regard to gas purity compared to a gas engine, the product gas has to be further cleaned. The further cleaning consists of a second scrubber, also operated with biodiesel, but contrary to the first scrubber its operating temperature is lower. In addition an adsorptive gas cleaning is installed in order to remove much of the trace components, which otherwise could lower the performance of the membrane. After undergoing these cleaning steps the product gas is compressed to a certain pressure level and fed into the membrane.

The separation process is realized as single stage process. The feed stream is split into two streams, obtaining one permeate and one retentate stream. The permeate stream represents the product stream, containing gas components which were transported through the membrane (mainly hydrogen). On the contrary, the retentate stream represents a residual stream, consisting of gas components which remained on the feed side of the membrane.

Separation of hydrogen from the product gas by means of a membrane separation technology is in this case based on the principle of gas permeation. Gas permeation allows separation of gas mixtures without a change in the phase. Separation of different gases or gas components is achieved due to differences in molecular size and gas solubility in the membrane. [4]

The ideal selectivity represents the most important parameter for describing membrane performance. Ideal selectivity is defined as permeability ratio of two gases or two components *i* and *j* of one gas and is given as

$$\alpha_{i/j} = \frac{P_i}{P_j} = \frac{D_i / D_j}{K_i / K_j}$$

P ... Permeability

D ... Diffusion coefficient

K ... Sorption coefficient

The ratio of diffusion coefficients indicates the relative motion of the molecules of the two components *i* and *j* and can therefore be considered as mobility selectivity. It is proportional to the ratio of molecular size of the two components.
The ratio of the sorption coefficients (sorption selectivity) indicates the relative concentration of the two components *i* and *j* in the membrane material and is proportional to the relative condensability of the components. [5]

The applied membrane separation process uses hollow-fiber membrane modules. More precisely, the actual membrane is constructed as a hollow-fiber and a certain number of hollow-fibers are bundled to form a module. The membrane consists of polyimide, which is a glassy polymer. Separation properties of glassy polymers heavily depend on the molecular size of the involved molecules [5]. Table 2 shows typical selectivities of the considered polyimide membrane for the mentioned components over longer alkanes (C_xH_y).

Table 2. Selectivities of the modeled polyimide membrane for main gas components of product gas

gas component	$\alpha_{component/CxHy}$
H_2	750.0
CO_2	83.3
CO	10.0
N_2	4.2
CH_4	2.5
C_xH_y	1.0

3 SIMULATION OF HYDROGEN PRODUCTION

3.1 Theoretical Background

Numerical modeling was employed in order to preliminarily investigate the applicability of the membrane separation process (gas permeation) for the separation of the hydrogen from product gas. The recently developed numerical algorithm uses a one-dimensional Gauß-Seidel finite difference method for the calculation of multicomponent transmembrane flows in membrane gas permeation systems. The algorithm was rigorously validated in a multicomponent permeation experiment and provided good agreement with the experimental results [6].

3.2 Boundary conditions of the simulation

In this work it was assumed that the gas transmembrane flow is ruled exclusively by the solution-diffusion mechanism. Moreover it is assumed that the membrane permeances are independent on other process parameters. Furthermore the flux-coupling effects as well as pressure losses along the membrane fibers in the feed channel and in the permeate channel were neglected.
The modeled case considered in this work is a single membrane stage operated in the counter-current configuration. It is assumed that the membrane stage is equipped with the membranes made of polyimide in the form of hollow-fibers.
The assumed feed gas composition for modeling is presented in table 3.

Table 3. Assumed feed gas composition for modeling

gas components	value	unit
H_2	39.8	vol%
CO	22.3	vol%
CO_2	22.4	vol%
CH_4	10.3	vol%
C_xH_y	3.2	vol%
N_2	2.0	vol%

3.3 Results

Figure 3 shows the hydrogen content in the permeate stream, what can be viewed as hydrogen purity, as a function of hydrogen recovery. Hydrogen recovery is defined as follows:

$$hydrogen\ recovery[\%] = \frac{hydrogen\ in\ permeate\ flow}{hydrogen\ in\ feed\ flow} * 100\% .$$

Furthermore, the figure also illustrates the pressure dependence of this function for pressures of five bar and 15 bar.

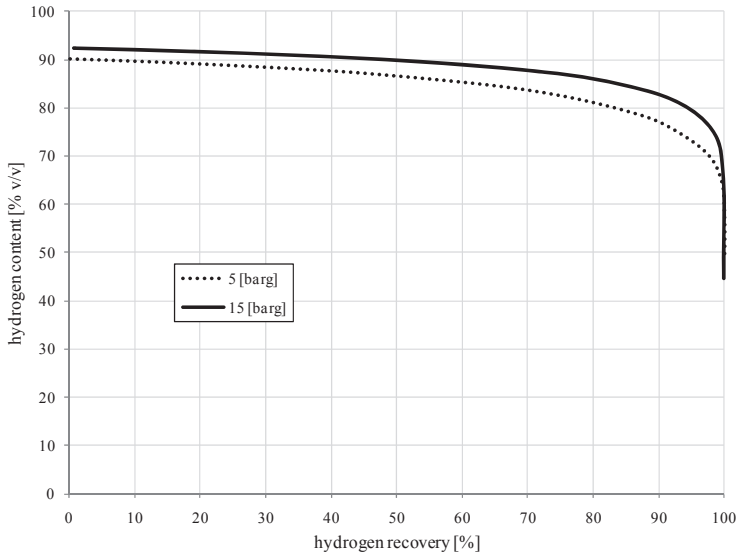

Figure 3. Hydrogen purity versus hydrogen recovery

The typical trade-off between recovery and purity can be observed. While at lower hydrogen recoveries hydrogen purities of above 90% are possible, an increase of hydrogen recovery leads to a decrease of hydrogen purity down to 80% or lower.
Referring to the pressure dependence, an increase of the operating feed gas pressure causes an improvement of the hydrogen purity. In order to give an example, at a hydrogen recovery of i.e. 60% the hydrogen purity would be about 87% at a pressure of five bar. However, at a pressure of 15 bar the hydrogen purity would increase up to a value of approximately 89%.

Figure 4 depicts the content of the gas components in the permeate stream versus the membrane stage-cut at an operating feed gas pressure of 15 bar. The membrane stage-cut is defined as follows:

$$membrane\ stage-cut = \frac{permeate\ flow}{feed\ flow} .$$

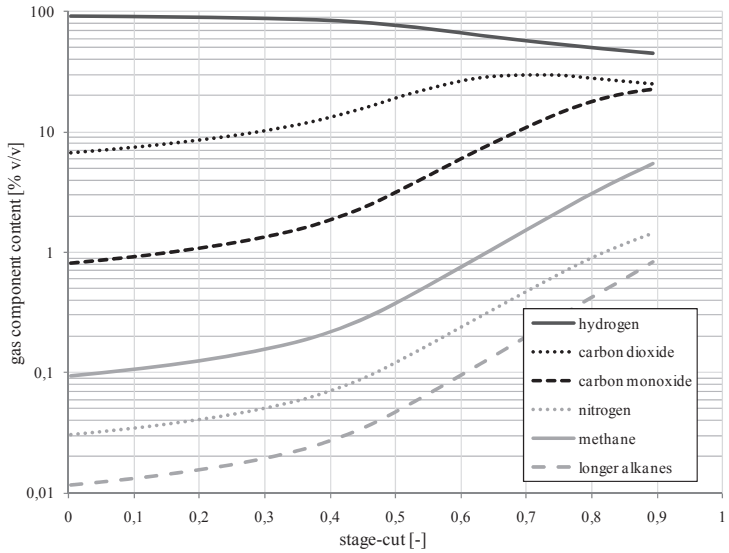

Figure 4. Gas composition of the permeate stream versus membrane stage-cut

As can be seen in this figure, the produced permeate stream is mainly composed of hydrogen. Apart from hydrogen, the gas also contains other gas components which also permeated at lower rate through the membrane. The amount of these gas components in the hydrogen-rich gas depends on the membrane stage-cut. In the range of lower stage-cuts (~ 0.15) a content of approximately 8 vol% of carbon dioxide can be expected in the produced gas (permeate stream). The next prevalent gas component is carbon monoxide with a content of approximately 1 vol%. The contents of other gases such as nitrogen, methane and lower alkanes are expected to be below 2000 ppmv.
In general, an increase of membrane stage-cut results in a decrease of the hydrogen content and in an increase of the amounts of other gases.

Figure 5 illustrates the content of the gas components in the retentate stream versus the membrane stage-cut at an operating feed gas pressure of 15 bar. This figure is a supplement to figure 4, since figure 4 shows the composition of the permeate stream under equal process conditions.

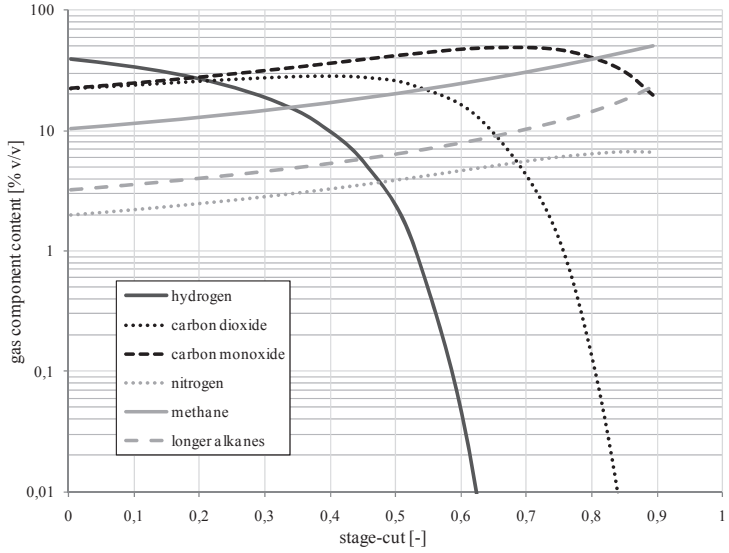

Figure 5. Gas composition of the retentate stream versus membrane stage-cut

In the range of average to higher membrane stage-cuts the predominate gas components are carbon monoxide and methane with contents from 20 vol% to 50 vol%. The contents of longer alkanes and nitrogen are expected to be 3 vol% and 5 vol% respectively at membrane stage-cuts of 0.5 and rising to 6 vol% and 14 vol% respectively at membrane stage-cuts of 0.8.
Hydrogen and carbon dioxide show similar behaviour regarding their content in the retentate stream at increasing stage-cuts. The content of both hydrogen and carbon dioxide sharply decreases at a certain stage-cut. The reason is that at this certain stage-cuts the whole amount of hydrogen and carbon dioxide contained in the feed gas has permeated through the membrane and therefore nothing remains at the retentate side of the membrane.

Corresponding to figures 4 and 5, figure 6 shows the expected gas composition of both permeate and retentate stream for an operating point with stage-cut of 0.14 an operating feed gas pressure of 15 bar.

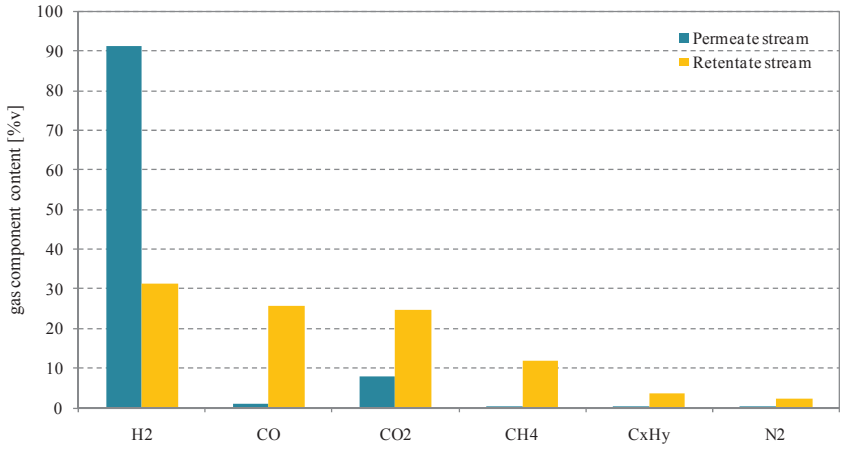

Figure 6. Gas composition of the permeate and retentate stream (stage-cut 0.14, 15 bar operating pressure)

Among the gas components of the permeate stream the most prevalent hydrogen, followed by carbon dioxide and carbon monoxide. The content of methane, longer alkanes and nitrogen is expected to be at a relatively low level.
On the contrary, the retentate stream is mainly composed of quite equal amounts of hydrogen, carbon monoxide and carbon dioxide. Apart from these three components, also methane, longer alkanes as well as nitrogen are present but to a lower extent.

4 CONCLUSION & OUTLOOK

This paper presents the polygeneration process which is going to be implemented at the biomass gasification plant in Oberwart, Austria. In addition to heat and electricity production, a hydrogen production process is going to be realized using a membrane separation process. A simulation of this process was carried out and results show that separation of hydrogen from product gas is basically possible. The content of hydrogen depends on several parameters such as the desired hydrogen recovery, the operating pressure and the stage-cut.
The hydrogen production process will be put into operation at the plant within the next few weeks. Results of the first operational experiments will give insight into the feasibility of this process and the obtained product gas qualities. Moreover, more information about how trace

components contained in the product gas of the gasification process affect the membrane will be gained.
If the obtained retentate stream composition possibly fits other process requirements, next steps could be evaluating more sophisticated applications of this gas instead of heat and electricity production only.

5 REFERENCES

[1] Hofbauer, H.; “Gas production for Polygeneration Plants”, International Conference on Polygeneration Strategies 2009, Vienna (2009)

[2] Potetz, A., Rauch, R. and Hofbauer, H.; „OptiBtLGas – Steam Reforming of Product Gas from Biomass Steam Gasification”, International Conference on Polygeneration Strategies 2009, Vienna (2009)

[3] Kotik, J.; Flow sheet Oberwart, Personal communication, Vienna (2010)

[4] Scott, K.; “Handbook of Industrial Membranes”, Elsevier (1995)

[5] Baker R.W. and Lokhandwala K.; “Natural Gas Processing with Membranes: An Overview”, Ind. Eng. Chem. Res. 47 (2008), p. 2109 – 2121

[6] Makaruk, A. and Harasek, M.; “Numerical algorithm for modeling multicomponent multipermeator systems”, Journal of Membrane Science 344 (2009), p. 258 – 265

IMPRESSUM

Verfasser
Technische Universität Wien, Institut für Verfahrenstechnik,
Umwelttechnik und technische Biowissenschaften
Ansprechpartner: Univ.Prof. Dipl.-Ing. Dr.techn. Hermann Hofbauer
Getreidemarkt 9/166, 1060 Wien
Tel: +43 (1) 58801-16601
Fax: +43 (1) 58801-16699
E-Mail: hermann.hofbauer@tuwien.ac.at
Web: http://www.vt.tuwien.ac.at

Projektpartner
- Energie Burgenland Biomasse GmbH & Co KG
- Binder Industrieanlagenbau GmbH

AutorInnen
- Hermann Hofbauer
- Klaus Bosch
- Horst Binder

Unter Mitarbeit von
- Michael Harasek
- Florian Benedikt
- David Konlechner
- Michael Kraussler

Eigentümer, Herausgeber und Medieninhaber
Klima- und Energiefonds
Gumpendorfer Straße 5/22
1060 Wien
E-Mail: office@klimafonds.gv.at
Web: www.klimafonds.gv.at

Gestaltung des Deckblattes
ZS communication + art GmbH